

A Appendices

Because of the numerous graphs and figures in the appendices, there has been chosen to print only the parts which consist mainly of text. However all appendices are included on the CD. In this way figures and graphs can be studied in detail on a computer. An overview of all appendices is given below. The ones only included on the cd are marked as well.

A.1	Description of the Western Scheldt: Additional Figures (CD).....	A-3
A.2	Human Interventions in the Last 50 Years.....	A-7
A.3	Sand Balance	A-16
A.3.1	Division in Compartments	A-16
A.3.2	Sand Balances for the Western Scheldt Estuary	A-18
A.3.3	Additional Figures and Tables (CD).....	A-25
A.4	Sediment Transport	A-28
A.4.1	Sediment Transport Mechanisms	A-28
A.4.2	Influence of Different Transport Formulations	A-29
A.4.3	Sediment Transport Formulae (CD)	A-31
A.5	1D-Equations for the Tidal Motion in a Channel with a Variable Width	A-38
A.6	Model Description	A-39
A.6.1	Model Properties	A-39
A.6.2	Bathymetry.....	A-41
A.6.3	Conventions in DELFT3D.....	A-42
A.7	Vertical Tidal Asymmetry.....	A-44
A.7.1	Applicability of the Model (CD)	A-44
A.7.2	Amplitude and Phase of the Tidal Constituents at the Different Stations in the Model.....	A-50
A.7.3	Evolution of the Vertical Tidal Asymmetry in Each Macro Cell.....	A-51

A.7.4	Depth Differences Between the Different Bathymetries (CD) ..	A-61
A.7.5	Cross-sections of the Bathymetry in Each Macro Cell (CD) .	A-68
A.7.6	Comparison with Previous Studies	A-80
A.7.7	Graphical Representation of the Amplitude Ratios and Phase Differences of the Vertical Tide (CD)	A-82
A.8	Horizontal Tidal Asymmetry	A-84
A.8.1	Location of the Cross-sections and Observation Points.....	A-84
A.8.2	Results per Macro Cell	A-88
A.8.3	Values of the Amplitude and Phase of the Velocity and the Direction of the Principal Axis in Every Observation Point ...	A-103
A.8.4	Values of the Amplitude and Phase of the Discharge through the Cross-sections in the Ebb and Flood Channel in Every Macro Cell	A-106
A.9	Residual Sediment Transport Patterns.....	A-108
A.9.1	Residual Sediment Transport Patterns (CD)	A-109
A.9.2	Differences in Direction and Magnitude of the Residual Sediment Transport.....	A-123
A.10	Sand Balance Derived from the Model	A-125
A.10.1	Cross-sections Used for the Calculation of the Sand Balance.	A-125
A.10.2	Transport at the Seaward Border of Macro Cell 1	A-127
A.10.3	Sand Balance Derived from the Model with the Engelund Hansen Transport Formulation.....	A-128
A.10.4	Comparison with Previous Studies	A-130
A.10.5	Possible Errors	A-131

A.1 Description of the Western Scheldt: Additional Figures

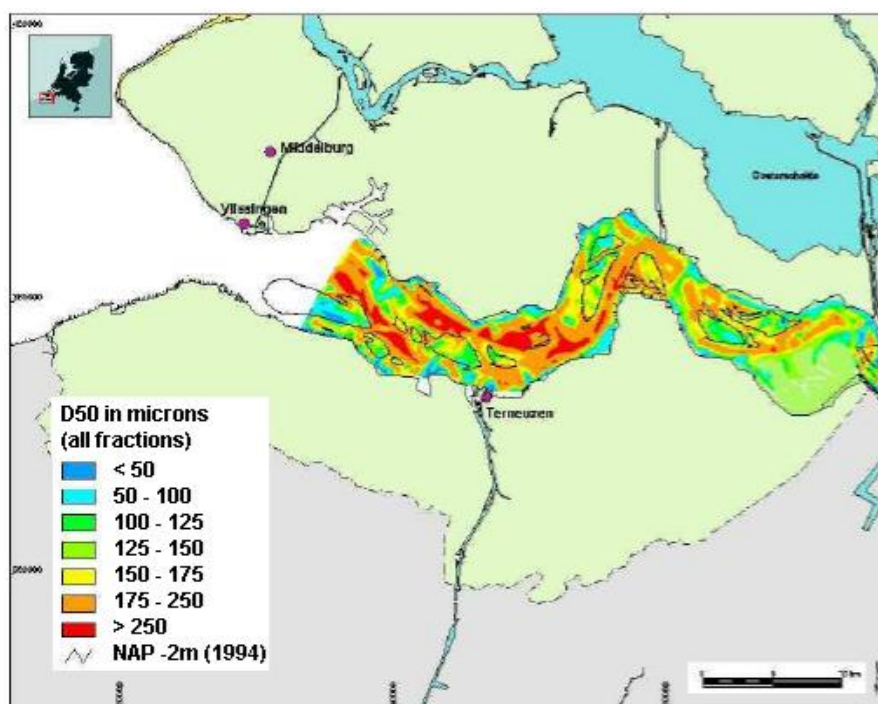


Figure A.1-1: Median grain size (d_{50}) in the Western Scheldt as measured in 1993 (Kuijper et al., 2004).

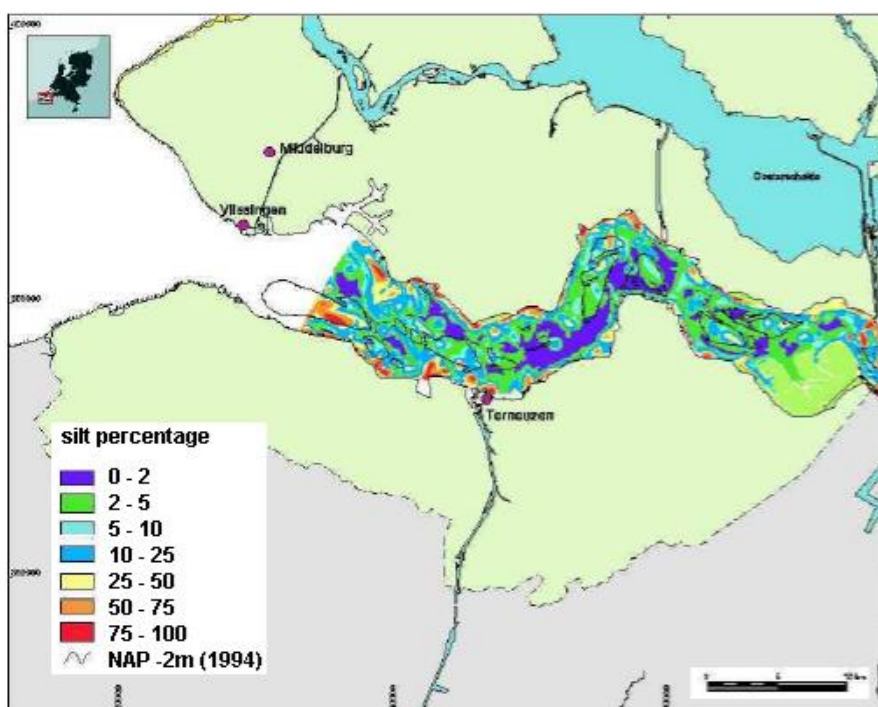


Figure A.1-2: Percentage of mud in the Western Scheldt as measured in 1993 (Kuijper et al., 2004).

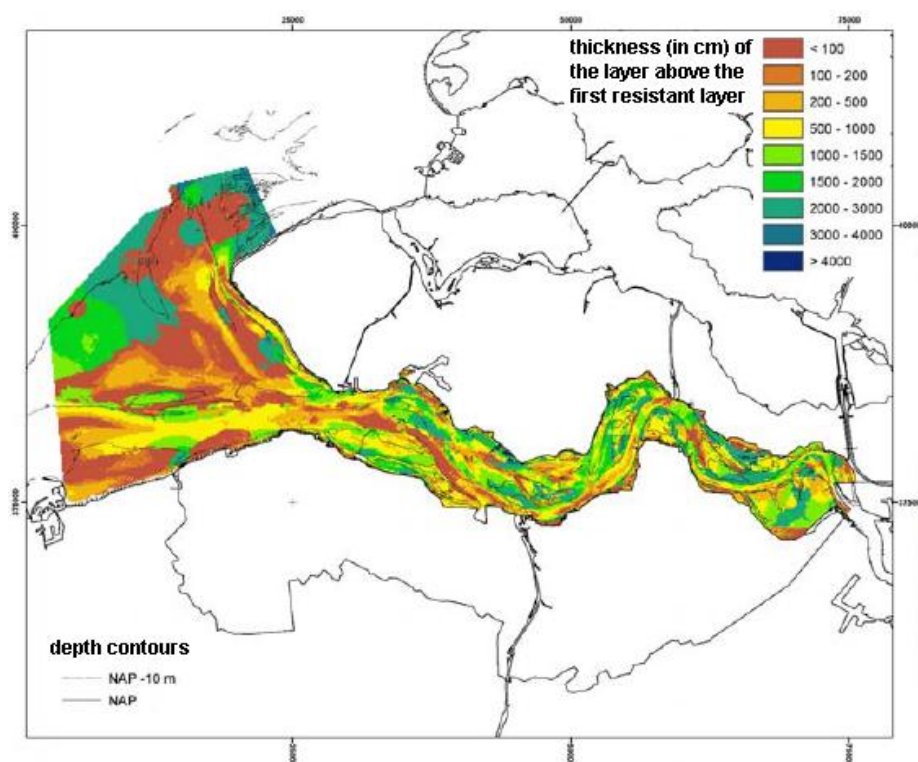


Figure A.1-3: Thickness of the upper erodible sand layer (Kuijper et al., 2004).

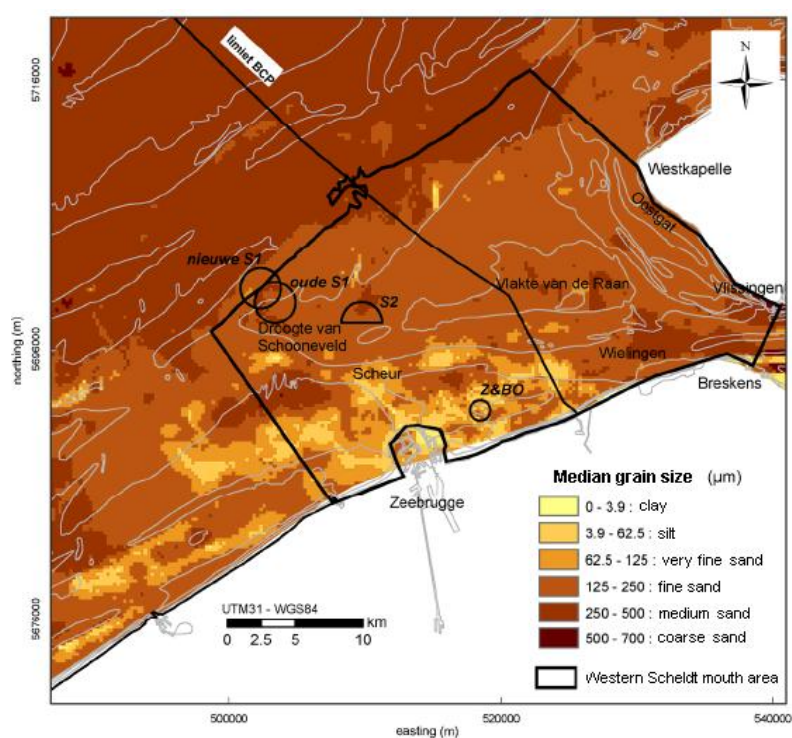


Figure A.1-4: Median grain size map, made based on an interpolation of the sediment data set (sedisurf@database, since 1976 made by RCMG (Renard Centre of Marine Geology) -Gent University), completed with sediment data from TNO (Dutch organisation for applied-natural scientific research), and steered by the variation of a bathymetric digital terrain model (Verfaillie et al., in press).

A.2 Human Interventions in the Last 50 Years

The human influences on the morphology of the Western Scheldt are not limited to the large land reclamation in the past, also in the last 50 years several interventions took place. Apart from almost continuous dredging, dumping and sand mining in the estuary, bank protection measures have been placed at the border of a number of channels Peters et al. (2003).

Also the morphological evolution of the mouth has been affected by human interventions. The expansion of the port of Zeebrugge (1972-1985) with the construction of the breakwaters and the dumping of large amounts of dredged material northwest of the Vlakte van de Raan for a long time, certainly have an influence although the exact impact can hardly be estimated (Dumon et al, 2006; Port of Zeebrugge, 2006). Also other edifices such as the delta-plan with the storm-surge barrier on the Eastern Scheldt (build between 1976 and 1986) have possibly affected the Western Scheldt mouth area (ibid.).

Dredging, Dumping and Sand Mining

The amount of dredged material varies during time. Since the beginning of the previous century till 2001, the total volume has increased from around 1 to nearly 11 million m³/year. The Table below gives an overview of the amount of maintenance dredging (= the dredging required to keep the channels and bars at the desired depth) in the Western Scheldt for different periods. Difference is made between the bars connecting the channels and the other areas. Since there is continuous sedimentation on the bars, most of the maintenance dredging takes place on these locations. A list of bars in the Western Scheldt and their location is given in Figure A.2-1. The evolution of the annual amount of dredging between 1955 and 2001 is shown on Figure A.2-2 (Peters et al., 2003).

Table A.2-1: Overview of the maintenance dredging in the Western Scheldt (Peters et al., 2003).

	Maintenance Dredging in the Western Scheldt (million m ³ /year)		
Period	Total	On Bars	Other Areas
begin previous century	1-2	-	-
1960's	5	4	1
1967-1978	first deepening: 44'/40'/34 feet deepening of the bars to minimal 14.5 m below NAP		
1978-1989	10-11	8-9	2
1989-1997	8.5-9	6.5-7	2
1997-1998	second deepening: 48'/43'/38' feet deepening of the bars to minimal 16 m below NAP		
1998-2001	10.5-11.5	6.5-7	4-4.5

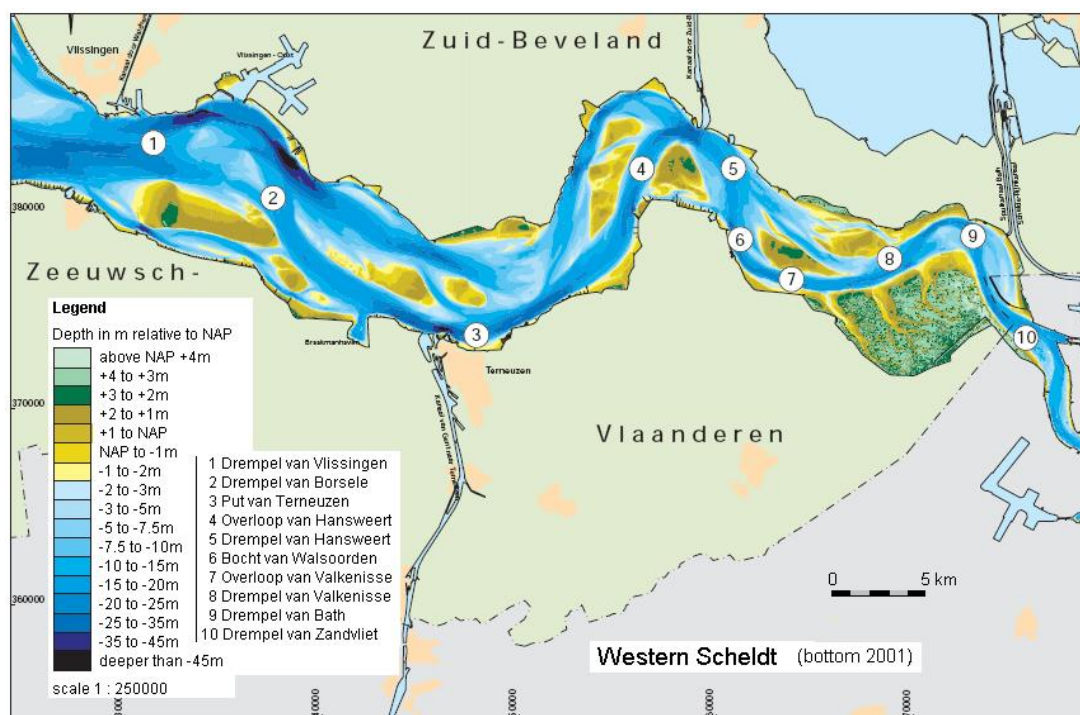


Figure A.2-1: Location of the bars in the Western Scheldt (Peters et al., 2003).

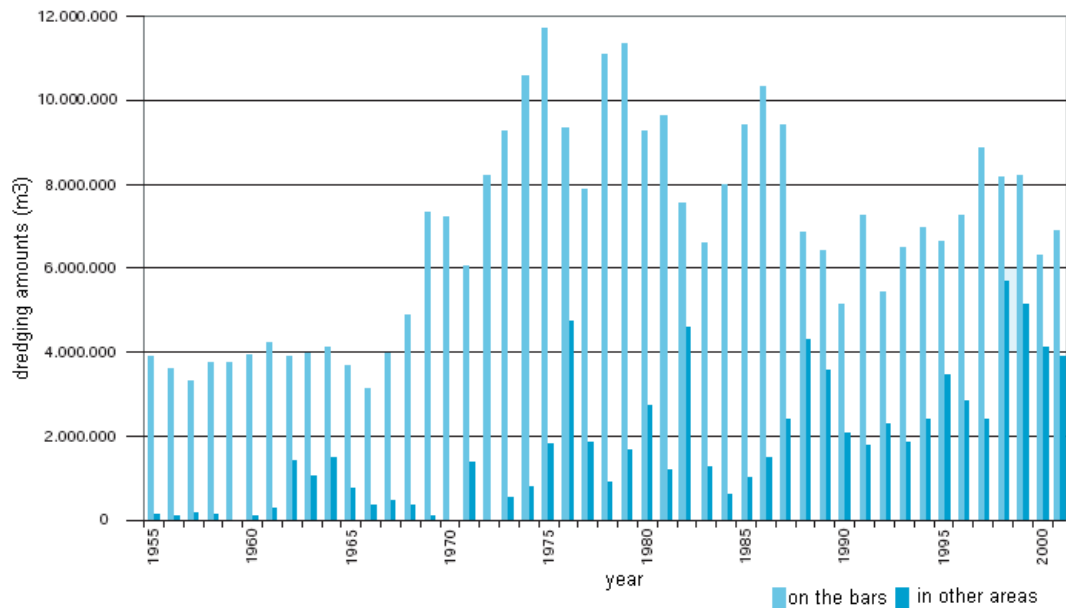


Figure A.2-2: Annual amounts of dredging in the Western Scheldt on the bars (light blue) and in the other areas (dark blue) (Peters et al., 2003).

To keep the total amount of sediments in the estuary constant, the material from the maintenance dredging of the channels is dumped elsewhere in the estuary. Before the second deepening, this material was mainly dumped in the eastern part of the Western Scheldt, in the secondary channels close to the place of extraction. After the second deepening, the dumping strategy has been changed. More dumping locations have been selected in the western and central part of the Western Scheldt to relieve the eastern part, to keep the dynamics of the multiple channel system and to limit the amount of maintenance dredging (Stikvoort et al, 2003; Peters et al., 2003).

Apart from dredging and dumping, there also occurs sand mining in the Western Scheldt. From 1993 on the maximal amount is 2.6 million m³/year (Huys et al., 2000). The sand mining is concentrated in the eastern part since 1991. Before this activity mainly took place in the western part. The annual values are shown on Figure A.2-3.

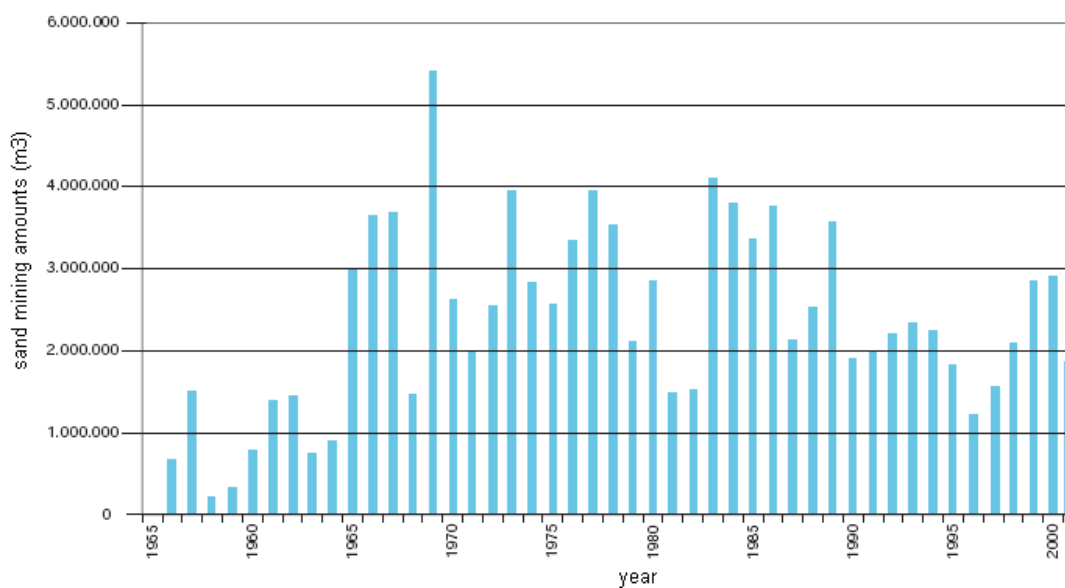


Figure A.2-3: Annual amounts of sand mining in the Western Scheldt (Peters et al., 2003).

Figure A.2-4 shows a map with the different areas where dredging, dumping or sand mining occurs. At the end of this appendix graphs are included with the annual amounts of material for each area.

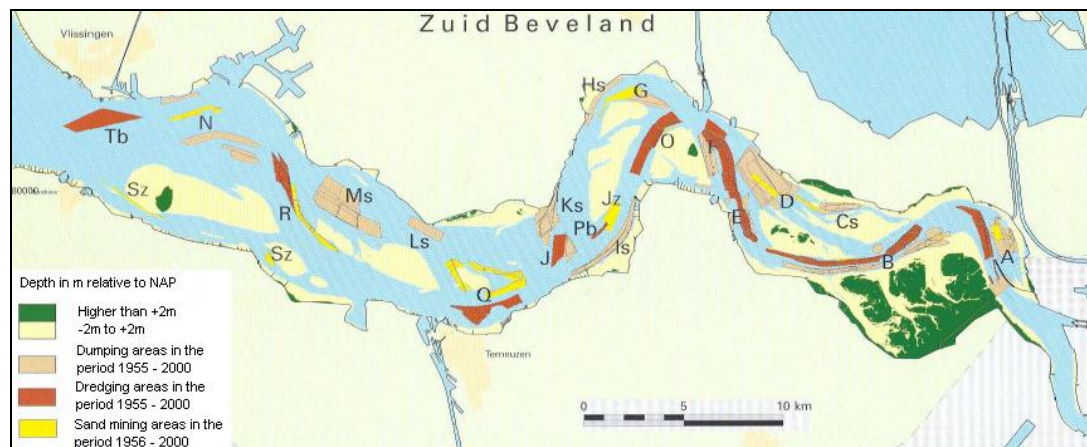


Figure A.2-4: Map of the Western Scheldt with the areas where dredging, dumping or sand mining occurs (adapted from Groenendaal, 2005).

Bank Protection Measures

As a part of the deepening agreement, several erosion protection measures have been placed in the central and eastern part of the Western Scheldt between 1996 and 2001 (Peters et al., 2003). They prevent further erosion of the banks and marshes in the outer bends of the channels. Their location is indicated on Figure A.2-5.

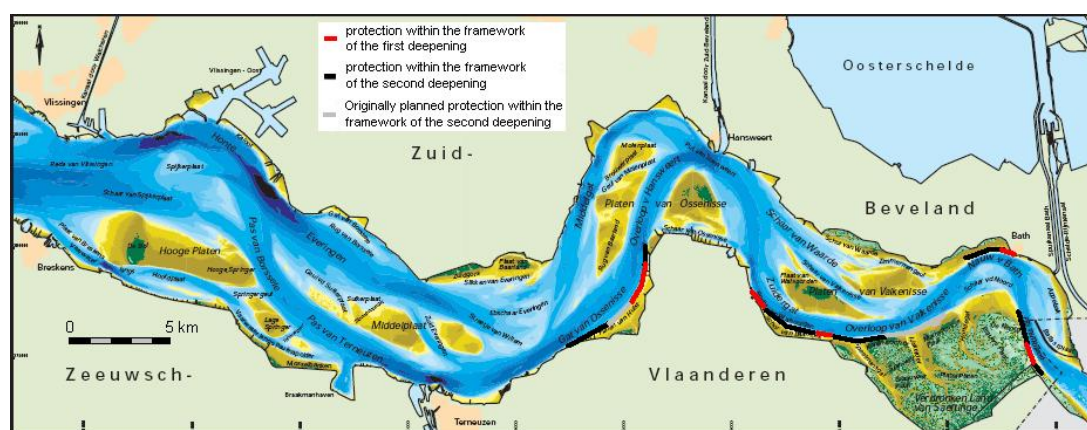


Figure A.2-5: Location of the erosion protection measures within the framework of the first and second deepening along the Western Scheldt (Adapted from Peters et al. (2003)).

The next graphs give the yearly amounts of dredging and dumping of sediments and the sand mining in the Western Scheldt for the period 1955-2000. The location of the areas is indicated on Figure A.2-4. The first capital letter stands for the location of the area, b stands for dredging, s for dumping and z for sand mining.

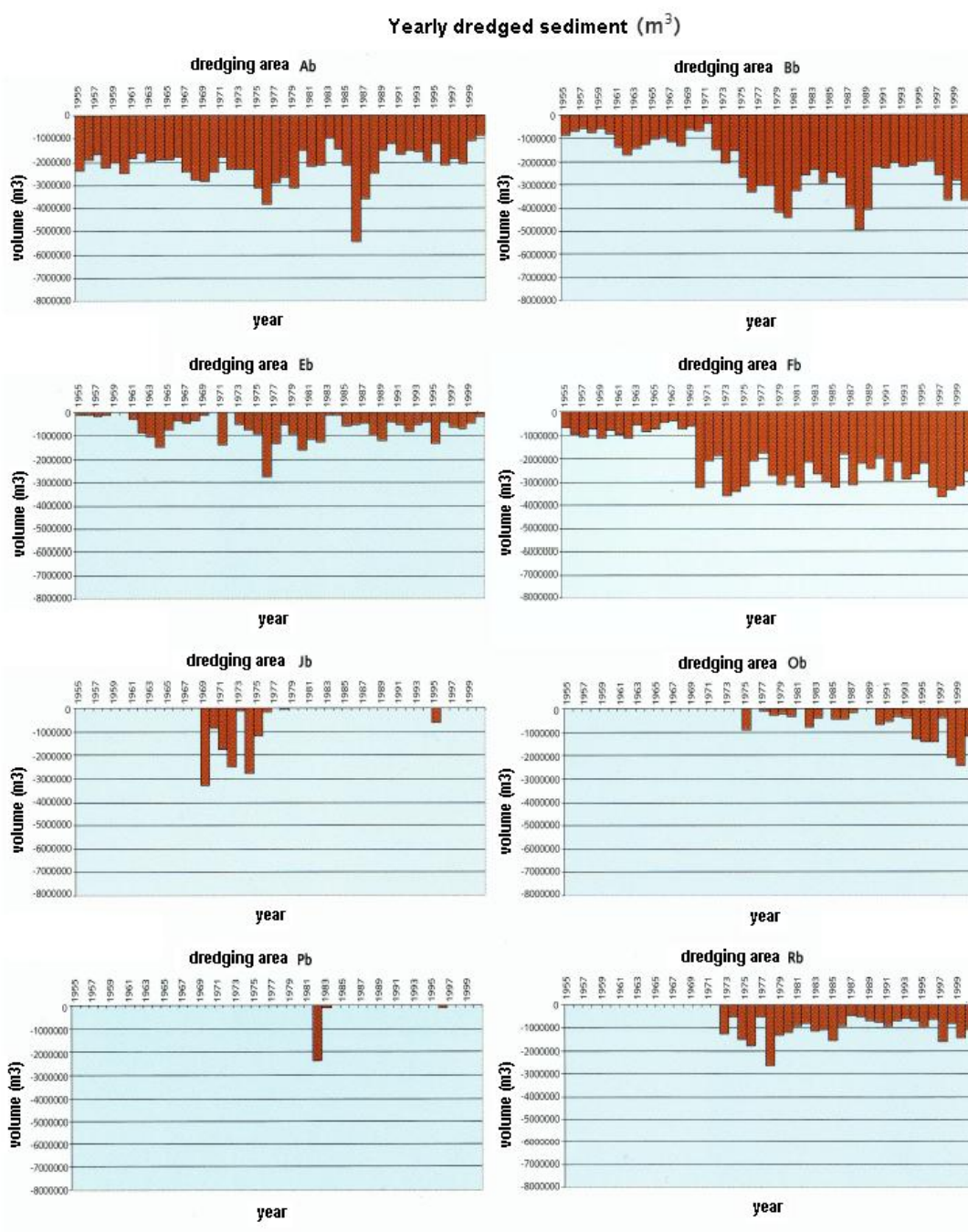


Figure A.2-6: Annual volumes of dredging, dumping and sand mining in the Western Scheldt estuary (Groenendaal, 2005).

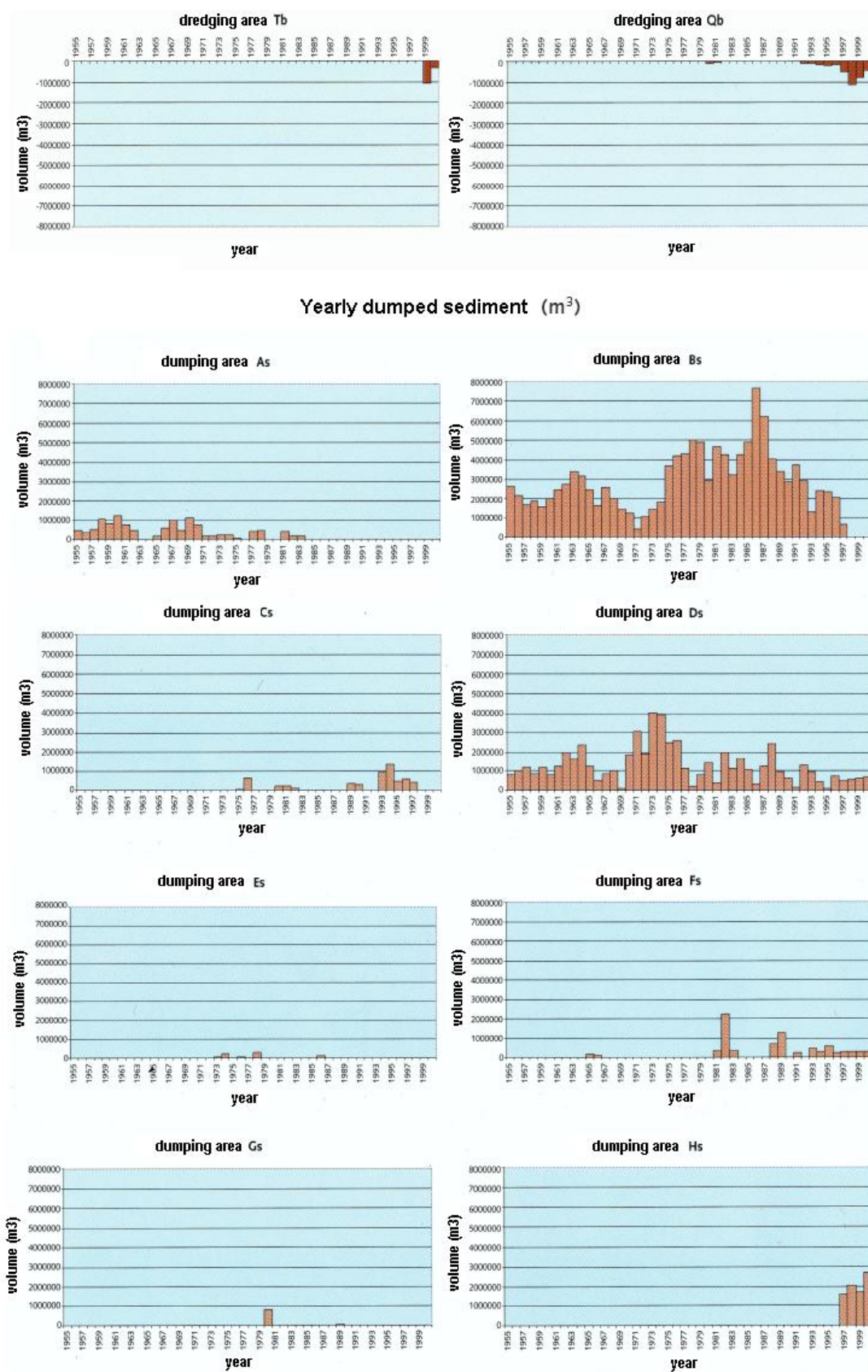


Figure A.2-7: Annual volumes of dredging, dumping and sand mining in the Western Scheldt estuary (part 2) (Groenendaal, 2005).

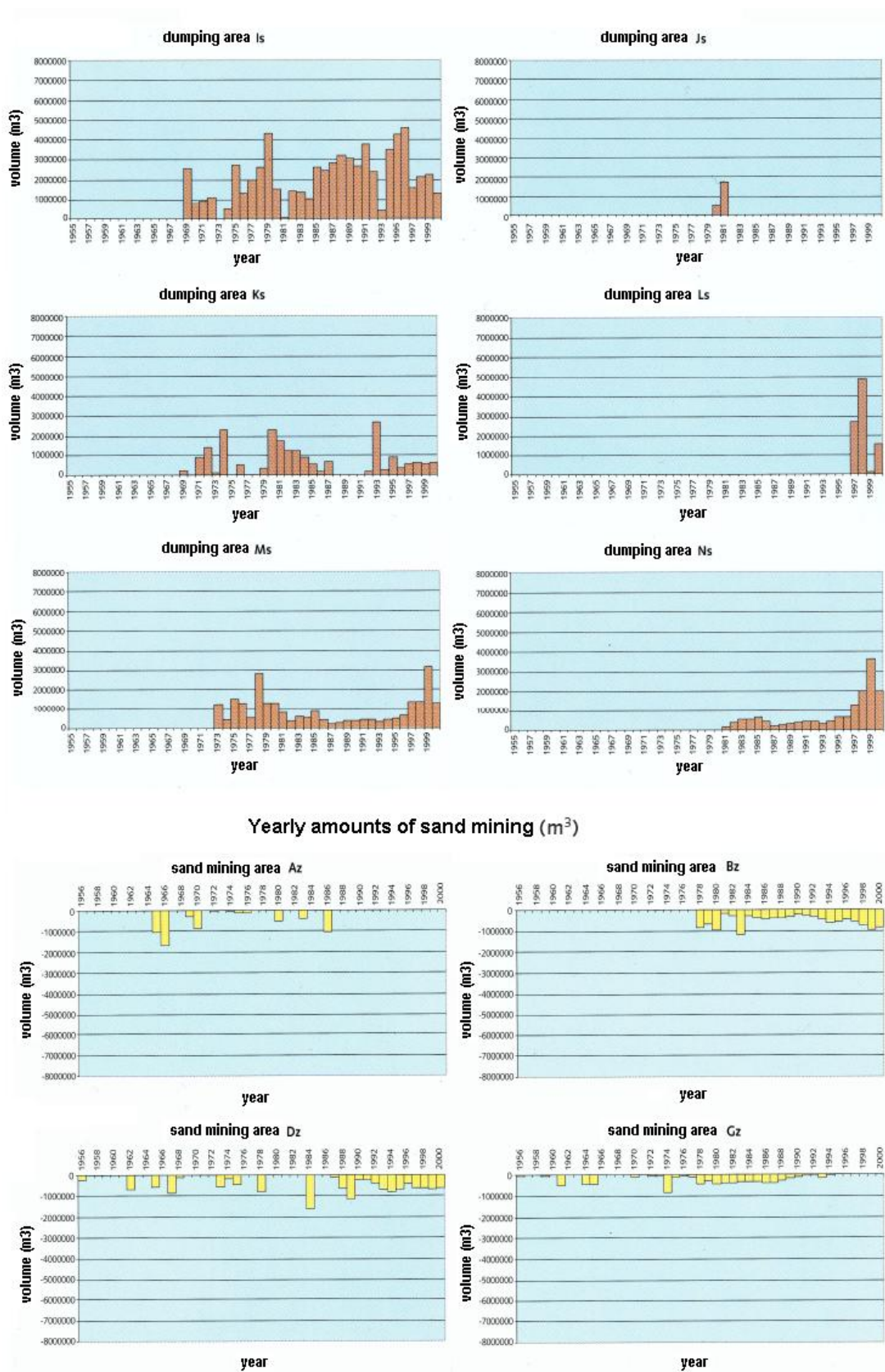


Figure A.2-8: Annual volumes of dredging, dumping and sand mining in the Western Scheldt estuary (part 3) (Groenendaal, 2005).

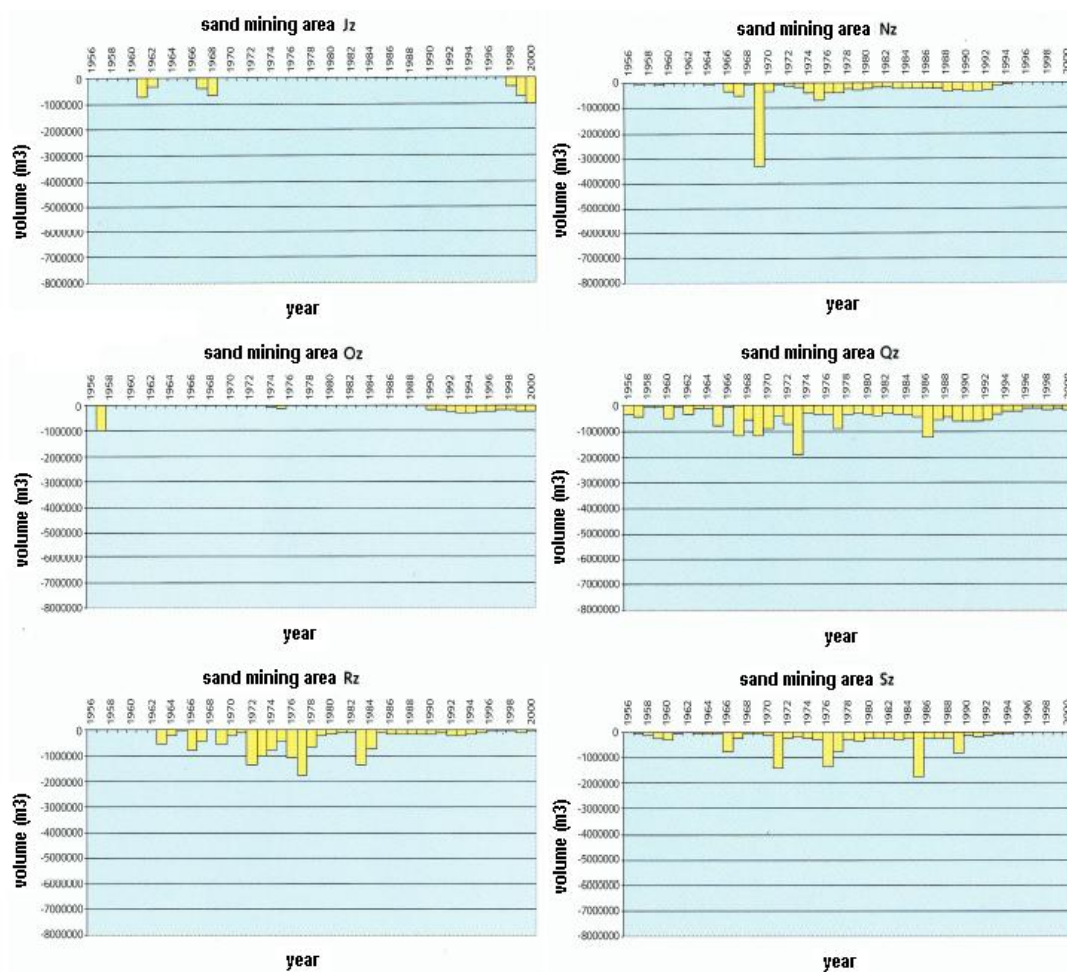


Figure A.2-9: Annual volumes of dredging, dumping and sand mining in the Western Scheldt estuary (part 4) (Groenendaal, 2005).

A.3 Sand Balance

A.3.1 Division in Compartments

Western Scheldt

Until the year 2000 the division in compartments of the Western Scheldt was kept the same as that of the bathymetric maps (the rectangles on Figure 3-2). Uit den Bogaard (1995) and De Jong (2000) constructed sand balances according to this partition.

Nowadays a morphological division is used (for example Nederbragt and Liek, 2004). This has the advantage that the configuration of the system of shoals and channels and their evolution in time is taken into account (Jeuken et al., 2002).

Different macro and meso cells are defined in the Western Scheldt (Winterwerp et al., 2000; Figure 2-4). Each of these cells can be split in smaller morphological units such as channels and shoals. Based on these units the channel-oriented morphological division in compartments for the Western Scheldt is made. For the sand balance, the compartments are aggregated to the level of ebb- and flood channels of the macro cells (Nederbragt and Liek, 2004; Figure 3-3).

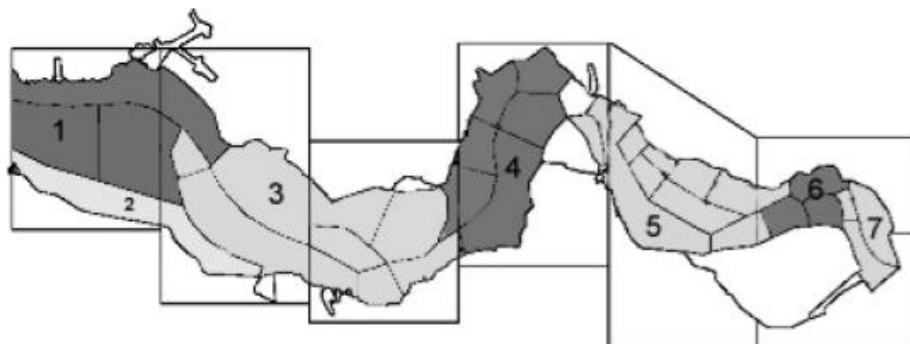


Figure A.3-1: The aggregated morphological division of the Western Scheldt into meso (cell 2) and macro cells (rest). The numbers of the cells agree with the macro-cells from Figure 2-3. The rectangles represent the echo-sounding areas (after Nederbragt and Liek, 2004).

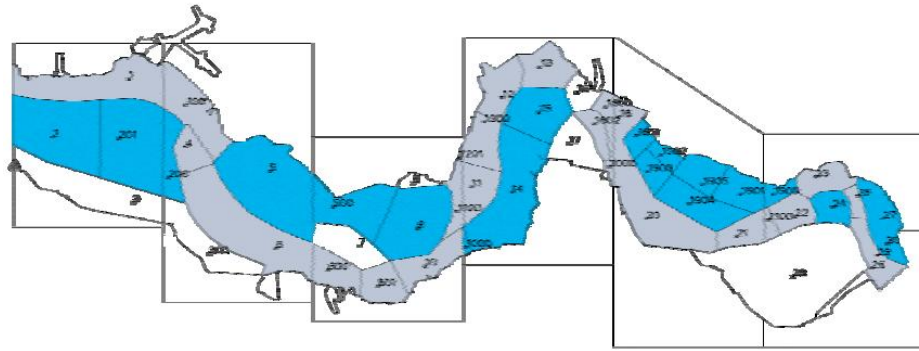


Figure A.3-2: The aggregated morphological division of the Western Scheldt into ebb channels (marked in grey) and flood channels (blue). The rectangles represent the echo-sounding areas (Nederbragt and Liek, 2004).

Western Scheldt Mouth

Sand balances for the Western Scheldt mouth have been created by Van der Slikke (1997, 1998) and Haecon (2000). Only in the study by Van der Slikke (1998) a morphological division has been used.

Also for the Western Scheldt mouth a new morphological and mostly channel-oriented division has been made by RIKZ (National Institute for Coastal and Marine Management) (Nederbragt and Liek, 2004). Here as well the compartments are aggregated to bigger morphological units as presented in Figure 3-4. A clear division is made between the Dutch and Belgian part of the mouth.

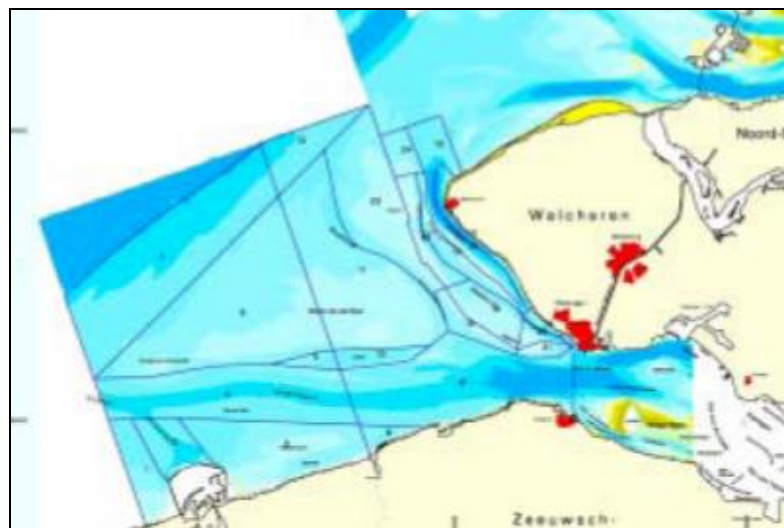


Figure A.3-1: The aggregated morphological division of the Western Scheldt mouth (Nederbragt and Liek, 2004).

A.3.2 Sand Balances for the Western Scheldt Estuary

A.3.2.1 Nederbragt and Liek (2004)

Nederbragt and Liek (2004) concluded from their sand balance study that since 1955 alternating periods with sand import and export occur. The Western Scheldt has become exporting since the 90's from the previous century. On average, the export was $1.5 \text{ Mm}^3/\text{year}$ over the period 1990-2001. The sediment transport from the west to the east has increased since 1997. The Western Scheldt combined with the mouth also shows an exporting trend over the period 1990-1996 (Figure A.3-4).

Varying assumptions for the conversion factor for the sediment volume of the interventions (10%) and the transports (sedimentation of the land of Saefthinge with $0.3 \text{ Mm}^3/\text{year}$ and no transport across the Belgian-Dutch boundary) do not change the exporting trend of the Western Scheldt, only the moment of the reversal from import to export is modified.

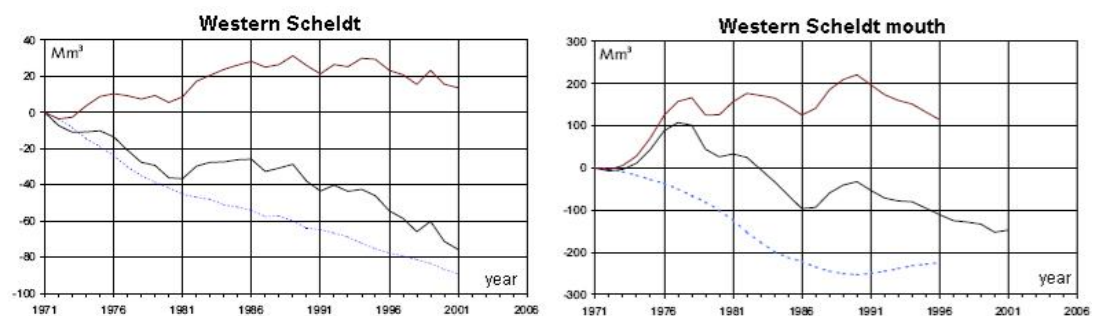


Figure A.3-2: Cumulative sand volumes since 1971 in the Western Scheldt (on the left) and the mouth (on the right). The black line gives the total volume V_{tot} , the blue line the cumulative interventions V_i and the red line the natural volume V_{nat} . A rising line means sedimentation, a descending line erosion (Nederbragt and Liek, 2004).

A.3.2.2 Duin (2005)

Walburg (2006) calculated a historical sand balance for the foundation (from NAP-20 m towards the land including all dunes and sea defences, excluding the Wadden Sea and the Western Scheldt) of the entire Dutch coast. On this data Duin (2005) performed a trend analysis for the period 1973-1997. He found that both the Western and the Eastern Scheldt delta show a significant erosion trend (due to natural transports) over this period of respectively 2.7 and $1.1 \text{ Mm}^3/\text{year}$ (Table A.3-3). On Figure A.3-5 there can be seen that the sedimentation of the coast foundation which took place since 1968 changed into erosion around 1980.

Table A.3-1: Trends in the natural volume changes due to natural transports for the subsystems and the coast foundation. The 90% confidence interval is given with the upper and lower limit. Significant trends are marked in grey (Duin, 2005).

Period 1973-1997	Trend in the Volume Change due to Natural Transports (ΔN) (Mm ³ /year)		
Subsystem ¹	Lower Limit	Trend	Upper Limit
Eems Dollard ²		-	
Friesche Zeegat	-1,7	-1,4	-0,7
Amelandse Zeegat	-1,0	0,1	2,7
Het Vlie	-2,3	-1,7	-0,9
Eierlandse Zeegat	-1,2	-0,9	-0,5
Marsdiep	-5,0	-3,2	-2,1
Waddenkust (exclusive Eems-Dollard)³	-10,0	-6,7	-0,5
Noord-Holland	-1,8	-0,1	0,8
IJ-geul ²		-	
Zuid-Holland ⁴	-0,9	-0,3	0,4
Maasgeul ²		-	
Hollandse kust³	-1,7	-0,4	1,2
Haringvliet delta ⁵	-1,2	0,1	0,8
Grevelingen delta	-2,8	-0,4	0,5
Oosterschelde delta	-3,6	-1,1	-0,1
Westerschelde delta	-3,3	-2,7	-1,5
Deltakust³	-10,6	-3,9	-0,4
Coast foundation³	-19,0	-15,0	-5,4
¹ For all subsystems the dune area is entirely missing. ² No bottom depth data available. The sand balance could not be calculated. ³ Summation of the separate trends doesn't give the trend of the compound area. This is related to the applied statistical method which is the Mann-Kendall technique. ⁴ There is assumed that all the dumped material on the Loswal Noord originates from the coast foundation. (internal redistribution). ⁵ Data about sand mining in 'het Slijkpat' are incomplete and this results in an underestimation			

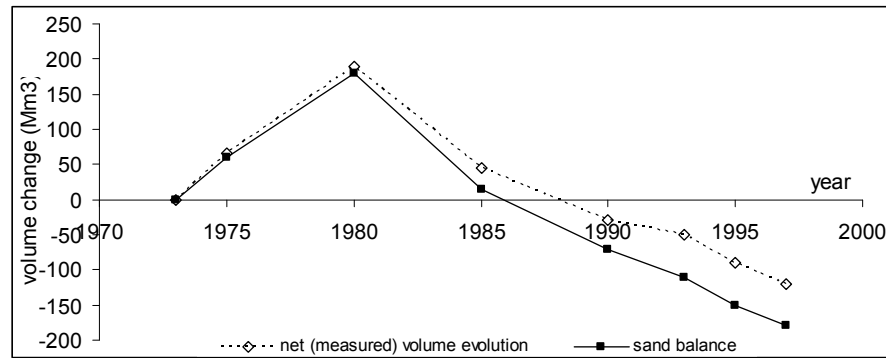


Figure A.3-3: Measured evolution and sand balance of the sand supplies of the coast foundation (after Nederbragt, 2006).

The evolution of the sediment in the Eastern Scheldt delta can be explained by the influence of the delta works: the construction of the Volkerakdam in 1969 enhanced the tidal prism of the Eastern Scheldt basin. This resulted in a growth of the outer delta. The construction of the Eastern Scheldt storm surge barrier narrowed the mouth. This decreased the tidal prism of the Eastern Scheldt and gave rise to erosion due to a relative increase of importance of the wave action compared to the tidal currents (de Bok, 2002). Since both deltas are closely related, this can also be expected to have an influence on the evolution of the Western Scheldt estuary.

A.3.2.3 Haecon (2006)

Recently the sand balance of the Western Scheldt has been updated by Haecon (2006). They expanded the previously developed sand balance model of Nederbragt and Liek (2004) on the landward side with the Sea Scheldt to Rupelmonde and on the western side with the areas between Zeebrugge and the Western Scheldt mouth (Figure A.3-6). This area is in accordance with results concerning the circulation of water, salt and sediment in the Scheldt estuary and the North Sea, and with the other research projects in the framework of the long term vision of the Western Scheldt estuary, which consider the Scheldt mouth as a part of the estuary (Peters, 2006).

The sand balance has been calculated over the entire area for the period 1955-2004 and all the available data have been taken into account. To allow comparison with the previous sand balances the same calculation method has been used. Also the assumption of a transport of 0.3 million m³/year towards the Verdonken land van Saefthinge has been kept the same.

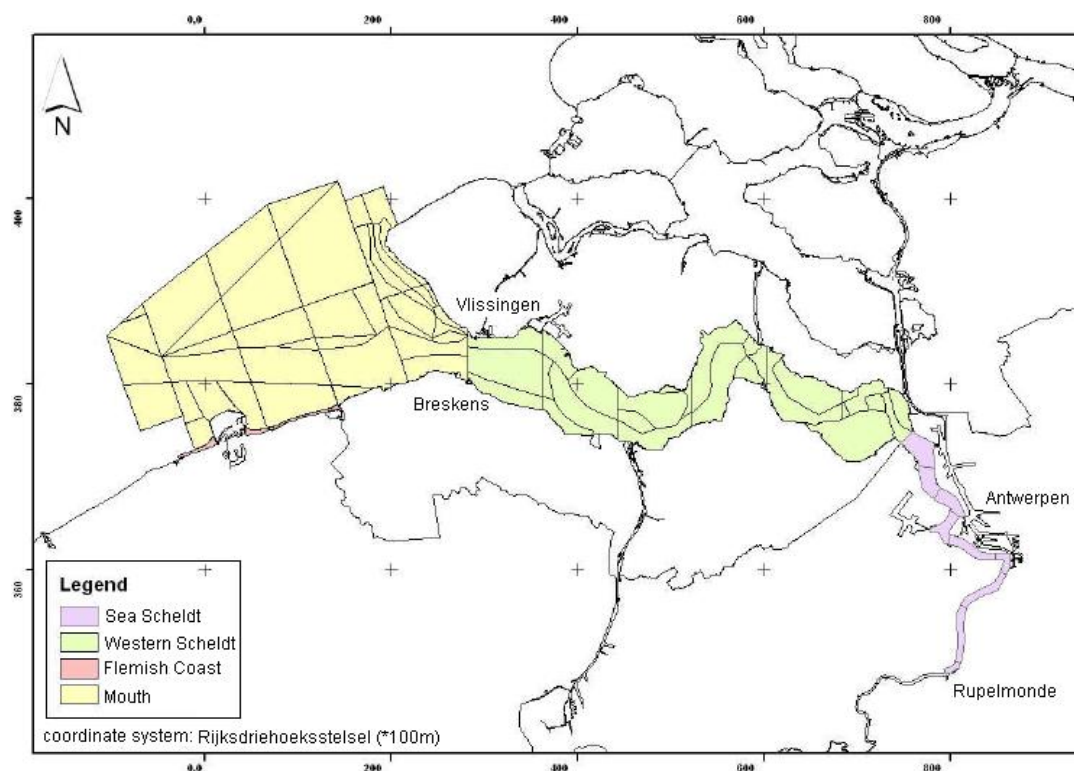


Figure A.3-4: Overview of the area included in the sand balance from Haecon (2006).

From the sand balance of the Sea Scheldt it comes out that the assumption in the previous sand balances of no transport across the Belgian-Dutch border is not valid. Between 1955 and 2004 there is a yearly import of 1.1 million m^3 , although there is a strong fluctuation as can be seen in Figure A.3-7. By considering this transport the change from import to export near Vlissingen takes place several years later (in 1997) compared to the previous balance (in 1990). This agrees with the findings of Nederbragt and Liek (2004).

The cumulative sand balance for the Western Scheldt is given in Figure A.3-8, the yearly import/export near Vlissingen is shown in Figure A.3-9. The change from import to export moves gradually upstream in the Western Scheldt (Haecon, 2006). The sharp fluctuations of the sediment transport are partly due to the applied calculation method, which works on a yearly base.

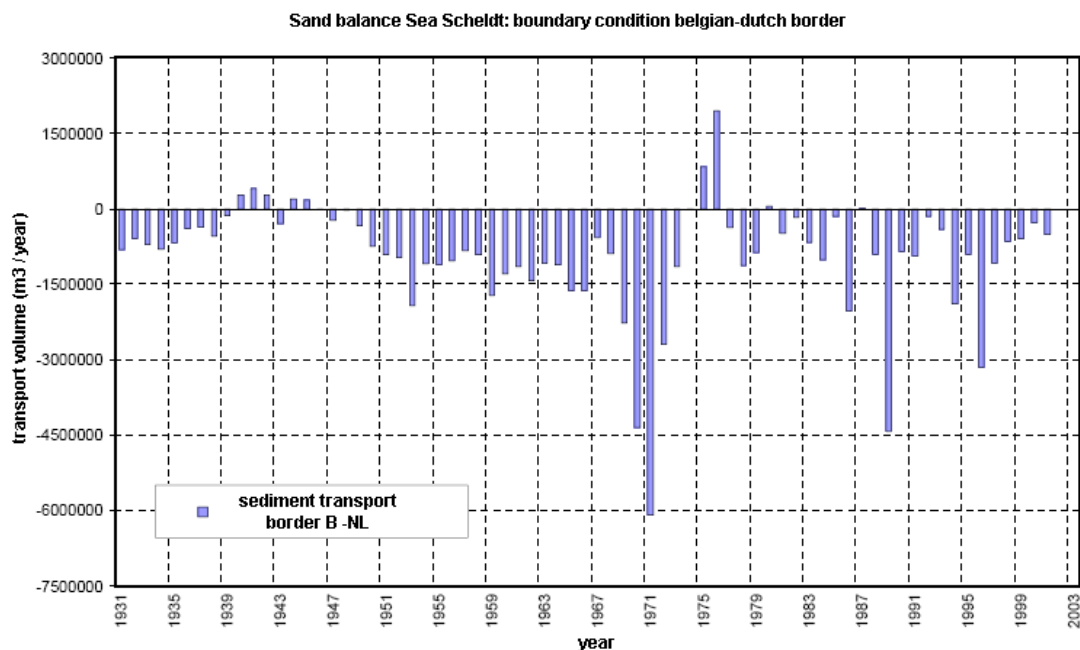


Figure A.3-5: Sand balance of the Sea Scheldt: boundary condition at the Belgian-Dutch boundary (Assumption of no transport near Rupelmonde; - = transport towards Belgium) (Haecon, 2006).

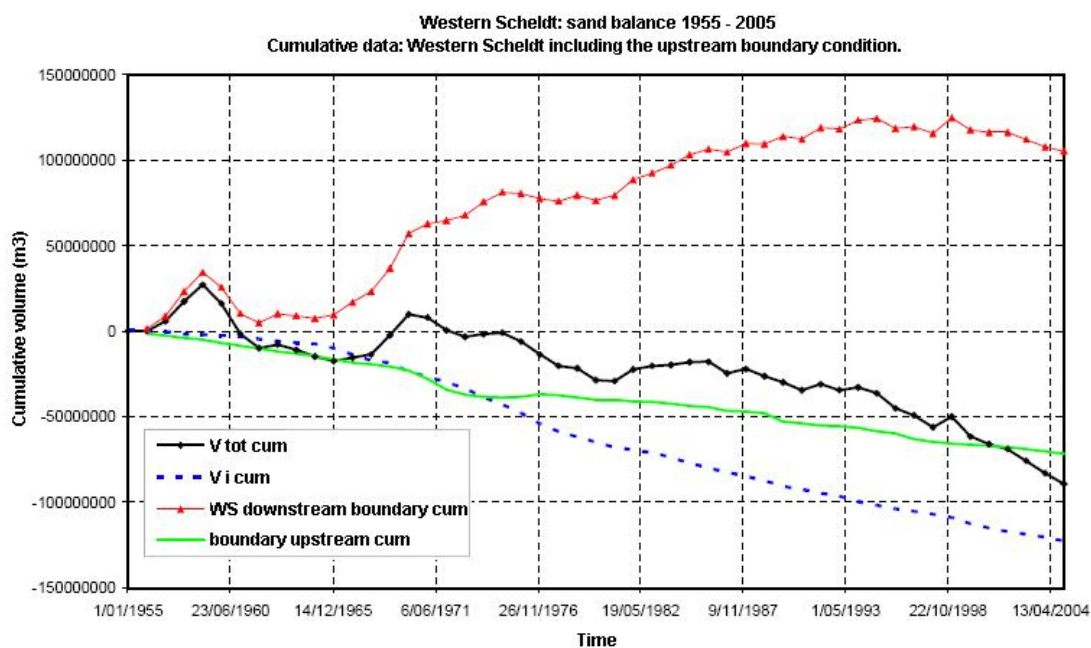


Figure A.3-6: Cumulative sand volumes since 1955 in the Western Scheldt. The black line gives the total volume V_{tot} , and the blue dashed line the cumulative interventions V_i . The green line is the upstream boundary condition near the Belgian-Dutch boundary. A descending green line means export from the Western Scheldt towards the Sea Scheldt or Saefthinge. The red line shows the downstream boundary near Vlissingen. A rising red line means import from the mouth towards the Western Scheldt (Haecon, 2006).

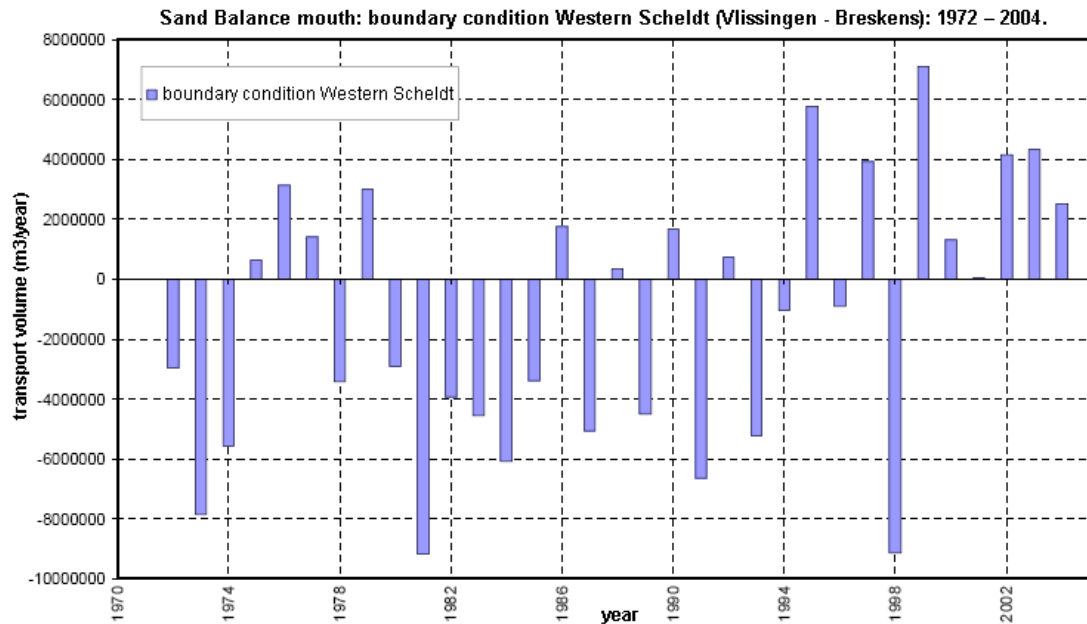


Figure A.3-7: Sand Balance mouth: boundary condition Western Scheldt (Vlissingen - Breskens): 1972-2004.
A negative value means transport from the mouth towards the Western Scheldt (Haecon, 2006).

Some other findings from Haecon (2006) are listed below.

- Due to human interventions, a lot of sand disappears from both the Western Scheldt and the Sea Scheldt. In the mouth this trend is less clear and the averaged yearly amounts are much smaller.
- Mainly during the last 15 years the transport from the mouth towards the sea is considerably ($10 \text{ million m}^3 / \text{year}$).
- In general, the bathymetry of the mouth has lowered. This is completely due to the deepening of the navigation channel and the surrounding areas. Also Walburg (2006) has noticed erosion of the Western Scheldt delta in the period 1973-1997.
- Only sand has been considered in the balance although especially in the mouth the ratio sand/silt is subject of discussion. Also the depth measurements in this area are possibly influenced by the occurrence of silt layers on the bottom which reflect the signal.
- The time series is still too short to perform a founded statistical analysis concerning the influence of the 18.6 yearly cycle.

The global balance of the Scheldt for the period 1972-2004 is shown in Figure A.3-10. The bottom profile has lowered during this period and 285 million m^3 sand has disappeared. Until 1989 sand was imported from the sea towards the mouth. Since 1990 export of sand occurs. However, this graph should be considered purely indicative since the ratio sand / silt

in the mouth is not well known and the depth measurements didn't always reach the solid bottom.

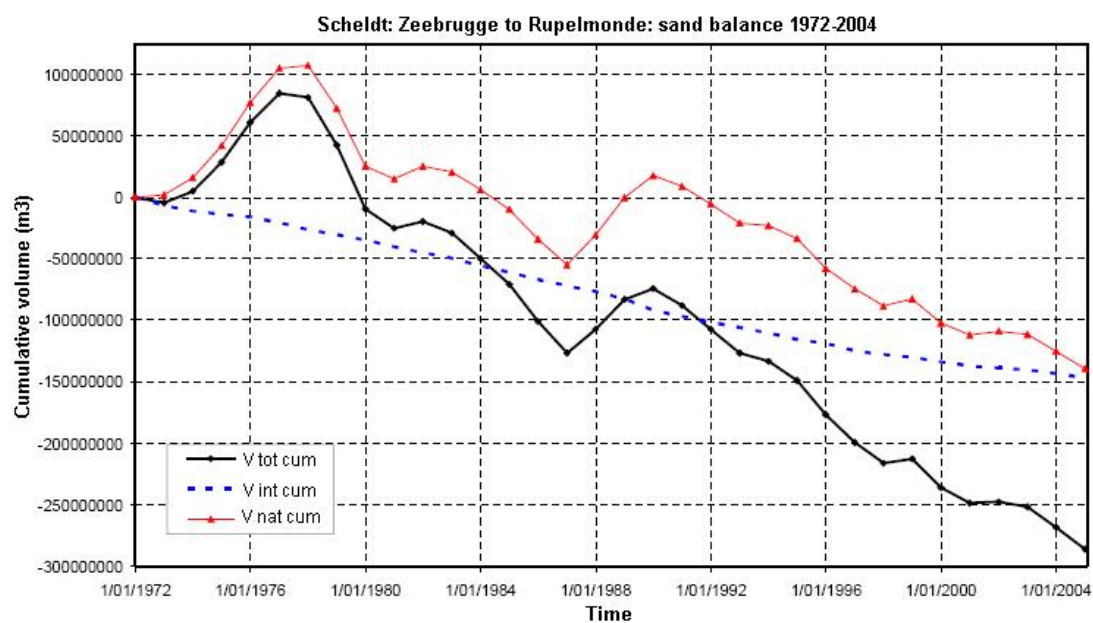


Figure A.3-8: Cumulative sand volumes since 1972 in the entire research area (Rupelmonde to Zeebrugge). The black line gives the total volume V_{tot} , the blue dashed line the cumulative interventions V_{int} and the red line the natural volume V_{nat} . A rising line means sedimentation, a descending line erosion (Haecon, 2006).

A.3.3 Additional Figures and Tables



Figure A.3-9: Division of the management area of "directie Zeeland" in echo-sounding areas, including the echo-sounding areas in the Belgian part of the Western Scheldt mouth (Nederbragt and Liek, 2004).

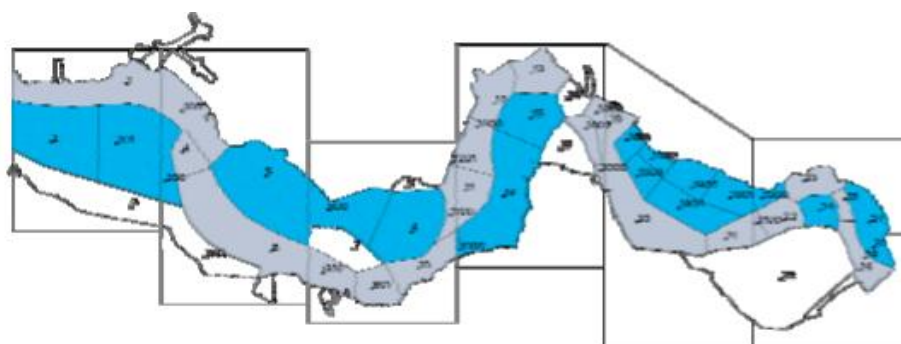


Figure A.3-10: Morphological division of the Western Scheldt. The flood channels are marked in dark blue, the ebb channels in grey. The channels also contain most of the shoals. The white areas aren't part of a macro-cel. The rectangular areas correspond with the borders of the echo-sounding areas (Nederbragt and Liek, 2004).

Table A.3-2: Aggregation of the compartments for the separate ebb- and flood-channels in the macro-cells (Nederbragt and Liek, 2004).

Macro Cell	Ebb Channel (EC)	Aggregated Compartments EC	Flood Channel (FC)	Aggregated Compartments FC
1	Honte	1, 100	Schaar van de Spijkerplaat	2, 201, 200
3	Pas van Terneuzen	4, 6, 600, 601, 10	Gat van Ossenisse	5, 500, 9
4	Middelgat	1100, 11, 1201, 1200, 12, 13	Schaar van Waarde / Schaar van Valkenisse	1000, 14, 15
5	Zuidergat / Overloop van Valkenisse	18, 1800, 1802, 2000, 20, 21, 2100	Schaar van de Noord	1801, 1903, 1904, 1902, 1905, 1901, 1900
6	Nauw van Bath	22, 23	Appelzak	24
7	Vaarwater boven Bath	25, 26		27

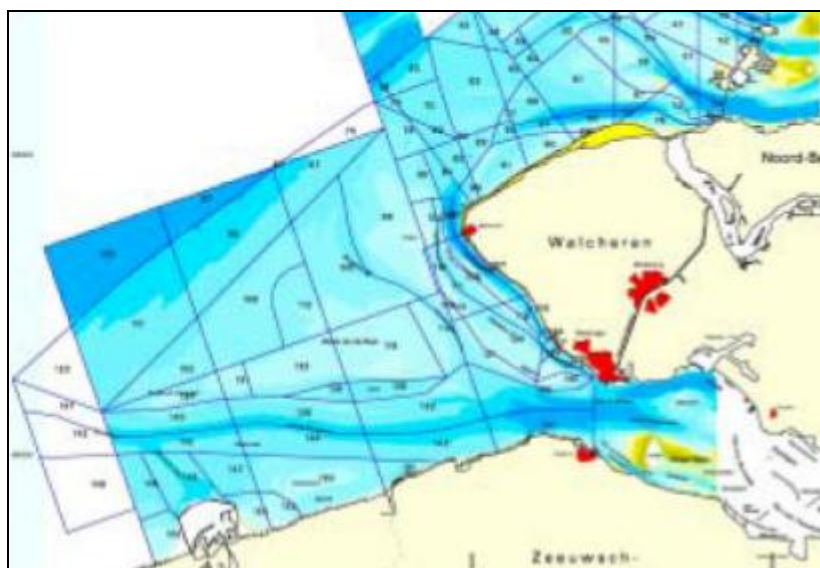


Figure A.3-11: Morphological division of the Western Scheldt mouth (Nederbragt and Liek, 2004).

Table A.3-3: Aggregation of the compartments in the Western Scheldt mouth (Nederbragt and Liek, 2004).

Balance Compartment	Name	Combined Compartments	Surface (km ²)
Belgian Part of the Mouth			
1	Zeebrugge west	148, 155	15.78
2	Pas van het Zand	146	13.00
3	Paardenmarkt/Appelzak	147, 150, 154, 153	45.10
4	Scheur/Wielingen (B)	139, 140, 144, 145	59.18
5	Spleet (B)	138	3.41
6	Vlakte van de Raan (B)	106, 113, 122, 125, 131, 134	93.68
7	Vooroever (B)	98, 110	82.74
Dutch Part of the Mouth			
8	Cadzand	151	4.46
9	Wielingen (NL)	132, 133, 141, 143	69.33
10	Spleet (NL)	136	6.57
11	Vlakte van de Raan (NL)	100, 114, 119	71.01
12	Vooroever (NL)	87	15.34
13	Oostgat noord	92, 94, 99	9.03
14	Walcheren	101, 107, 116, 124	6.83
15	Vlissingen	127, 128	2.29
16	Bankje van Zoutelande oost	102, 108, 117, 126	9.70
17	Bankje van Zoutelande west	103, 109, 118	9.60
18	Walvischstaart oost	120	12.24
19	Walvischstaart west	121	6.94
20	Nolleplaat noord	129, 130	3.06
21	Nolleplaat zuid	135	3.16
22	Rassen oost	104, 111, 112	9.59
23	Rassen west	88, 115, 156	42.62
24	Rassen noord	95	6.10

A.4 Sediment Transport

A.4.1 Sediment Transport Mechanisms

Depending on the grain size and the energy of the flow, sediment in an estuary may be transported in two different modes (Heathershaw, 1988):

- Bed-load in which grains roll or saltate along the seabed, directly related to the local instantaneous flow velocity.
- Suspended load in which grains are transported within the body of the fluid. The flow conditions upstream and in the past play a role as well because of the settling lag effect of the suspended sediment concentration.

In this study we only consider the transport of non-cohesive material.

Waves and currents influence the sediment motion. Elias et al. (2006) pointed out that especially in the ebb-tidal delta waves can be an important factor governing sand transports. Off course, these processes are also important in the basin on shallow areas where only small waves are needed to generate large sediment transports. As a first step, to reduce complexity, wave effects won't be considered. This study focusses mainly on the interaction between tide and bathymetry

In estuaries there is, apart from the general physical principles, another additional factor which influences the sediment transport. The interaction between the fresh water from the river and the salt water from the sea also determines the distribution and circulation of fine sediments within an estuary. In contrast to salt wedge estuaries (with little or no mixing) where accumulation of sediments occurs at the turbidity maximum, there is a net landward movement of sediments in partially and well mixed estuaries.

The influence of density differences on the water movement and water levels in the Western Scheldt is small since it is a partially to well-mixed estuary. Therefore this effect is ignored in most numerical models (Technische Scheldecommissie, 1984; Verlaan, 1998).

Non-Tidal Sediment Transport Mechanisms

In addition to the tidal forcing also non-tidal mechanisms such as estuarine circulation, wind and waves can contribute significantly to the transport in a tidal inlet (Elias et al., 2006).

As demonstrated for the Texel tidal inlet by Elias et al. (2006), waves can contribute to sand transports on the ebb-tidal delta in two different ways:

- directly via currents due to radiation stresses generated by wave breaking of obliquely incident waves and due to wave asymmetry
- indirectly by enhancing the bed-shear stresses and stirring up sediment, allowing more sediment into suspension to be transported by the tidal- and wind-driven flow.

Waves are larger on the ebb-tidal delta than in the more sheltered landward areas and therefore promotes spatial gradients in sediment concentration and sediment import into the basin. The importance of this effect depends not only on the local wave climate, but also on the ebb-tidal delta geometry. In case of Texel inlet this effect seems to enhance sediment import.

However, wave influences are an extensive subject when considered separately and are not included in this study. This research is limited to the tide-driven flow, which is probably the most important mechanism for sediment transport in the Western Scheldt.

A.4.2 Influence of Different Transport Formulations

Sand transport models are often based on semi-empirical transport formulae that relate sediment fluxes to physical properties such as velocity, depth and characteristic sediment grain sizes. Errors in these properties affect the accuracy of the sediment fluxes. Furthermore most of the formulae have been compared and fitted to a case-dependent data set (experimental or field data) which results in a restricted range of applicability.

Camenen and Larroudé (2003) investigated the limits of the Bijker, Bailard, Van Rijn, Dibajnia and Watanabe, and Ribberink formulae and their sensitivity to certain parameters in a coastal environment. With respect to the grain size, which plays an important role in estimating sediment flux (via roughness, settling velocity etc.), none of the five considered formulae gave satisfactory behaviour in their applications. To start with only the Van Rijn and Ribberink formulae take into account a critical value for the Shields parameter. The Bijker formula is not recommended for grain sizes over 1 mm due to its extreme sensitivity

to roughness. The Ribberink formula is less sensitive to roughness, but its behaviour in relation to grain size seems to be too insensitive since it takes into account the bed load only.

The error propagation from the input physical properties to the sediment fluxes has been analysed by Pinto et al. (2006) for four total load formulae (Ackers and White, Engelund and Hansen, van Rijn, and Karim and Kennedy) and one bed load formulation (van Rijn). They found that the current velocity and the sediment median grain size d_{50} control the errors in the total sediment transport formulations, whereas bed-load transport estimates are mainly affected by current velocity. The analysis of the d_{50} variation showed that the Engelund and Hansen, and the Karim and Kennedy formulae are less sensitive to sediment grain size than the other two.

The accuracy in the sediment flux evaluation is dominated by errors in the physical properties, rather than by the limitations of the formulae themselves. Although the van Rijn formula is often regarded as the most accurate formulation for situations without waves, and is the most commonly used, it emerges as the most sensitive to errors in the physical properties in the study of Pinto et al. (2006).

All this stresses the need for more and better field observations to specify the input physical properties, especially for the current velocity and the sediment median grain size. For both parameters Pinto et al. (2006) advise it is better to underestimate than overestimate their value when they are not known with precision.

The mentioned sediment transport formulae can be found in Appendix A.3.

A.4.3 Sediment Transport Formulae

A.4.3.1 Engelund and Hansen (1967)

$$q_s = 0.05 \frac{\bar{u}^5}{(s_d - 1)^2 g^{0.5} d_{50} C^3} \quad \text{Equation A.4-1}$$

where q_s = total load

\bar{u} = mean flow velocity

s_d = specific density = ρ_s/ρ

g = acceleration of gravity

d_{50} = particle diameter

C = Chézy coefficient

According to the authors, this formula can only be applied for when $d_{50} > 0.15$ mm and the geometric standard deviation of the sediment grain size is greater than 2. The Manning formula has to be used to calculate the bottom stress coefficient. This formula is frequently used in rivers and estuaries.

A.4.3.2 Bijker (1968)

$$q_{sb} = C_b d \sqrt{\frac{\mu_c \tau_c}{\rho}} \exp\left(-0.27 \frac{(\rho_s - \rho) g d}{\mu_c \tau_{cw}}\right),$$

$$q_{ss} = 1.83 q_{sb} \left(I_1 \ln \left[\frac{33h}{\delta_c} \right] + I_2 \right),$$

where

$$\mu_c = \left(\frac{f_{ct}}{f_c} \right)^{3/2},$$

$$\tau_{cw} = \left[1 + 0.5 \left(\xi_B \frac{U_w}{U_c} \right)^2 \right] \tau_{cf},$$

$$I_1 = \int_{\delta}^1 \left(\frac{1-y}{y} \right)^A dy,$$

$$I_2 = \int_{\delta}^1 \left(\frac{1-y}{y} \right)^A \ln y dy$$

Equation A.4-2

- where
- q_{sb} = sediment volume flux for bedload
 - q_{ss} = sediment volume flux for suspended-load
 - d_{50} = particle diameter
 - h = water depth
 - C_b = wave breaking parameter
 - μ_c = ripple parameter
 - τ_c = shear stress due to current only
 - τ_{cw} = shear stress due to wave-current interaction
 - ρ_s, ρ = sediment and water densities
 - I_1, I_2 = Einstein integrals (suspended load)
 - δ_c = $100d/h$ = dimensionless thickness of the bed load layer
 - μ_c = ripple parameter
 - f_{ct} = total friction coefficient due to current
 - f_c = skin friction coefficient due to current
 - C_b = breaking wave coefficient
 - = 2 if $H_w/h < 0.05$
 - = $2 + 3 (H_w/h - 0.05)$ if $0.05 < H_w/h < 0.4$
 - = 5 if $0.4 < H_w/h$

H_w	= wave height
ξ_B	= $\sqrt{(f_{wt}/f_{ct})}$ = parameter due to wave interaction
f_{wt}	= total friction coefficient due to waves
U_w	= peak value of the wave orbital velocity at the bottom
U_c	= mean current velocity
A	= $W_s/\kappa(\tau_{cw}/\rho)0.5$ = function determining the rate of suspension
K	= 0.41 = Von Karman constant
W_s	= settling velocity

This formula is derived from the Frijlink (1952) formula for a current only with modification of the bottom shear stress using a wave-current model.

A.4.3.3 Ackers and White (1973)

$$q_s = \frac{s_d k d_{35}}{d} \left(\frac{\bar{u}}{u_*} \right)^n \left(\frac{F_{gr} - A}{A} \right)^m,$$

Equation A.4-3

$$F_{gr} = \frac{u_*}{\sqrt{g d_{35} (s_d - 1)}} \left[\frac{\bar{u}}{\sqrt{32} \log(10d / d_{35})} \right]^{1-n}$$

where q_s	= total load
F_{gr}	= sediment mobility number
u^*	= stress velocity
A	= value of F_{gr} at nominal initial motion
k, m and n	= empirical coefficients
d	= flow depth
\bar{u}	= mean flow velocity
s_d	= specific density = ρ_s/ρ
g	= acceleration of gravity
d_{35}	= particle diameter

The values of A , k , m and n were obtained from experimental studies that showed how these parameters vary with the dimensionless particle size d_{gr}

$$d_{gr} = d_{35} \left[g (s_d - 1) / v^2 \right]^{1/3}$$

Equation A.4-4

where ν = kinematic viscosity of the fluid

if $d_{gr} > 60$ then $n = 0.00$, $m = 1.50$, $A = 0.17$, $k = 0.025$ and

if $1 < d_{gr} \leq 60$ then $n = 1.00 - 0.56 \log d_{gr}$, $m = (9.66/d_{gr}) + 1.34$, $A = (0.23/\sqrt{d_{gr}})$,
 $\log k = 2.86 \log d_{gr} - (\log d_{gr})^2 - 3.53$

This equation is applicable to sediment mixtures with $d_{gr} > 1$, i.e. d_{35} above about 0.04 mm.

The Manning formula has to be used to calculate the bottom stress coefficient.

This formulation gives a general sediment transport function to calculate sediment flux based on experiments with established sediment movement. It is mostly applied in river cases.

A.4.3.4 Bailard (1981)

$$q_s = q_{sb} + q_{ss} \propto \Omega$$

$$\Omega = 0.5 \rho f_{cw} |\vec{u}(t)|^3$$

Equation A.4-5

$$\vec{q}_s = \frac{0.5 f_{cw}}{g(s-1)} \left(\frac{\varepsilon_b}{\tan \phi} \langle |\vec{u}|^2 \vec{u} \rangle + \frac{\varepsilon_s}{W_s} \langle |\vec{u}|^3 \vec{u} \rangle \right)$$

where Ω = energy flux due to waves and currents

f_{cw} = friction coefficient due to wave-current interaction

= instantaneous velocity vector

U_c = current velocity averaged over the depth

$u_w(t)$ = instantaneous wave velocity

ε_b = bed load efficiency (=0.1)

ε_s = suspended load efficiency (=0.02)

Φ = friction angle of the sediment

$\langle \rangle$ = average over several periods of wave

ρ = water density

The estimation of the friction coefficient due to wave-current interaction is not specified by Bailard. The formula is derived from the Bagnold model.

A.4.3.5 Van Rijn (1984)

The total transport is computed as:

$$q_s = 0.053 \left[(s_d - 1)g \right]^{0.5} \frac{d_{50}^{1.5}}{d_*^{0.3}} T^{2.1} + F d c_a \bar{u},$$

$$F = \frac{\left[\frac{a}{d} \right]^Z - \left[\frac{a}{d} \right]^{1/2}}{\left[1 - \frac{a}{d} \right]^Z \left[1.2 - Z \right]}$$

Equation A.4-6

where q_s = total load
 d^* = $d_{50} ((s_d - 1)g/\nu)^{1/3}$ = dimensionless particle diameter
 T = $(u_*^2 - u_{*cr}^2) / u_{*cr}^2$ = transport stage parameter
 u^* = stress velocity
 u_{*cr} = critical stress velocity
 c_a = reference concentration
 a = reference level
 Z = suspension number
 d = flow depth
 \bar{u} = mean flow velocity
 s_d = specific density = ρ_s/ρ
 g = acceleration of gravity
 d_{50} = particle diameter

The first and second terms on the right hand side of the equation for q_s represent the bed and the suspended load transport, respectively. The formula can be applied for cases in which the sediment size varies between 0.2 and 2.0 mm.

A.4.3.6 Karim and Kennedy (1990)

$$q_s = 10^{-2.821 + 3.369 \log(X1) + 0.840 \log(X2)} \sqrt{(s_d - 1)g d_{50}^3},$$

$$X1 = \bar{u} / \sqrt{(s_d - 1)g d_{50}},$$

$$X2 = (u_* - u_{*c}) / \sqrt{(s_d - 1)g d_{50}}$$

Equation A.4-7

where q_s = total load

u^*	= stress velocity
u_c^*	= critical stress velocity
\bar{u}	= mean flow velocity
s_d	= specific density = ρ_s/ρ
g	= acceleration of gravity
d_{50}	= particle diameter

The Manning formula has to be used to calculate the bottom stress coefficient. The formula allows a direct computation of the total transport.

A.4.3.7 Dibajnia and Watanabe (1992)

$$\bar{q}_s = A_{dw} W_s d \frac{\bar{\Gamma}}{\Gamma} \Gamma^{B_{dw}} \quad \text{Equation A.4-8}$$

$$\bar{\Gamma} = \frac{T_{wc} \bar{u}_{wc} (\Omega_c^3 + \Omega_c'^3) + T_{wt} \bar{u}_{wt} (\Omega_t^3 + \Omega_t'^3)}{(u_{wc} + u_{wt}) T_w}$$

where A_{dw}	= 0.001 = calibration coefficient
B_{dw}	= 0.55 = calibration coefficient
T_w, T_{wc}, T_{wt}	= period and half-periods of wave taking into account the effect of a current
Ω_c, Ω_t	= amount of sand entrained and settled during the half period T_{wc} and T_{wt}
Ω_c', Ω_t'	= amount of suspended sand remaining from the positive and negative half-cycle
u_{wc}, u_{wt}	= quadratic velocity (wave + current) over each half-period

This formulation takes into account a possible quantity of sand still in suspension after each half-cycle, and hence moving in the other direction (= phase-lag).

A.4.3.8 Ribberink (1998)

$$q_{sb} = m_{rib} \sqrt{(s-1)gd^3} \times \left\langle \left(|\bar{\Psi}(t)| - \Psi_{cr} \right)^{n_{rib}} \frac{\bar{\Psi}(t)}{|\bar{\Psi}(t)|} \right\rangle$$

$$\bar{\Psi}(t) = 0.5 f_{cw} |u(t)| \bar{u}(t) / [(s-1)gd]$$

$$k_{st} = \max \left(k_s; d \left[1 + 6 \left(\langle |\Psi(t)| \rangle / \Psi_{cr} - 1 \right) \right] \right)$$

Equation A.4-9

- where
- ψ_t = time dependent shields parameter
 - \vec{u} = instantaneous velocity vector
 - U_c = current velocity averaged over the depth
 - $u_w(t)$ = instantaneous wave velocity
 - f_{cw} = friction coefficient due to wave-current interaction
 - ψ_{cr} = critical shields parameter
 - $\langle \rangle$ = average over several periods of wave
 - m_{Rib} = 11 = adjusted coefficient
 - n_{Rib} = 1.65 = adjusted coefficient
 - k_s = skin roughness height

This is a quasi steady model of bed load transport where the instantaneous solid flux is assumed to be proportional to a function of the difference between the actual time-dependent bed shear stress and the critical bed shear stress.

A.5 1D-Equations for the Tidal Motion in a Channel with a Variable Width

The cross-sectionally integrated, 1D-equations of motion for well-mixed, channelised flow in an intertidal embayment with intertidal flats may be expressed according to Speer and Aubrey (1985) as:

Momentum equation:

$$\underbrace{\frac{\partial u}{\partial t}}_{(A)} + \underbrace{u \frac{\partial u}{\partial x}}_{(B)} + \underbrace{g \frac{\partial \zeta}{\partial x}}_{(C)} + \underbrace{c_f \frac{u|u|}{h_0 + \zeta}}_{(D)} = 0 \quad \text{Equation A.5-1}$$

Continuity equation:

$$\underbrace{b \frac{\partial \zeta}{\partial t}}_{(E)} + \underbrace{\frac{\partial}{\partial x} \{b_c u (h_0 + \zeta)\}}_{(F)} = 0 \quad \text{Equation A.5-2}$$

where t = time
 x = distance to channel entrance
 $u(x,t)$ = cross-sectionally averaged flow velocity
 $\zeta(x,t)$ = water surface elevation relative to mean sea level
 h_0 = water depth below mean sea level
 g = acceleration due to gravity
 c_f = bed friction factor
 b = total embayment width (including flats)
 b_c = the channel width

A = the local inertia term
 B = the advective inertia term
 C = the slope term
 D = the bottom friction term
 E = the storage term
 H = the discharge gradient term

A.6 Model Description

A.6.1 Model Properties

The original model has been described by Kuijper et al. (2004). Additional information concerning the present model is also included in the Table below.

Table A.6-1: Model description of the original and present model.

Water movement	
program	DELFT3D-FLOW
version number	<i>Original model</i>
release date	<i>(calibration & validation):</i> Version 3.33; November 06, 2003 <i>Present model:</i> Version 3.54.10.00; May 05, 2006
changes in the source	-
bottom schematisation	Bathymetry corresponding with: original model: 2001 and 1972 present model: 1970, 1983 and 2002
grid	curvilinear $\Delta x = 60 \text{ m} - 900 \text{ m}$ $\Delta y = 50 \text{ m} - 1400 \text{ m}$
m_{\max}	$m_{\max} = 129$
n_{\max}	$n_{\max} = 239$
number of domains	1 single domain
number of layers (+ division) per domain	100%
model parameters (friction etc.)	<i>friction</i> : space-varying Manning roughness ($0.02 - 0.04 \text{ s/m}^{1/3}$) originating from the Scalwest schematisation <i>sediment</i> : sand, uniform $200 \mu\text{m}$
different model parameters	-
parameters varied in the study	-
boundary conditions: type, location, representation, details	<i>Original model</i> <i>(calibration & validation):</i> * open sea boundaries: astronomical forcing (25 tidal constituents); boundary signal: Riemann

	<p>invariant; boundaries originating from the Scalwest model</p> <p>* open river boundary: astronomical forcing (21 tidal constituents); boundary signal: discharges; boundary conditions originating from time series computed with the Scalwest model for the period 17/06/2000 to 05/07/2000 which were transformed into amplitudes and phases of the most important tidal constituents by means of tidal analysis to allow astronomical forcing.</p> <p><i>Present model:</i></p> <p>* open sea boundaries: harmonical forcing (13 tidal constituents); boundary signal: Riemann invariant</p> <p>* open river boundary: harmonical forcing (13 tidal constituents); boundary signal: discharges</p>
simulation time step	$\Delta t_{\text{sim}} = 1 \text{ minutes}$
output time step	$\Delta t_{\text{history}} = 10 \text{ minutes}$
calibration period	2000, 2001, 2002
calibration data	water levels, discharge measurements and velocity measurements
validation period	1972
validation data	water levels and discharge measurements

A.6.2 Bathymetry

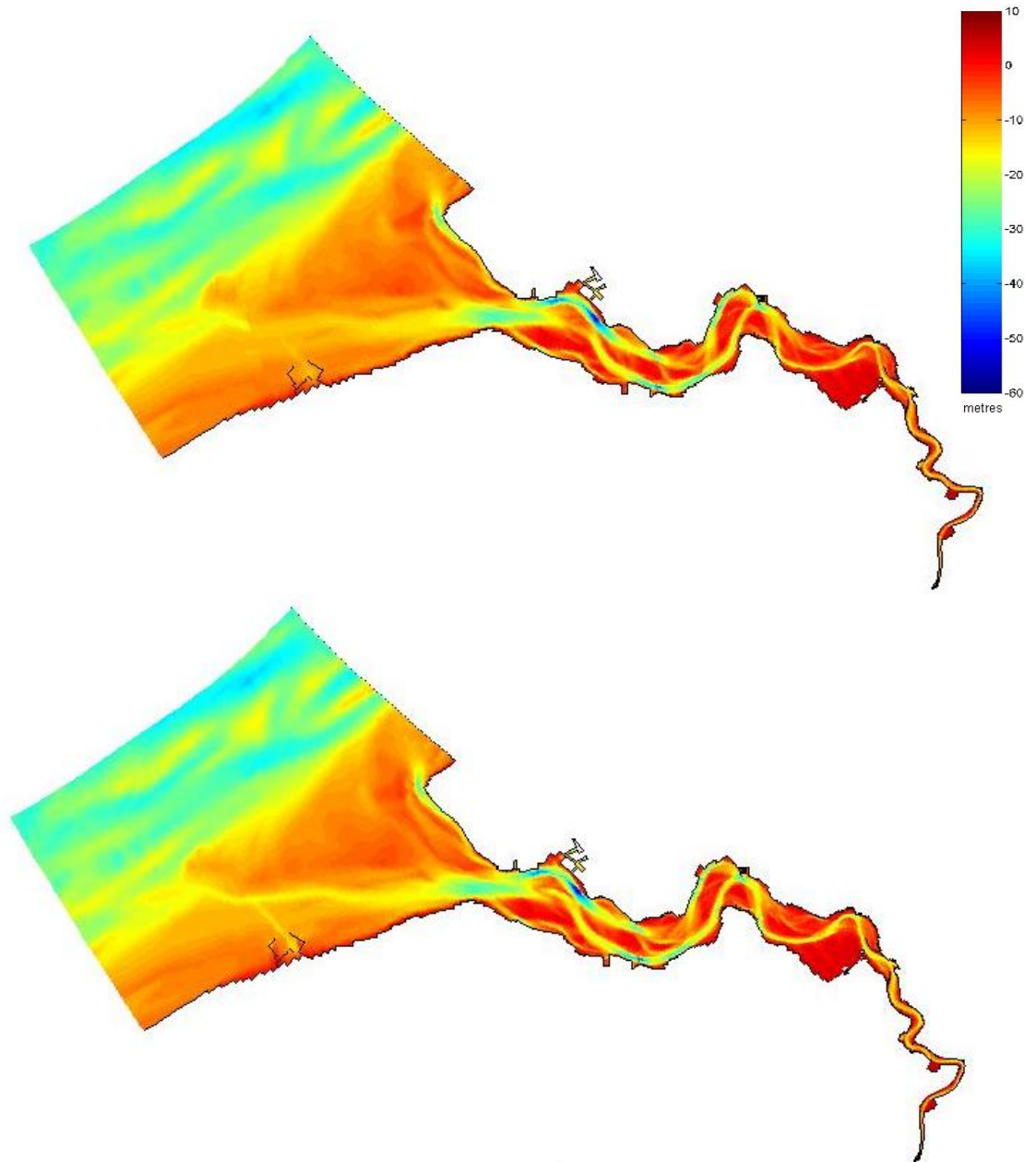


Figure A.6-1: Bathymetry 1970 (top) and 1983 (bottom).

A.6.3 Conventions in DELFT3D

In DELFT3D-FLOW a staggered grid is applied. This means that not all quantities are defined at the same location in the numerical grid. The Figure below shows the locations on the grid where the different quantities are measured in the model.

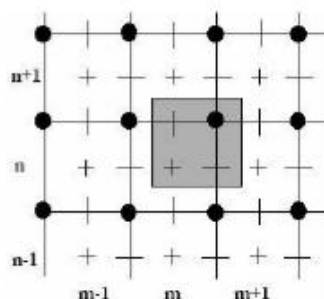


Figure A.6-2: The numerical grid of DELFT3D.

Table A.6-2: Legend for Figure A.6-2.

full lines	the numerical grid
grey area	items with the same grid co-ordinates (m, n)
+	water level, concentration of constituents, salinity, temperature
-	horizontal velocity component in x- or ξ -direction (also called u and m-direction)
	horizontal velocity component in y- or η -direction (also called v and n-direction)
●	depth below mean (still) water level (reference level)

The orientation of the curvi-linear grid applied in the Western Scheldt model is shown on Figure A.6-3.

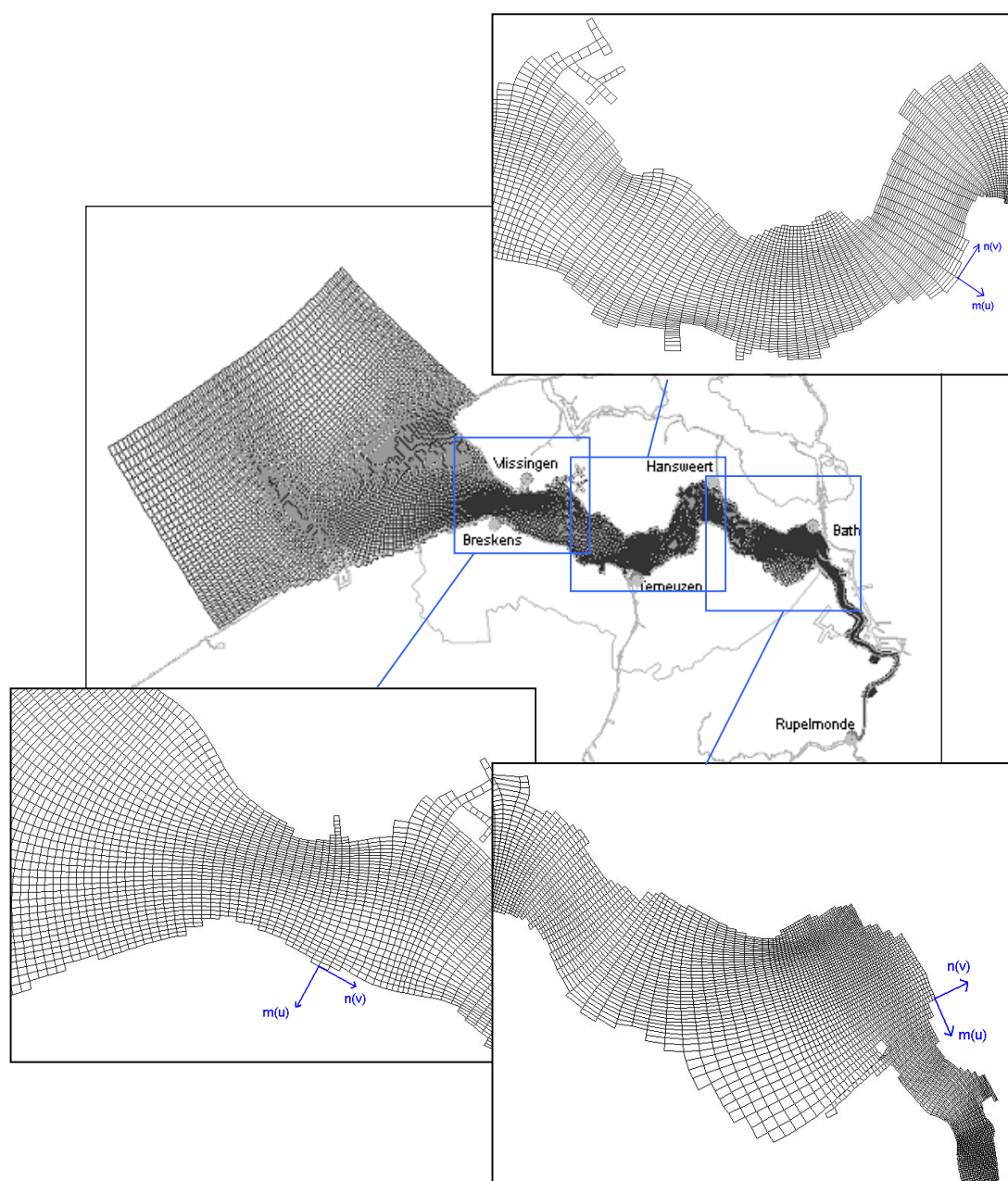


Figure A.6-3: Orientation of the curvilinear grid along the estuary.

A.7 Vertical Tidal Asymmetry

A.7.1 Applicability of the Model

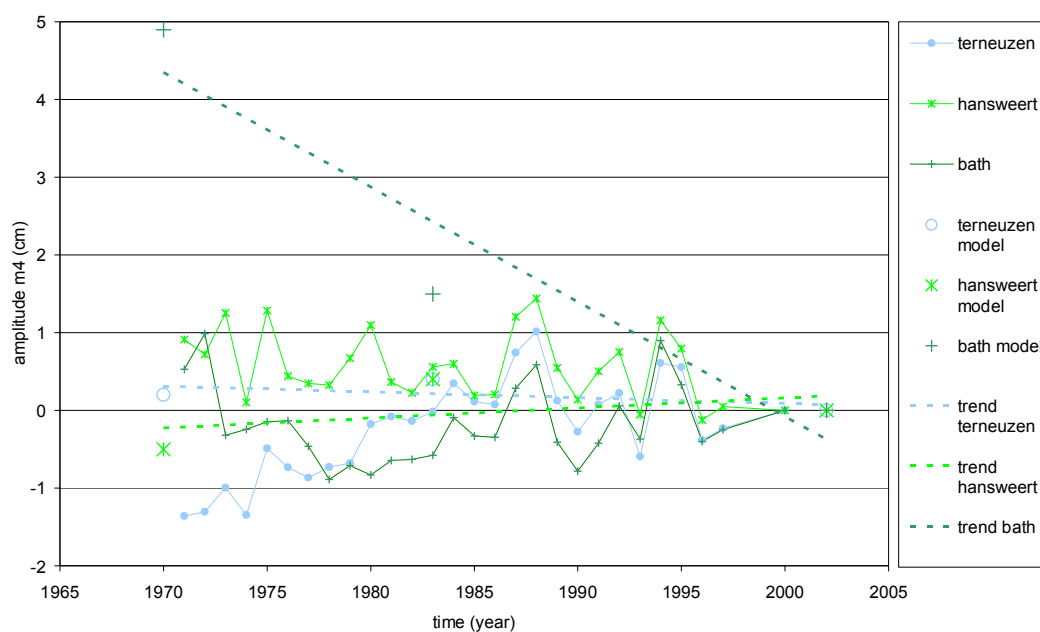


Figure A.7-1: Comparison of the amplitude of M_4 derived from the model (relative to 2002) with the measurements (relative to 2000) at the stations Terneuzen, Hansweert and Westkapelle.

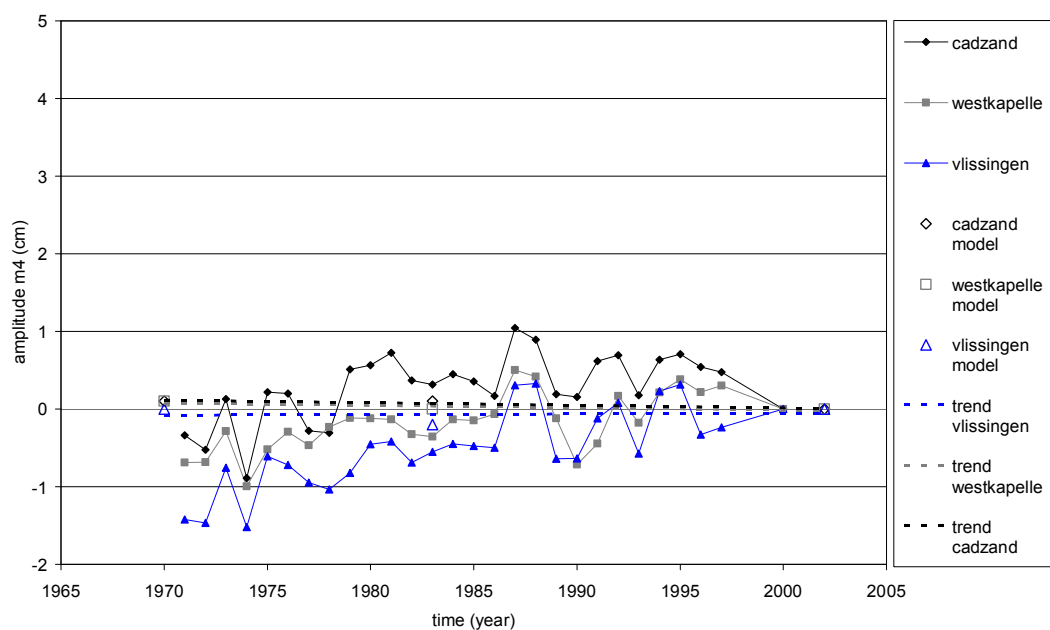


Figure A.7-2: Comparison of the amplitude of M_4 derived from the model (relative to 2002) with the measurements (relative to 2000) at the stations Westkapelle, Cadzand and Vlissingen.

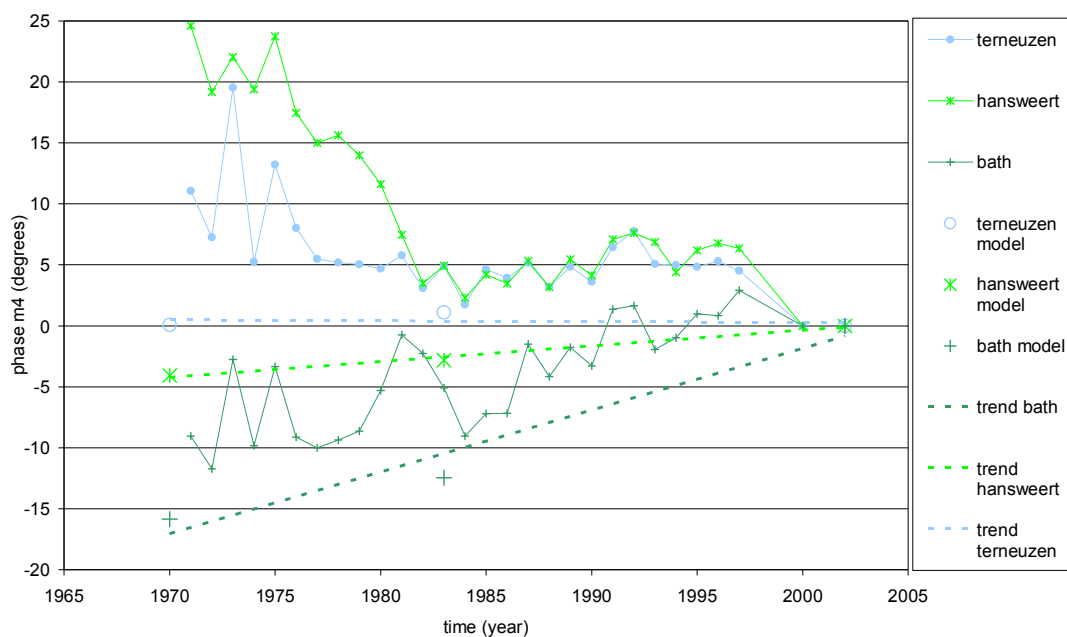


Figure A.7-3: Comparison of the phase of M_4 derived from the model (relative to 2002) with the measurements (relative to 2000) at the stations Terneuzen, Hansweert and Westkapelle.

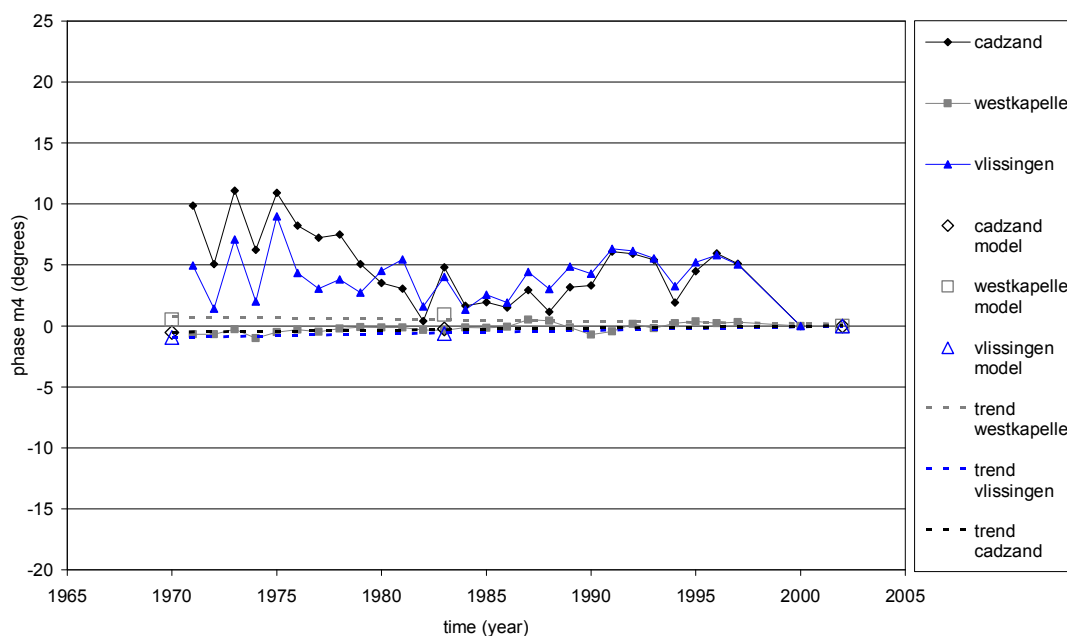


Figure A.7-4: Comparison of the phase of M_4 derived from the model (relative to 2002) with the measurements (relative to 2000) at the stations Westkapelle, Cadzand and Vlissingen.

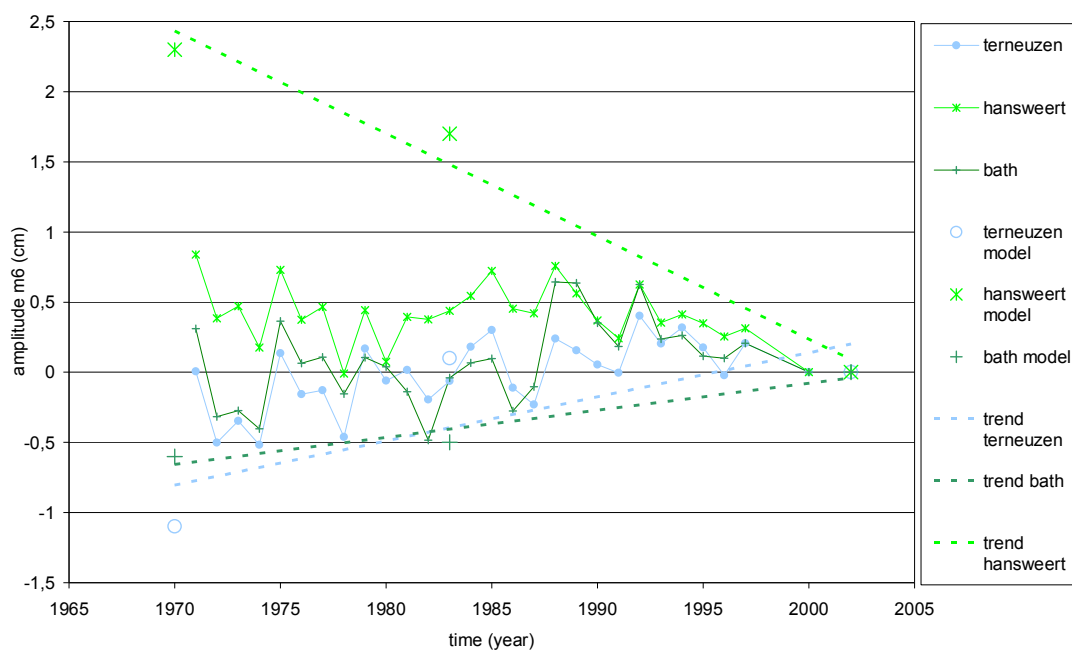


Figure A.7-5: Comparison of the amplitude of M_6 derived from the model (relative to 2002) with the measurements (relative to 2000) at the stations Terneuzen, Hansweert and Westkapelle.

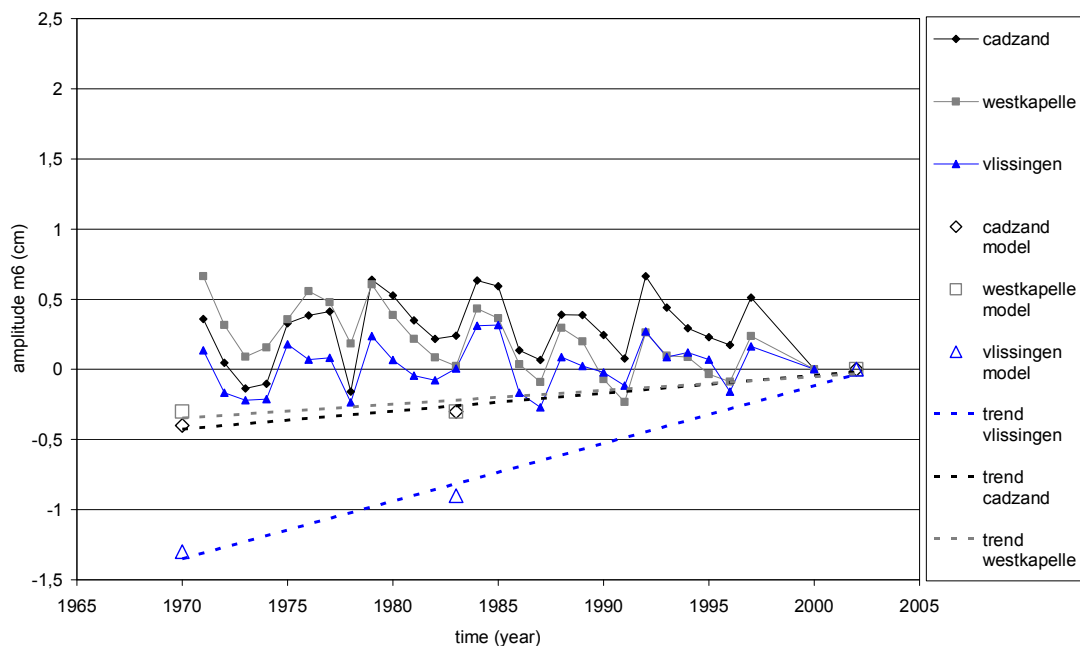


Figure A.7-6: Comparison of the amplitude of M_6 derived from the model (relative to 2002) with the measurements (relative to 2000) at the stations Westkapelle, Cadzand and Vlissingen.

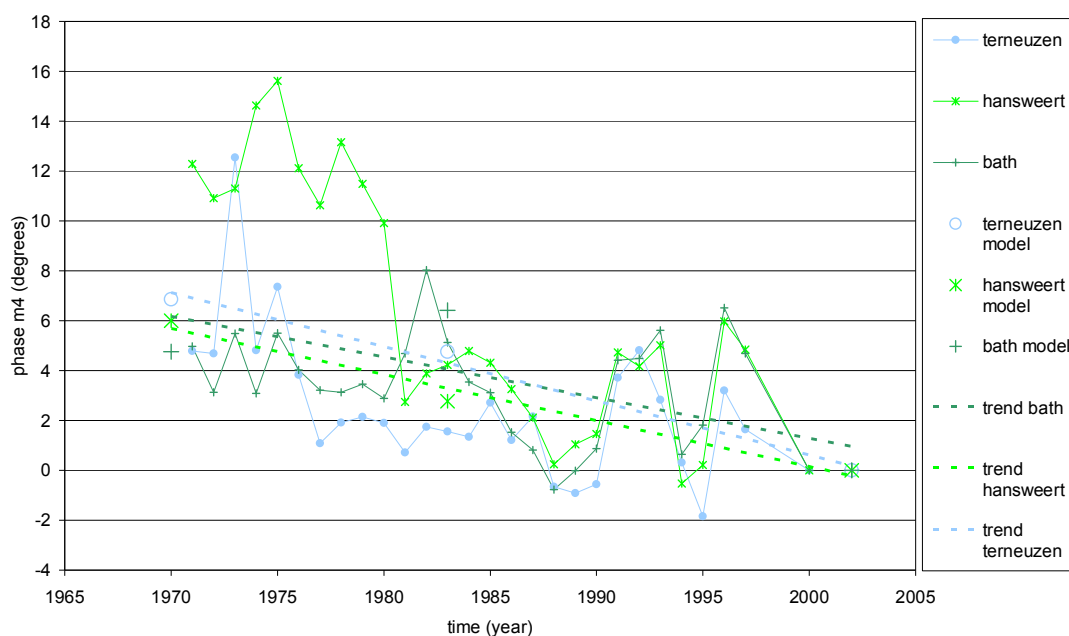


Figure A.7-7: Comparison of the phase of M_6 derived from the model (relative to 2002) with the measurements (relative to 2000) at the stations Terneuzen, Hansweert and Westkapelle.

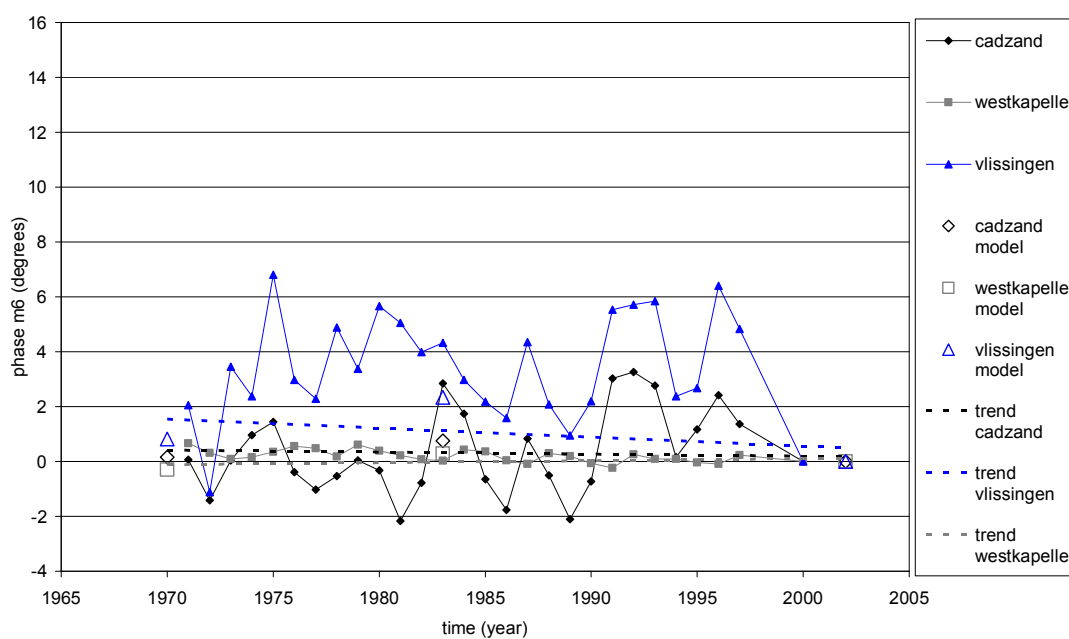


Figure A.7-8: Comparison of the phase of M_6 derived from the model (relative to 2002) with the measurements (relative to 2000) at the stations Westkapelle, Cadzand and Vlissingen.

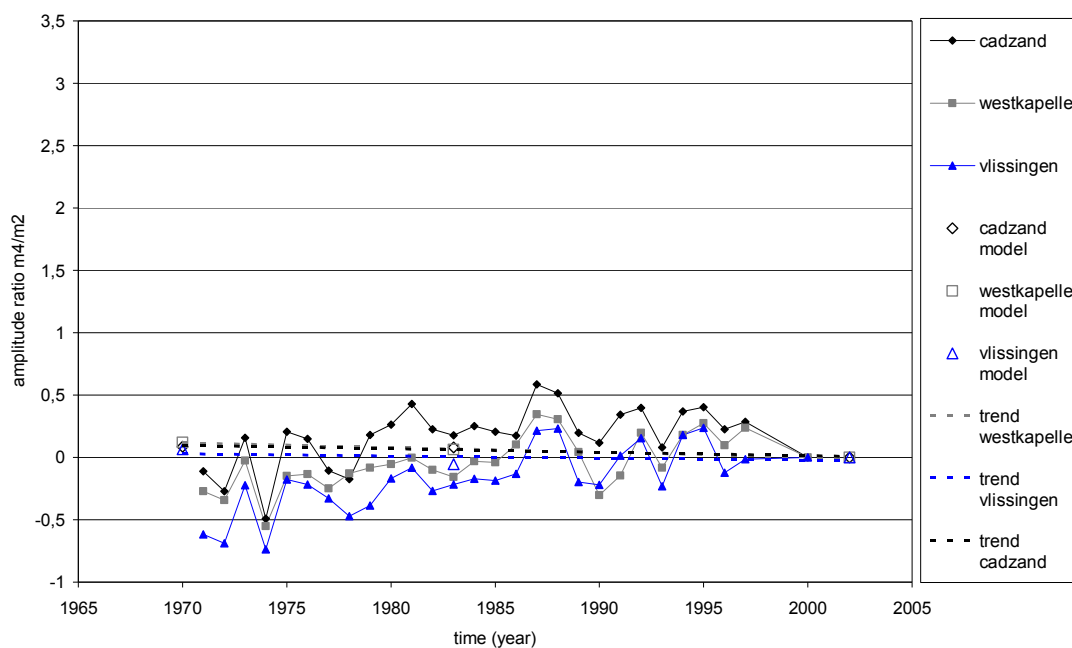


Figure A.7-9: Comparison of the amplitude ratio M_4/M_2 derived from the model (relative to 2002) with the measurements (relative to 2000) at the stations Westkapelle, Cadzand and Vlissingen.

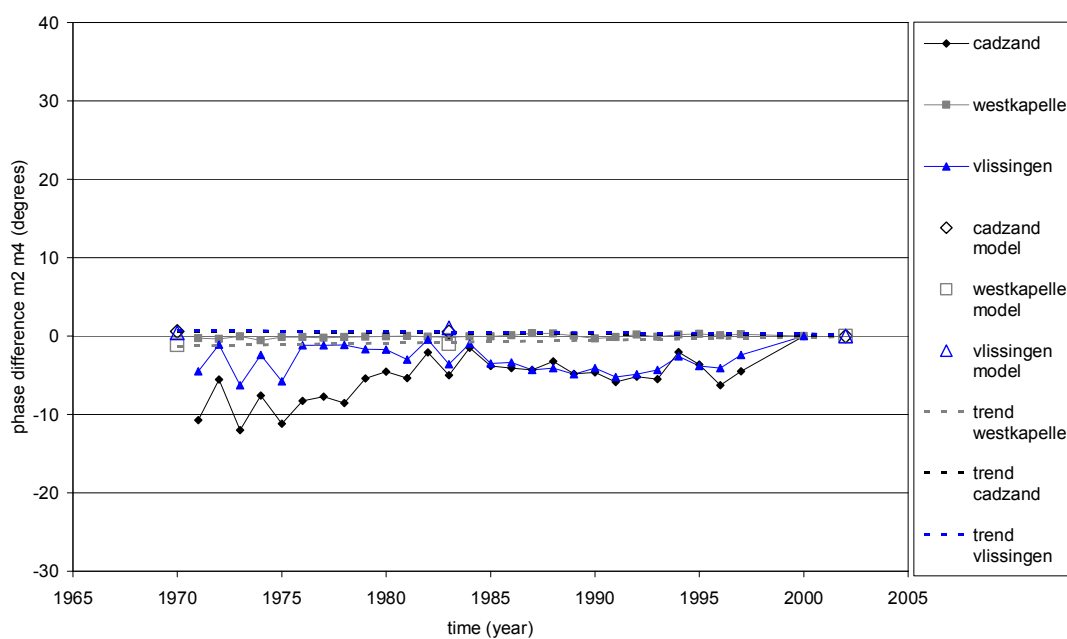


Figure A.7-10: Comparison of the phase difference $2\phi_2 - \phi_4$ derived from the model (relative to 2002) with the measurements (relative to 2000) at the stations Westkapelle, Cadzand and Vlissingen.

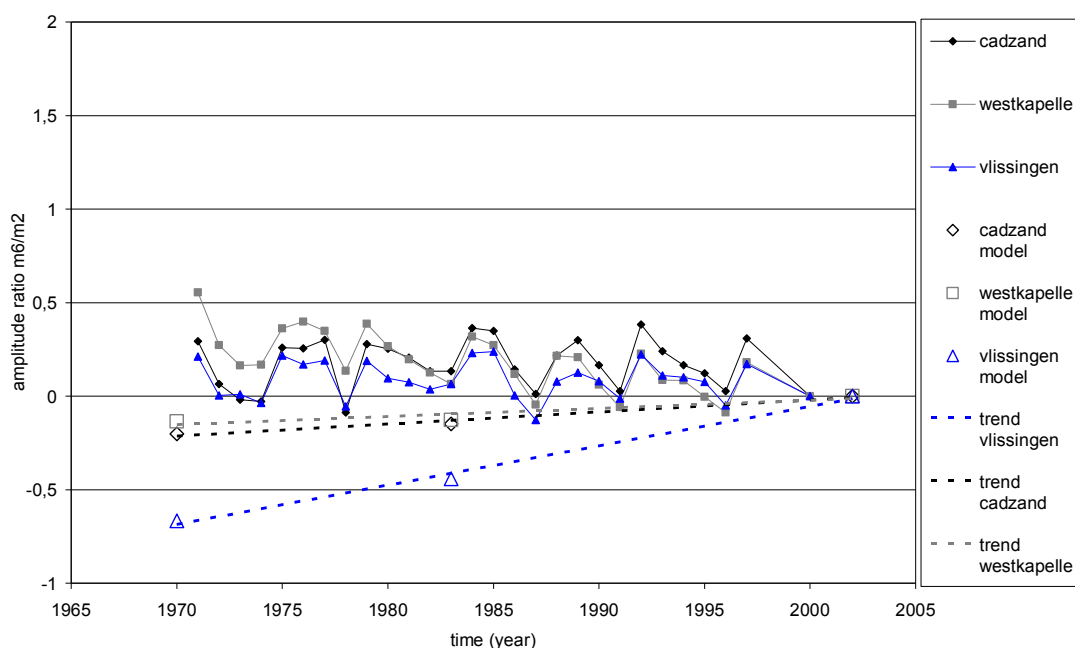


Figure A.7-11: Comparison of the amplitude ratio M_6/M_2 derived from the model (relative to 2002) with the measurements (relative to 2000) at the stations Westkapelle, Cadzand and Vlissingen.

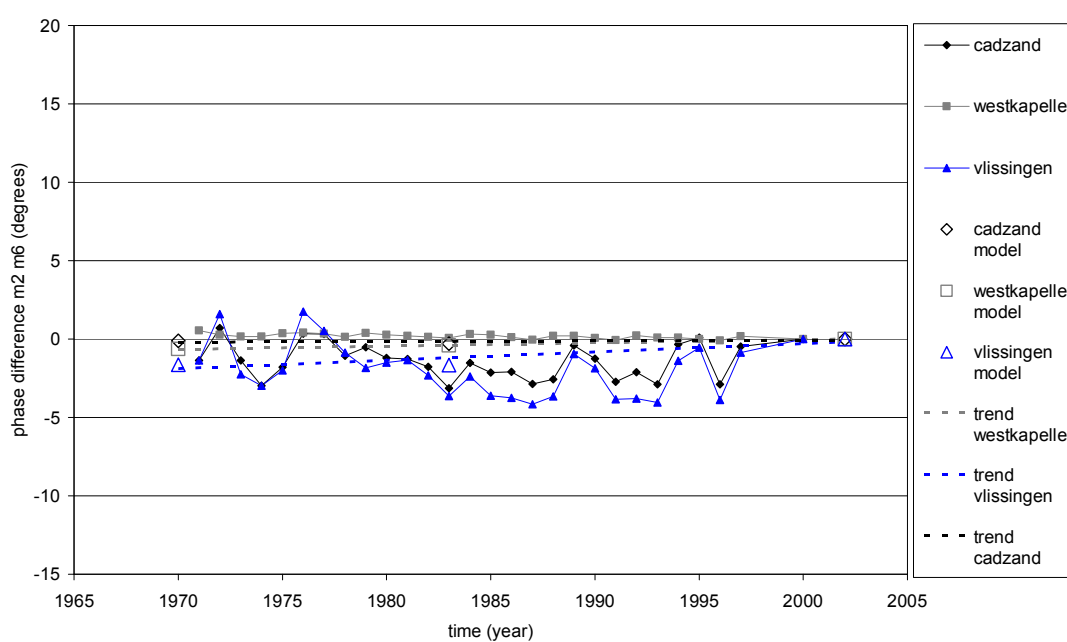


Figure A.7-12: Comparison of the phase difference $3\phi_2 - \phi_6$ derived from the model (relative to 2002) with the measurements (relative to 2000) at the stations Westkapelle, Cadzand and Vlissingen.

A.7.2 Amplitude and Phase of the Tidal Constituents at the Different Stations in the Model

Table A.7-1: Overview of the amplitudes (absolute value) and phases (relative to Cadzand) of the tidal components M_2 , M_4 and M_6 derived from the model and from field data.

	Cadzand		Westkapelle		Vlissingen		Terneuzen		Hansweert		Bath		
	amplitude (m)	phase (degrees)	amplitude (m)	phase (degrees)	amplitude (m)	phase (degrees)	amplitude (m)	phase (degrees)	amplitude (m)	phase (degrees)	amplitude (m)	phase (degrees)	
from model													
M ₂	1970	1,70	3	1,55	7	1,74	13	1,85	23	1,93	36	1,92	58
	1983	1,70	3	1,55	7	1,74	13	1,86	24	1,96	37	2,06	56
	2002	1,70	3	1,56	7	1,76	13	1,88	24	2,01	38	2,18	51
M ₄	1970	0,15	-12	0,17	-6	0,16	15	0,14	28	0,12	73	0,18	74
	1983	0,15	-12	0,17	-5	0,15	16	0,14	29	0,13	75	0,15	77
	2002	0,15	-12	0,17	-6	0,16	16	0,14	28	0,12	78	0,13	90
M ₆	1970	0,19	-78	0,18	-73	0,17	-40	0,19	12	0,24	63	0,20	108
	1983	0,20	-77	0,18	-73	0,18	-39	0,21	10	0,23	59	0,20	110
	2002	0,20	-78	0,18	-73	0,19	-41	0,20	5	0,22	57	0,21	104
from measurements													
M ₂	1971	1,65	49	1,52	54	1,72	59	1,85	69	1,95	80	1,97	95
	1983	1,68	50	1,53	53	1,75	59	1,87	68	1,99	79	2,10	93
	1997	1,67	50	1,54	54	1,74	60	1,86	70	1,97	81	2,07	93
M ₄	1971	0,11	97	0,13	102	0,12	119	0,11	140	0,12	185	0,13	163
	1983	0,12	92	0,13	95	0,13	118	0,12	134	0,12	165	0,12	167
	1997	0,12	92	0,14	97	0,13	119	0,12	134	0,11	166	0,12	175
M ₆	1971	0,10	72	0,10	86	0,09	106	0,09	155	0,10	212	0,13	256
	1983	0,10	75	0,09	81	0,09	108	0,09	152	0,10	204	0,12	256
	1997	0,10	74	0,09	81	0,09	109	0,09	152	0,10	204	0,12	256
amplitude = absolute value, phase = relative to Cadzand													

A.7.3 Evolution of the Vertical Tidal Asymmetry in Each Macro Cell

The complete description of macro cell 6 is included in the main text. Hereafter, the evolution in macro cells 1 to 5 is described in detail.

A.7.3.1 Macro cell I

Between 1970 and 2002 of the amplitude of M_2 increased slightly, the amplitude of M_4 decreased a bit and also the amplitude of M_6 increased. As a result M_4/M_2 decreases lightly and M_6/M_2 increases. The phase hardly changes in this period, although $3\varphi_2 - \varphi_6$ increases between 1983 and 2002. These evolutions occur in both the ebb and flood channel.

The ‘Drempel of Borsele’ (at the upstream end of the ebb channel) became deeper (Figure A.7-1). This is probably related to the dredging which took place in area R (Table A.7-2). The ebb channel in general became narrower but also deeper. Also the flood channel became slightly deeper. Furthermore it is visible that the shoal area in the middle of this cell evolves a lot over the years.

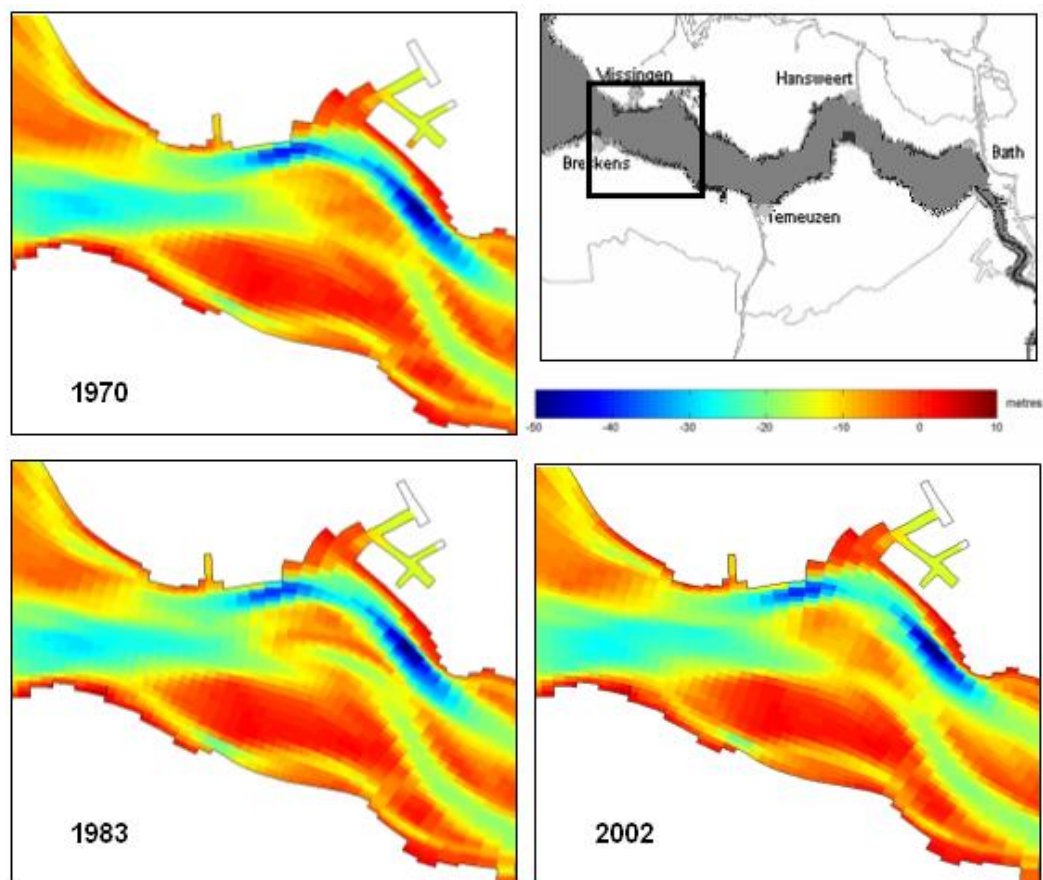
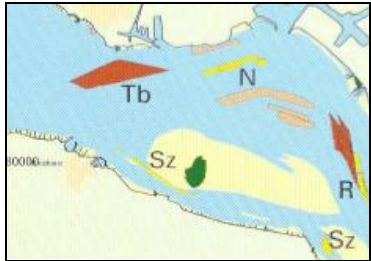


Figure A.7-13: Bathymetry in macro cell 1 for the years 1970, 1983 and 2002.

Table A.7-2: Overview of the dredging, dumping and sand mining activities in macro cell 1.

Activity	Amount (m ³ /year)	Period (years)	
Dredging in area R	1000000	1972 - 2000	
Dredging in area T	1500000	1999 - 2000	
Dumping in area N	500000	1981 - 1997	
	2000000	1997 - 2000	
Sand mining in area R	500000	1962 - 1972	
	1000000	1972 - 1985	
	200000	1985 - 2000	
Sand mining in area N	250000	1966 - 1994	
	325000	1969	

A.7.3.2 Macro cell 3

The amplitude of M_2 increases between 1983 and 2002 in macro cell 3, whereas M_4 increases slightly between 1970 and 1983 but decreases from 1983 to 2002. The amplitude of M_6 increases between 1970 and 2002, but decreases in the upstream part of the ebb channel from 1983 to 2002. φ_2 and φ_4 hardly change in the ebb and flood channels, whereas φ_6 decreases from 1970 to 2002.

This results in a slight increase of M_4/M_2 between 1970 and 1983 and a decrease from 1983 to 2002. The ratio M_6/M_2 also decreases from 1970 to 1983 but in the period 1983 – 2002 this ratio decreases only in the upstream part of the cell. The phase difference $2\varphi_2 - \varphi_4$ remains stable from 1970 to 2002, whereas $3\varphi_2 - \varphi_6$ increases during this period, with the highest change from 1983 to 2002.

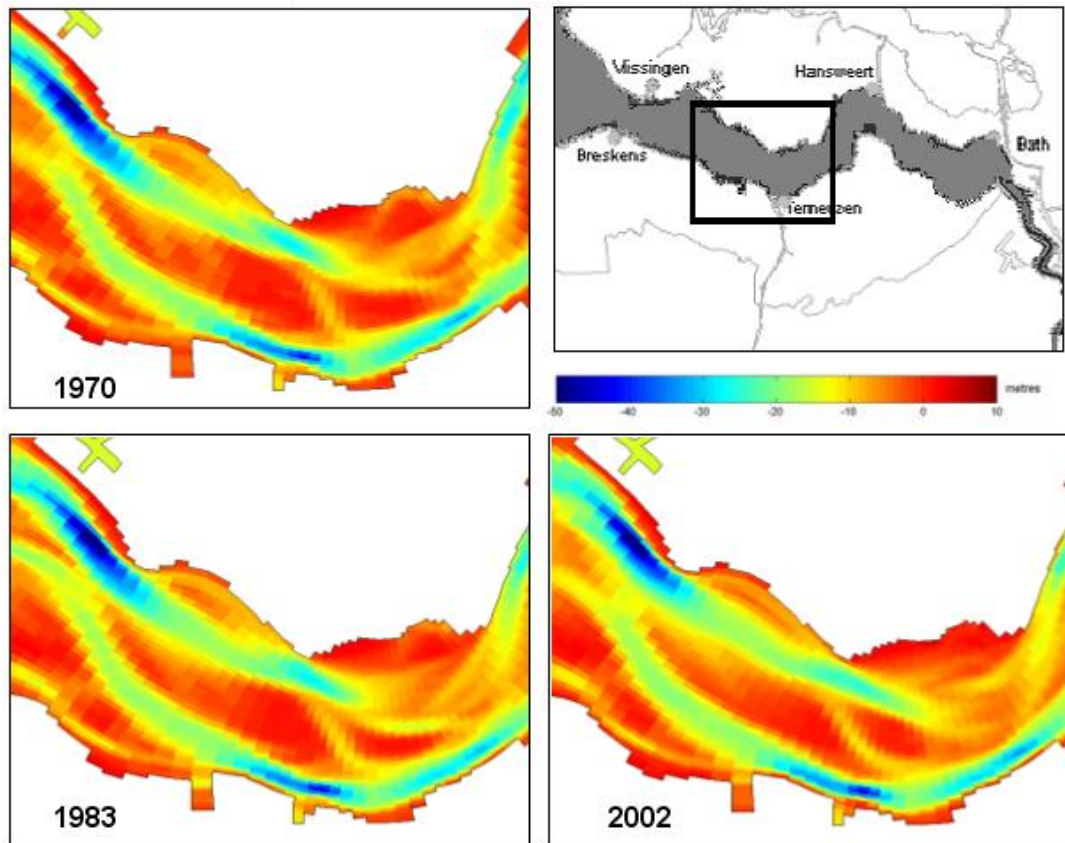


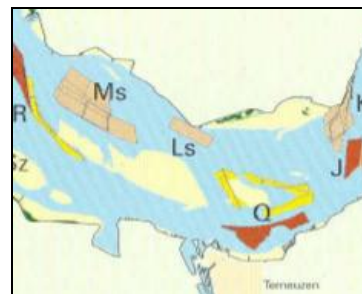
Figure A.7-14: Bathymetry in macro cell 3 for the years 1970, 1983 and 2002.

The most important change in the bathymetry of this area is the deepening of the ebb channel from 1970 to 2002 (Figure A.7-2). However upstream in this cell there occurs temporarily a bit shallower part in the ebb channel in 1983. The deepening after 1983 in this upstream part can be related to the dredging in area Q and probably gives rise to the local decrease of M_6 from 1983 to 2002 (Table A.7-3).

Sedimentation takes place in the downstream part of the flood channel from 1983 to 2002. This is probably related to the dumping in area M which has increased at the end of the 90's. Also the shoal area evolves significantly over the years. The sand mining in area Q can influence this evolution.

Table A.7-3: Overview of the dredging, dumping and sand mining activities in macro cell 3.

Activity	Amount (m ³ /year)	Period (years)
Dredging in area Q	500000	1993 - 2000
Dredging in area R	1000000	1972 - 2000
Dredging in area J	2000000	1969 - 1977
Dumping in area M	1000000	1973 - 1982
	500000	1982 - 1997
	1500000	1997 - 2000
Dumping in area L	3000000	1997 - 2000
Dumping in area K	1000000	1970 - 1987
	750000	1991 - 2000
Dumping in area J	1100000	1979 - 1981
Sand mining in area R	500000	1962 - 1972
	1000000	1972 - 1985
	200000	1985 - 2000
Sand mining in area Q	1000000	1964 - 1974
	300000	1974 - 1985
	600000	1985 - 1993
	200000	1993 - 2000



A.7.3.3 Macro cell 4

The amplitude of M_2 increases between 1970 and 2002, with the highest change between 1983 and 2002. The M_4 amplitude increases slightly between 1970 and 1983 but decreases from 1983 to 2002. The amplitude of M_6 decreases continuously between 1970 and 2002. φ_2 and φ_4 slightly increase in the ebb and flood channels from 1970 to 2002, whereas φ_6 decreases. φ_4 increases more in the ebb channel than in the flood channel.

This results in a slight increase of M_4/M_2 between 1970 and 1983 and a decrease from 1983 to 2002. M_6/M_2 decreases from 1970 to 2002. The phase difference $2\varphi_2 - \varphi_4$ decreases a bit from 1970 to 2002, whereas $3\varphi_2 - \varphi_6$ increases significantly during this period.

The most important change in the bathymetry is the deepening and widening of the flood channel, which is even more pronounced upstream (Figure A.7-3). The biggest difference occurs between 1983 and 2002. Dredging occurs in area O (in the upstream part of the flood channel) since 1975 and has been increased in the period 1993-2000 (Table A.7-4). In area J in the downstream part of this channel sand mining takes place. Also significant

sedimentation of the ebb channel is noticed. The different evolution in both channels can explain why ϕ_4 increases more in the ebb channel than in the flood channel.

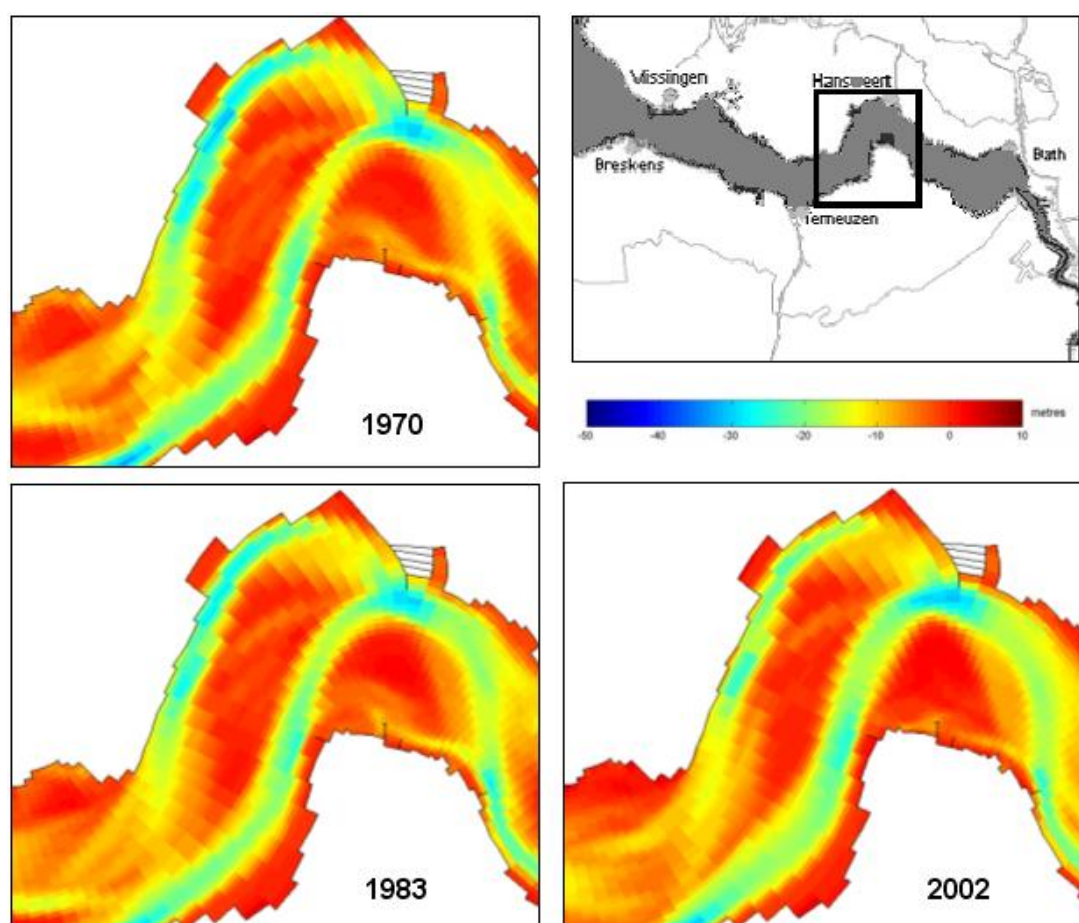
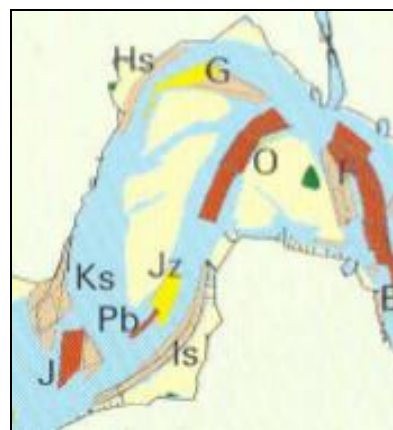


Figure A.7-15: Bathymetry in macro cell 4 for the years 1970, 1983 and 2002.

Table A.7-4: Overview of the dredging, dumping and sand mining activities in macro cell 4.

Activity	Amount (m ³ /year)	Period (years)
Dredging in area J	2000000	1969 - 1977
Dredging in area O	500000	1975 - 1993
	1500000	1993 - 2000
Dredging in area F	800000	1955 - 1970
	2500000	1970 - 2000
Dredging in area E	750000	1961 - 1968
	1200000	1973 - 1983
	600000	1983 - 2000
Dumping in area K	1000000	1970 - 1987
	750000	1991 - 2000
Dumping in area J	1100000	1979 - 1981
Dumping in area I	1500000	1969 - 1985
	2500000	1985 - 2000
Dumping in area H	2000000	1997 - 2000
Dumping in area G	900000	1979
Dumping in area F	300000	1981 - 2000
Sand mining in area J	500000	1960 - 1962
	500000	1966 - 1968
	800000	1998 - 2000
Sand mining in area G	400000	1961 - 1966
	400000	1974 - 1990



A.7.3.4 Macro cell 5

The amplitude of M_2 increases significantly between 1970 and 2002. The M_4 amplitude increases slightly in the flood channel whereas it decreases significantly in the ebb channel. The amplitude of M_6 decreases between 1970 and 2002 in both channels, although the decrease is larger in the flood channel. The phases don't change significantly in the flood channel in the period 1970-2002, whereas in the ebb channel both φ_2 and φ_6 decrease slightly, and φ_4 increases a lot.

This results in a significant decrease of M_4/M_2 and M_6/M_2 in the ebb channel. The trend for M_4/M_2 in the flood channel is less clear, a slight decrease is noticed. The ratio M_6/M_2 also decreases significantly in this part. The phase difference $2\varphi_2 - \varphi_4$ decreases heavily from 1970

to 2002 in the ebb channel. $3\phi_2 - \phi_6$ increases in the most western part of macro cell 5 but decreases in the eastern part.

In the downstream part of macro cell 5 the ebb channel deepens from 1970 to 1983, but becomes shallower again in 2002 (Figure A.7-4). This is possibly due to the fact that the amount of dredging in area E decreases after 1983 (Table A.7-5). The flood channel is shallower in 1983 than in 1970, but becomes deeper again in 2002. The amount of sand mining in area D is since 1984 the double of that in the period before. The dumping in the same area has decreased significantly since 1977.

In the upstream part deepening and widening of the ebb channel occurs. This is related to the high amounts of dredging in area B. The flood channel in this part is deepening from 1970 to 1983, but becomes shallower in 2002 than it was in 1970.

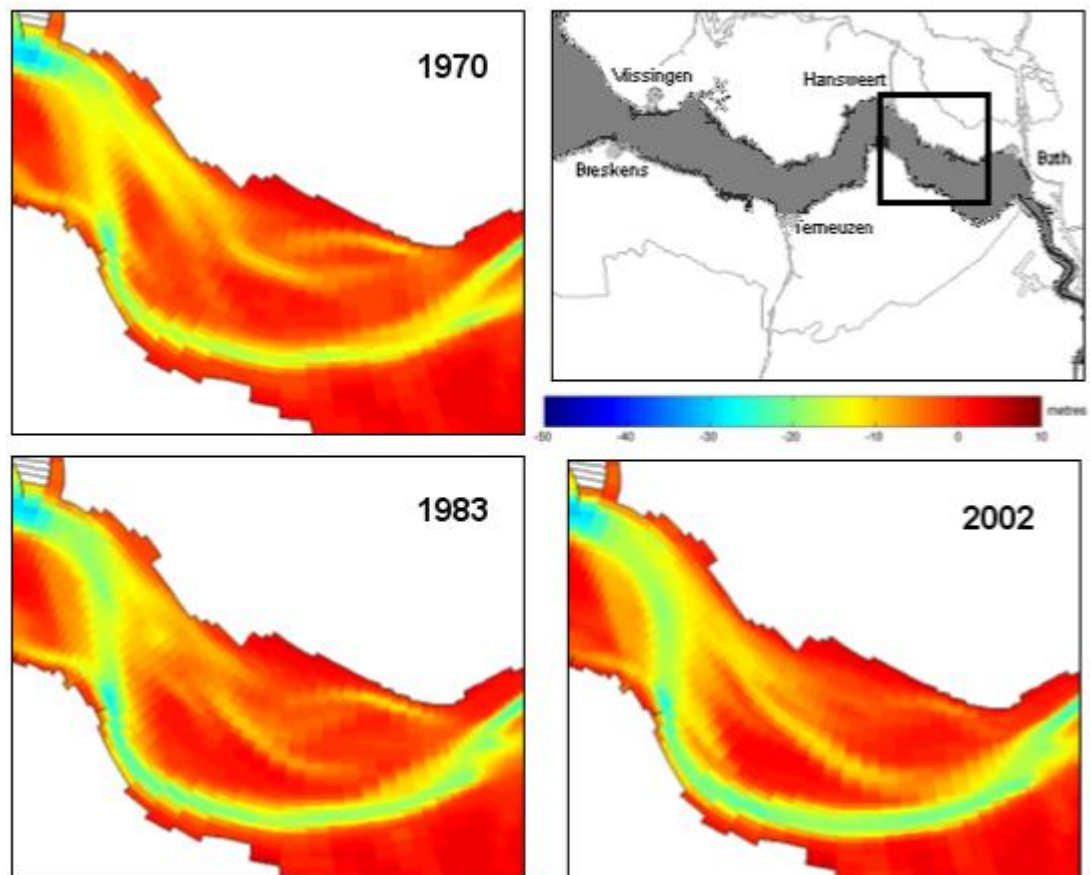


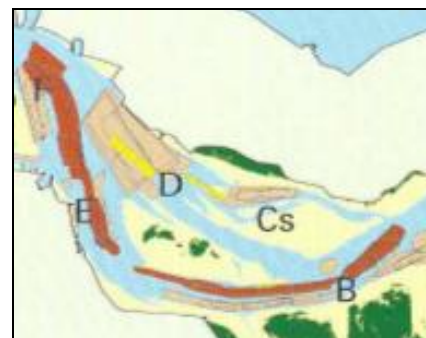
Figure A.7-16: Bathymetry in macro cell 5 for the years 1970, 1983 and 2002.

The significant deepening of the ebb channel from 1970-2000 and the sedimentation of the flood channel can explain why the amplitude of M_4 increases slightly in the flood channel but decreases significantly in the ebb channel.

The bigger changes in the ebb channel can be related to the significant increase of φ_4 in the ebb channel. The different evolution of the western and eastern part of this cell can be brought in relation with the evolution of the phase difference $3\varphi_2 - \varphi_6$ which increases in the most western part of macro cell 5 but decreases in the eastern part.

Table A.7-5: Overview of the dredging, dumping and sand mining activities in macro cell 5.

Activity	Amount (m ³ /year)	Period (years)
Dredging in area F	800000	1955 - 1970
	2500000	1970 - 2000
Dredging in area E	750000	1961 - 1968
	1200000	1973 - 1983
	600000	1983 - 2000
Dredging in area B	1000000	1955 - 1969
	2500000	1969 - 2000
Dumping in area D	1200000	1955 - 1970
	2500000	1970 - 1977
	1000000	1977 - 2000
Dumping in area F	300000	1981 - 2000
Dumping in area C	200000	1975 - 1983
	400000	1989 - 1997
Dumping in area B	2200000	1955 - 1973
	4500000	1973 - 1991
	2000000	1991 - 1997
Sand mining in area D	400000	1962 - 1968
	400000	1972 - 1978
	800000	1984 - 2000



A.7.3.5 Macro cell 6 and 7

The amplitude of M_2 increases significantly in both channels between 1970 and 2002 whereas the amplitude of M_4 decreases significantly. The biggest change occurs in the period 1970 to 1983. The amplitude of M_6 increases slightly in the ebb channel, but hardly changes in the flood channel. φ_2 decreases and φ_4 increases heavily in both channels from 1970 to 2002. φ_6 decreases as well, but changes less than φ_4 .

This results in a significant decrease of M_4/M_2 , M_6/M_2 , $2\phi_2-\phi_4$ and $3\phi_2-\phi_6$ in this macro cell. The decrease of the amplitude differences is more pronounced in the period 1970-1983, whereas for the phase differences the largest change occurs in the period 1983-2002.

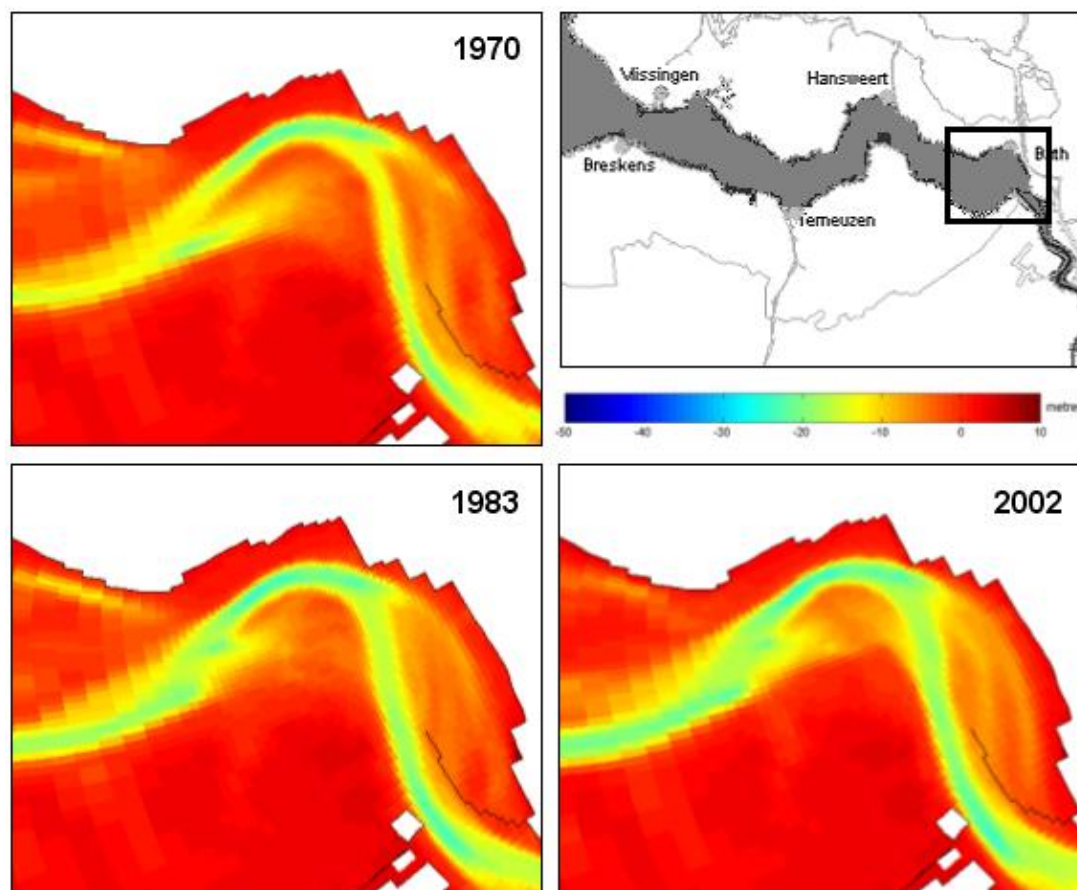


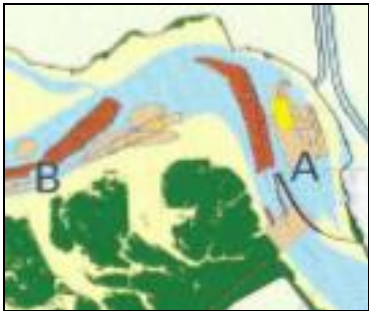
Figure A.7-17: Bathymetry in macro cell 6 and 7 for the years 1970, 1983 and 2002.

Both the ebb and flood channel became deeper from 1970 to 2002 (Figure A.7-5). It's also clearly visible that the ebb channel became wider during the years. This is due to the high amounts of dredging which took place in areas A and B in the ebb channel (Table A.7-6). Further, steepening and a northwards movement of the southern border of the flood channel is noticed. This is due to the dumping of material in area B. High amounts of material have been dumped in area B until 1991, from then the amount has been halved. As a result the flood channel becomes narrower but also somewhat deeper. In the period 1970-1983 sedimentation also took place at the landward end of the flood channel.

Deepening of both channels gave rise to an increase of the M_2 amplitude and a decrease of the amplitude of M_4 . Deepening of the ebb channel through the entire macro cell has

occurred from 1970 to 1983. This explains why the biggest change is noticed in the period 1970-1983.

Table A.7-6: Overview of the dredging, dumping and sand mining activities in macro cell 6.

Activity	Amount (m ³ /year)	Period (years)	
Dredging in area B	1000000	1955 – 1969	
	2500000	1969 – 2000	
Dredging in area A	2300000	1955 – 1985	
	3200000	1985 – 1989	
	1500000	1989 – 2000	
Dumping in area B	2200000	1955 – 1973	
	4500000	1973 – 1991	
	2000000	1991 – 1997	
Dumping in area A	800000	1955 – 1971	
	200000	1971 – 1983	
Sand mining in area A	800000	1964 – 1970	
	100000	1972 – 1976	
	300000	1980 – 1986	

A.7.4 Depth Differences Between the Different Bathymetries

In this section the depth on all the figures is according to the depth scale in Figure A.7-6. The difference between the years 2002 & 1983, 1983 & 1970 and 2002 & 1970 are presented.

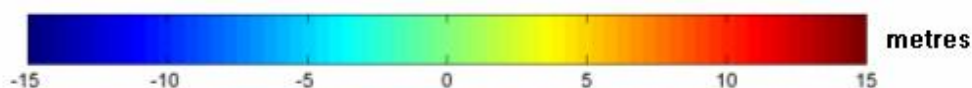


Figure A.7-18: Depth scale.

A.7.4.1 Macro cell I

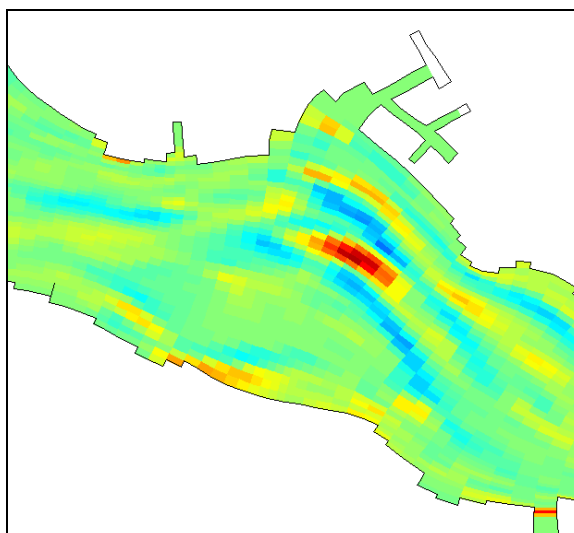


Figure A.7-19: Depth differences between the bathymetry of 2002 and 1983 in macro cell I.

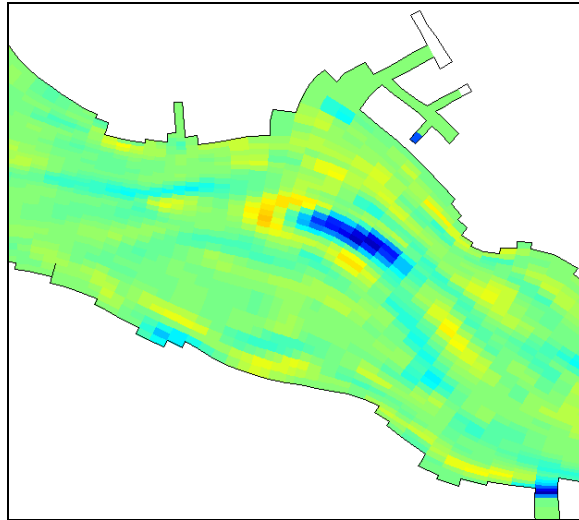


Figure A.7-20: Depth differences between the bathymetry of 1983 and 1970 in macro cell 1.

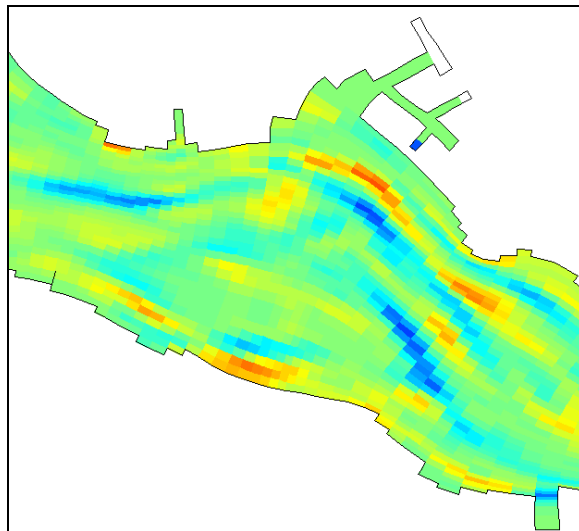


Figure A.7-21: Depth differences between the bathymetry of 2002 and 1970 in macro cell 1.

A.7.4.2 Macro cell 3

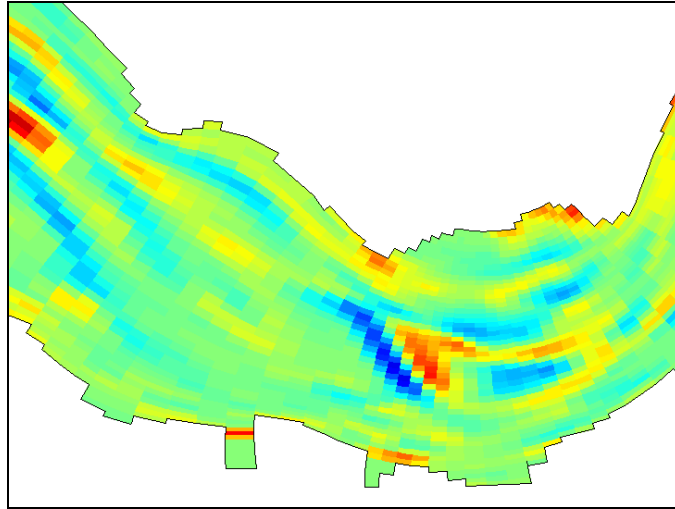


Figure A.7-22: Depth differences between the bathymetry of 2002 and 1983 in macro cell 3.

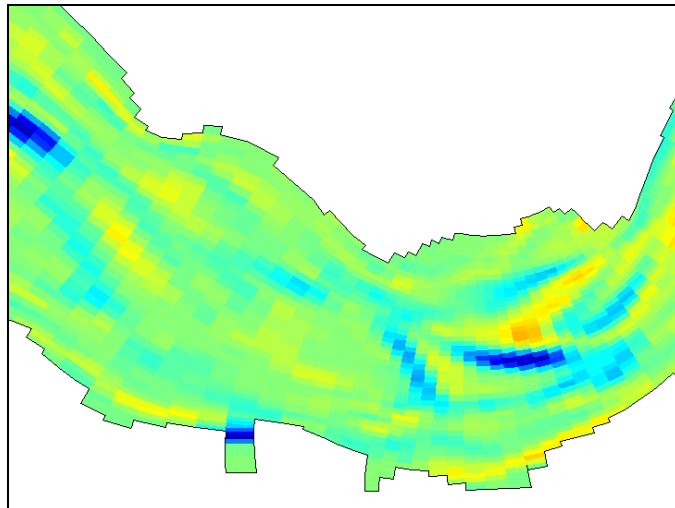


Figure A.7-23: Depth differences between the bathymetry of 1983 and 1970 in macro cell 3.

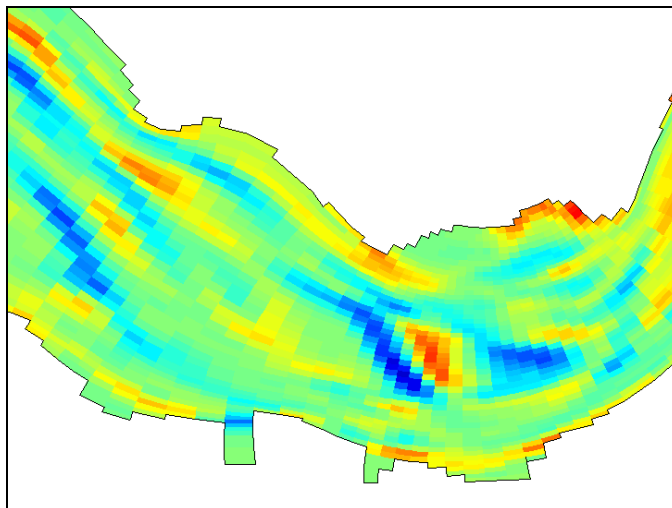


Figure A.7-24: Depth differences between the bathymetry of 2002 and 1970 in macro cell 3.

A.7.4.3 Macro cell 4

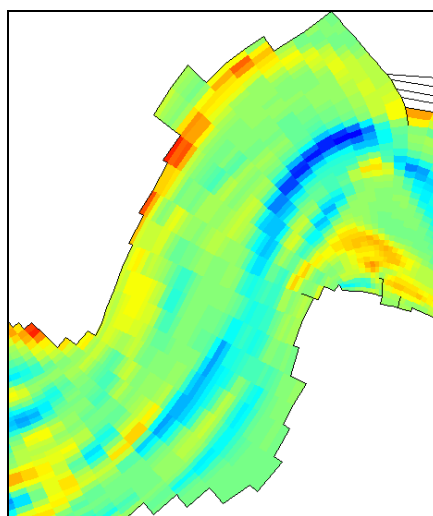


Figure A.7-25: Depth differences between the bathymetry of 2002 and 1983 in macro cell 4.

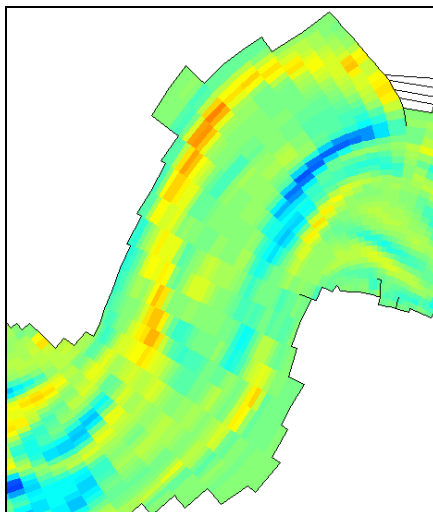


Figure A.7-26: Depth differences between the bathymetry of 1983 and 1970 in macro cell 4.

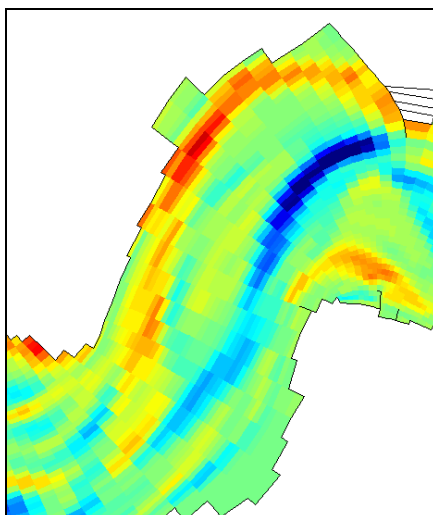


Figure A.7-27: Depth differences between the bathymetry of 2002 and 1970 in macro cell 4.

A.7.4.4 Macro cell 5

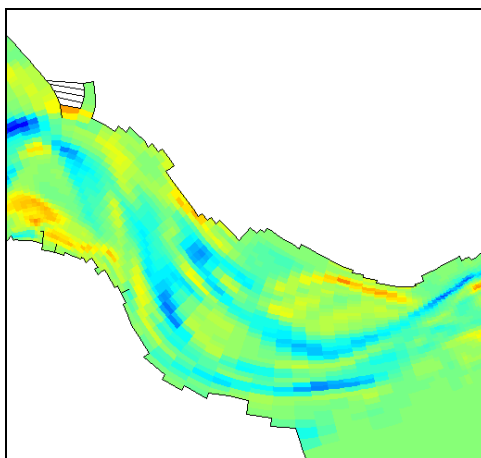


Figure A.7-28: Depth differences between the bathymetry of 2002 and 1983 in macro cell 5.

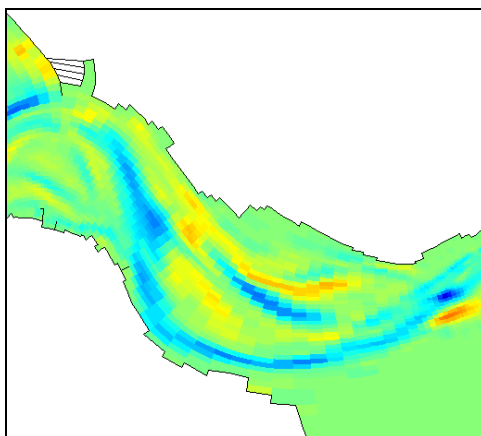


Figure A.7-29: Depth differences between the bathymetry of 1983 and 1970 in macro cell 5.

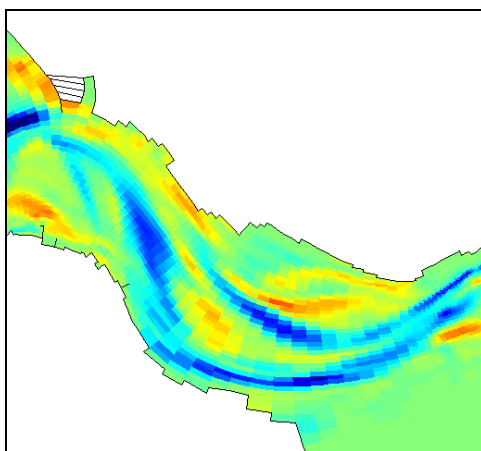


Figure A.7-30: Depth differences between the bathymetry of 2002 and 1970 in macro cell 5.

A.7.4.5 Macro cell 6 and 7

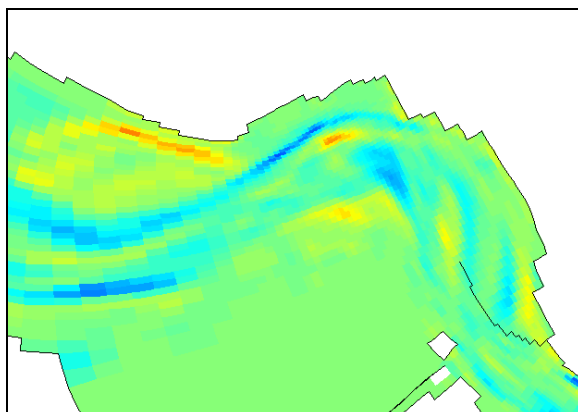


Figure A.7-31: Depth differences between the bathymetry of 2002 and 1983 in macro cell 6 and 7.

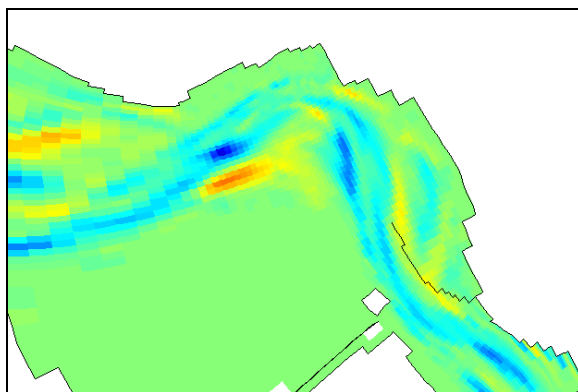


Figure A.7-32: Depth differences between the bathymetry of 1983 and 1970 in macro cell 6 and 7.

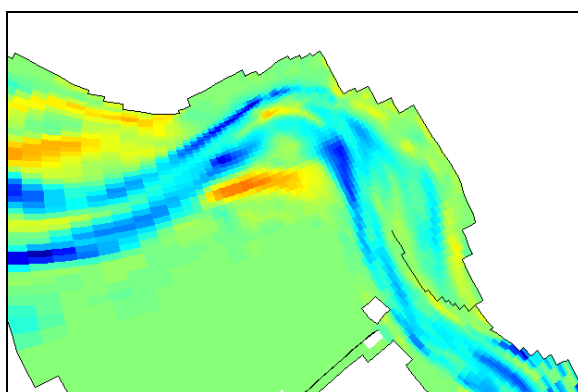


Figure A.7-33: Depth differences between the bathymetry of 2002 and 1970 in macro cell 6 and 7.

A.7.5 Cross-sections of the Bathymetry in Each Macro Cell

A.7.5.1 Locations of the Cross-sections

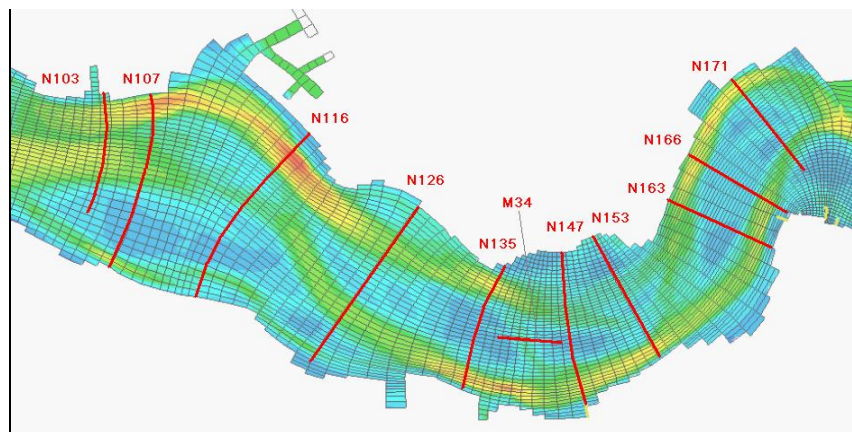


Figure A.7-34: Location of the cross-sections in the western part of the Western Scheldt.

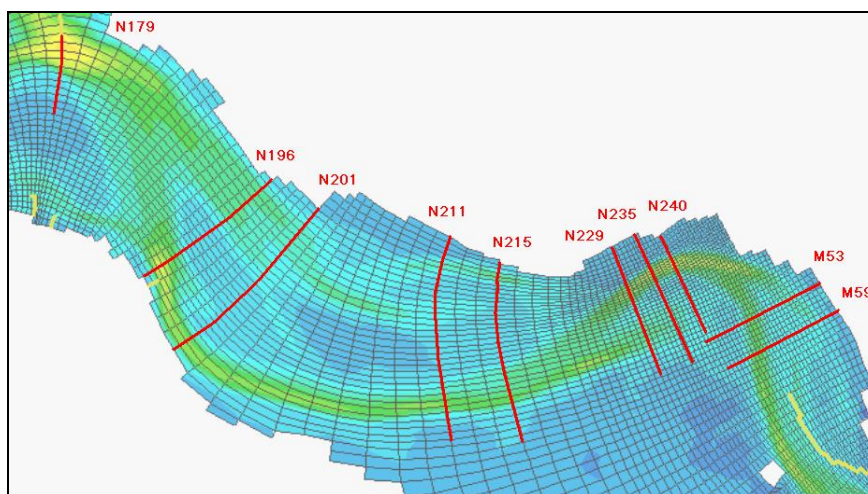


Figure A.7-35: Location of the cross-sections in the eastern part of the Western Scheldt.

A.7.5.2 Cross-sections

All the cross-sections in this section are according to the legend below.

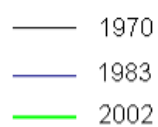


Figure A.7-36: Legend for the cross-sections.

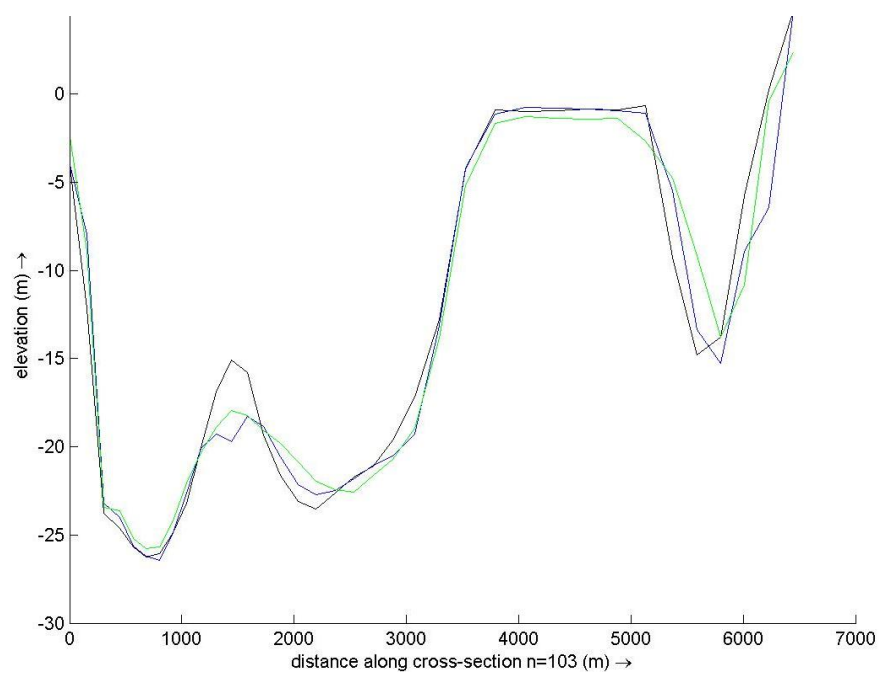


Figure A.7-37: Cross-sections of the bathymetry at location N103 for the years 1970, 1983 and 2002.

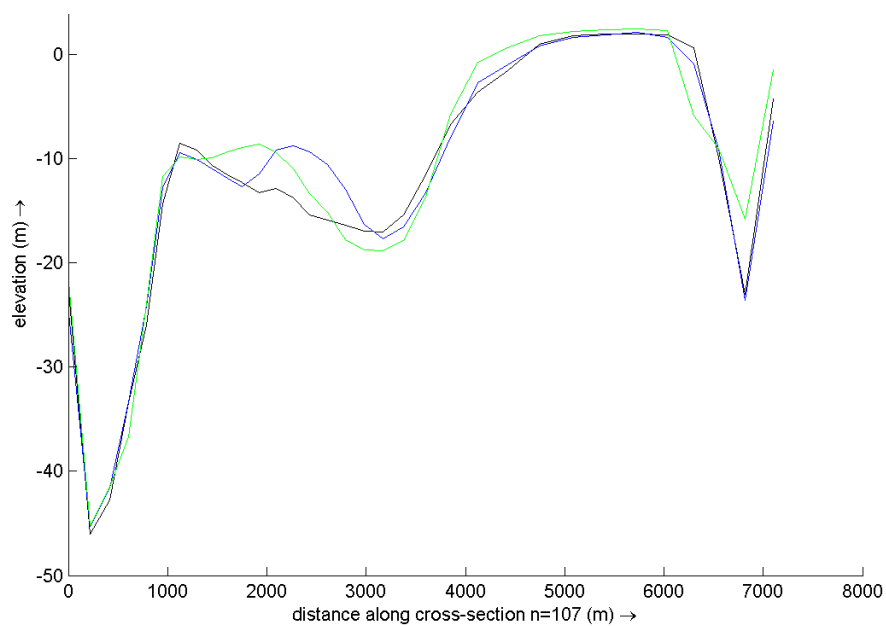


Figure A.7-38: Cross-sections of the bathymetry at location N107 for the years 1970, 1983 and 2002.

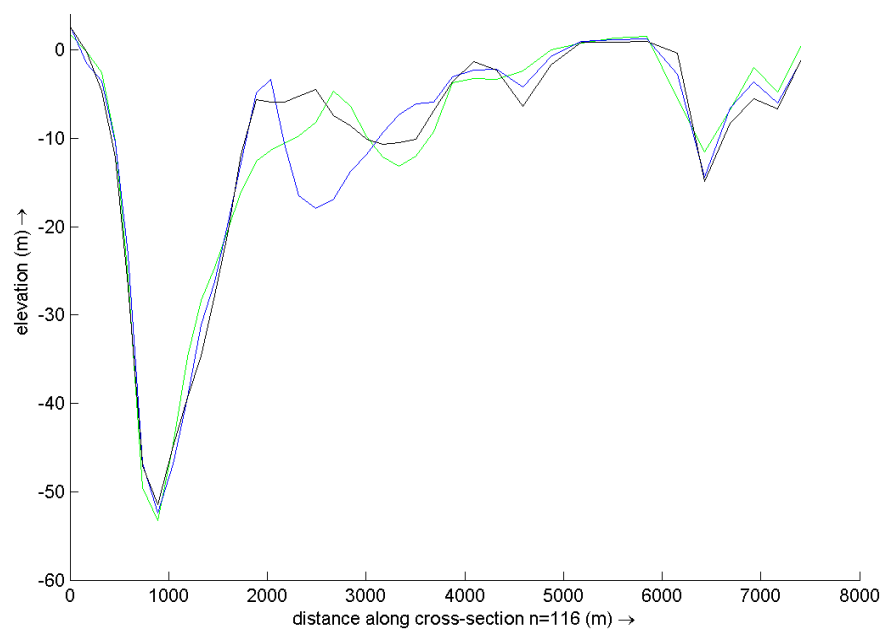


Figure A.7-39: Cross-sections of the bathymetry at location N116 for the years 1970, 1983 and 2002.

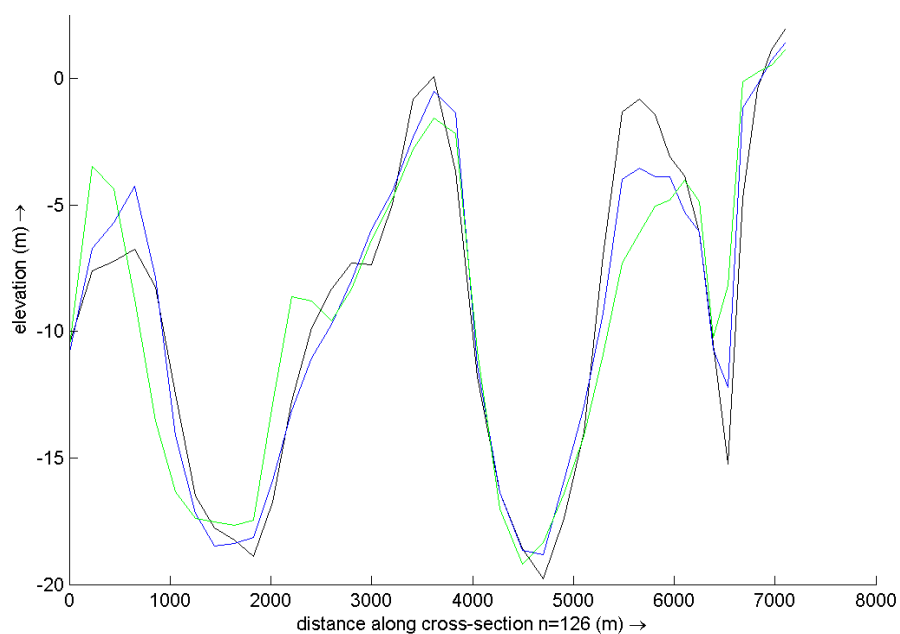


Figure A.7-40: Cross-sections of the bathymetry at location N126 for the years 1970, 1983 and 2002.

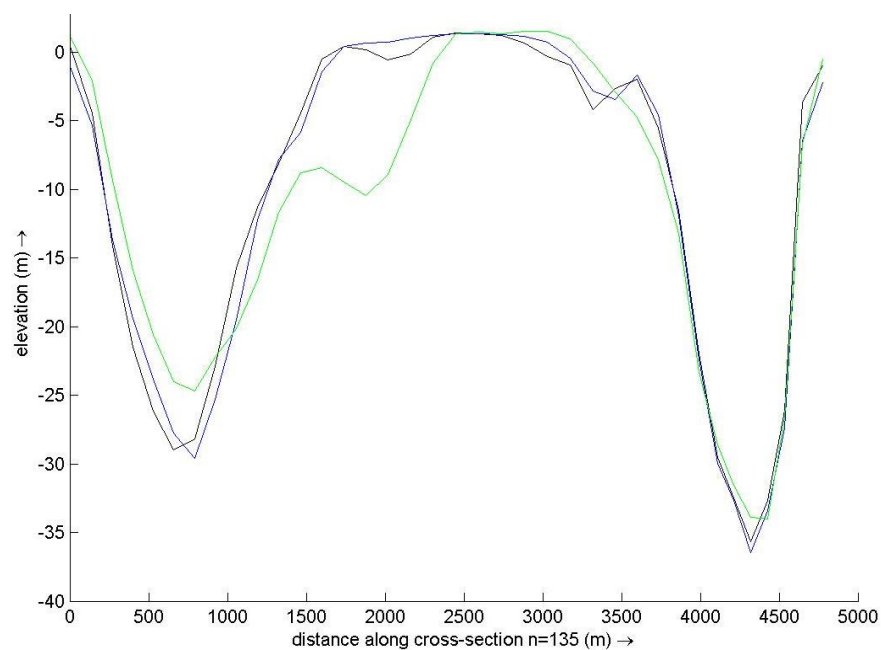


Figure A.7-41: Cross-sections of the bathymetry at location N135 for the years 1970, 1983 and 2002.

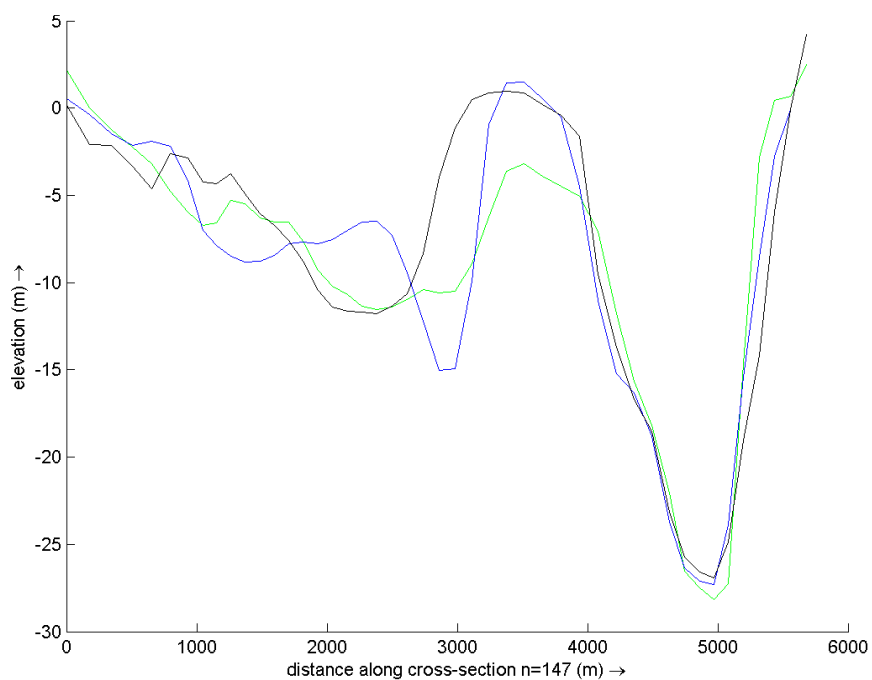


Figure A.7-42: Cross-sections of the bathymetry at location N147 for the years 1970, 1983 and 2002.

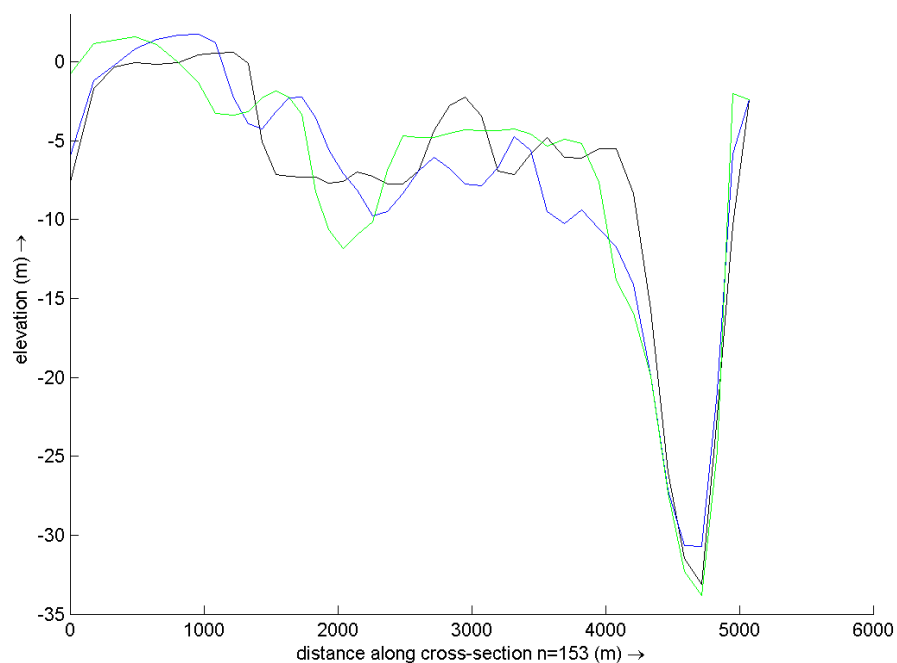


Figure A.7-43: Cross-sections of the bathymetry at location N153 for the years 1970, 1983 and 2002.

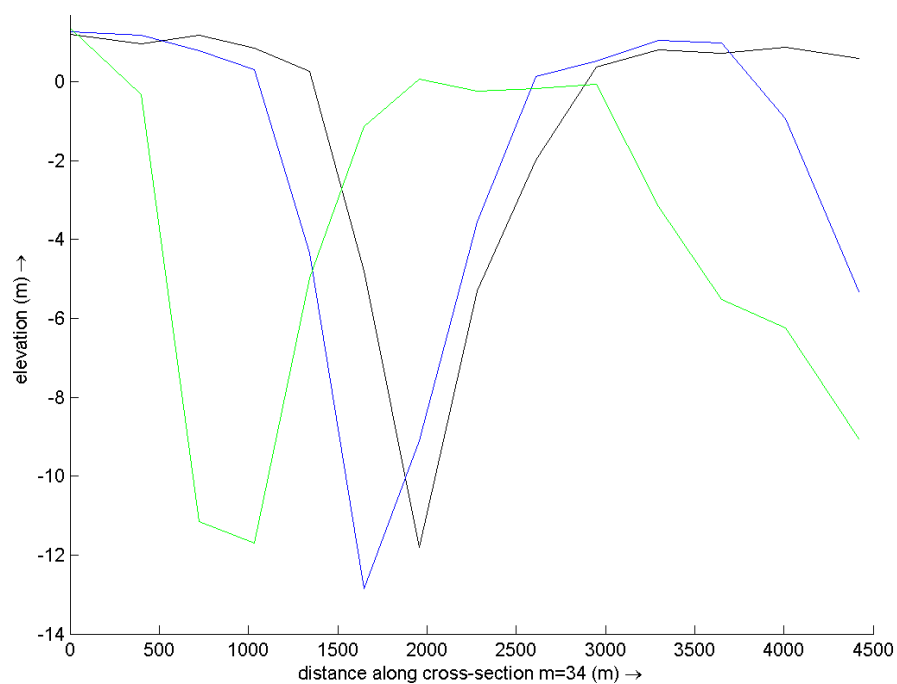


Figure A.7-44: Cross-sections of the bathymetry at location M34 for the years 1970, 1983 and 2002.

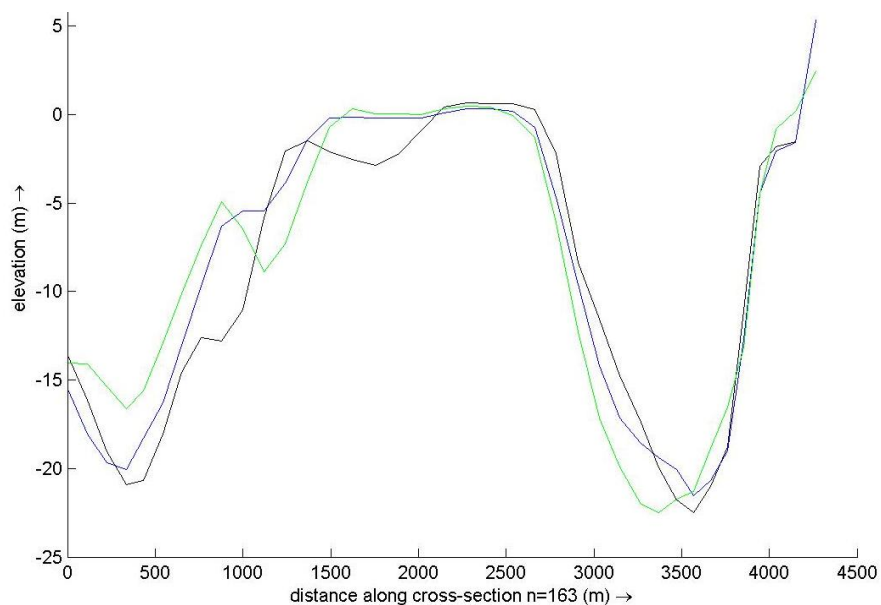


Figure A.7-45: Cross-sections of the bathymetry at location N163 for the years 1970, 1983 and 2002.

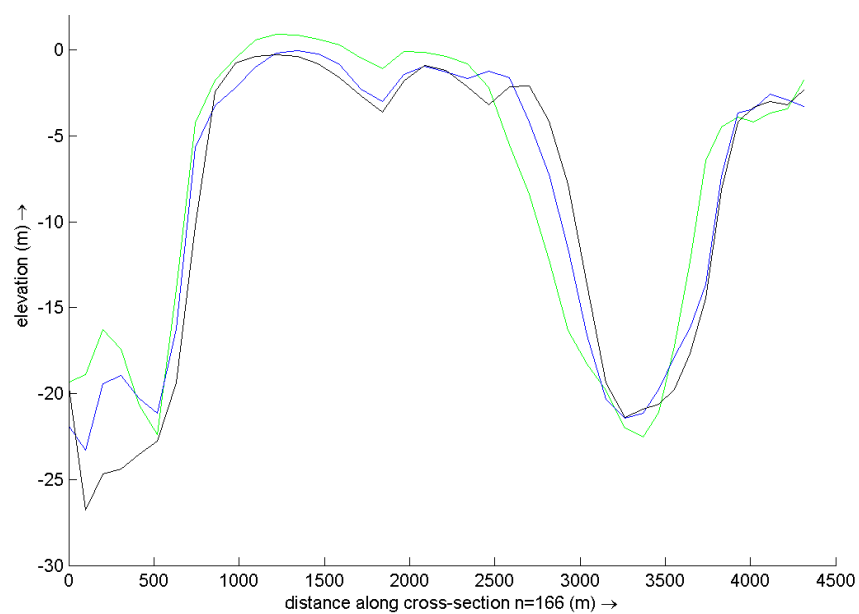


Figure A.7-46: Cross-sections of the bathymetry at location N166 for the years 1970, 1983 and 2002.

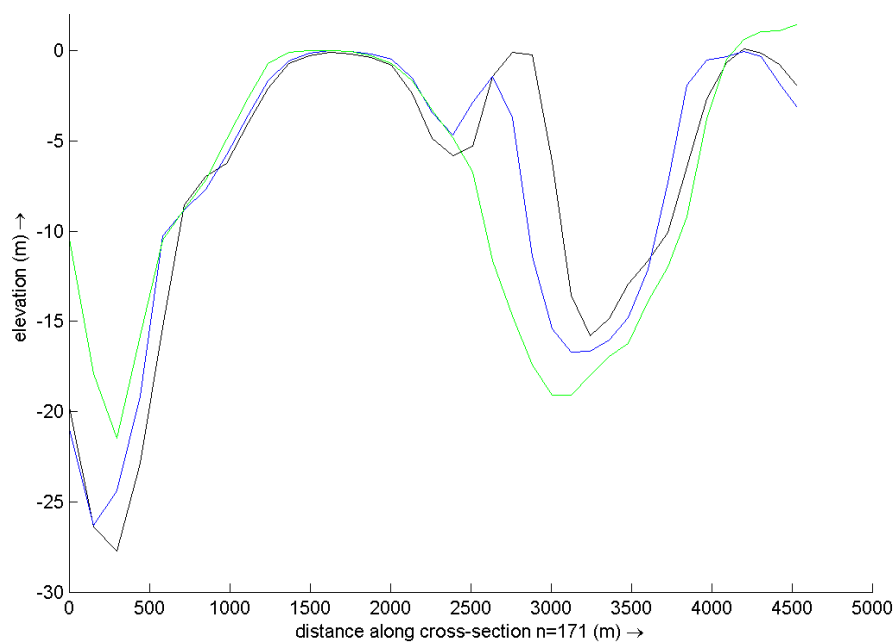


Figure A.7-47: Cross-sections of the bathymetry at location N171 for the years 1970, 1983 and 2002.

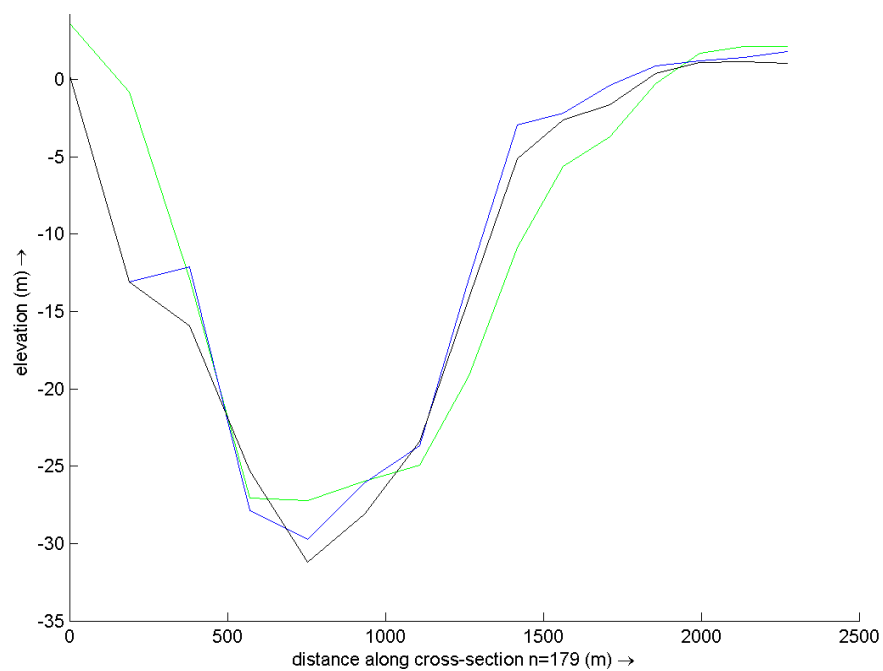


Figure A.7-48: Cross-sections of the bathymetry at location N179 for the years 1970, 1983 and 2002.

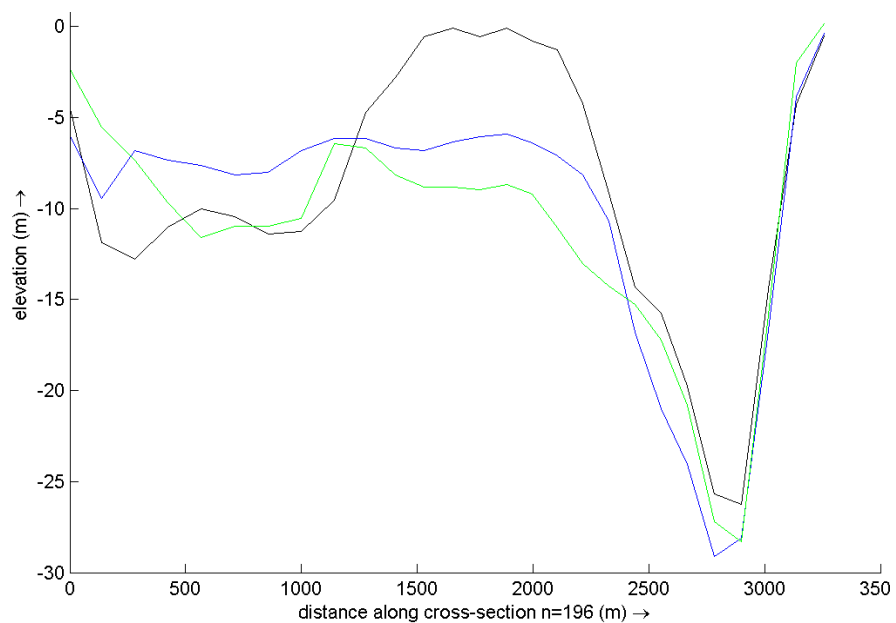


Figure A.7-49: Cross-sections of the bathymetry at location N196 for the years 1970, 1983 and 2002.

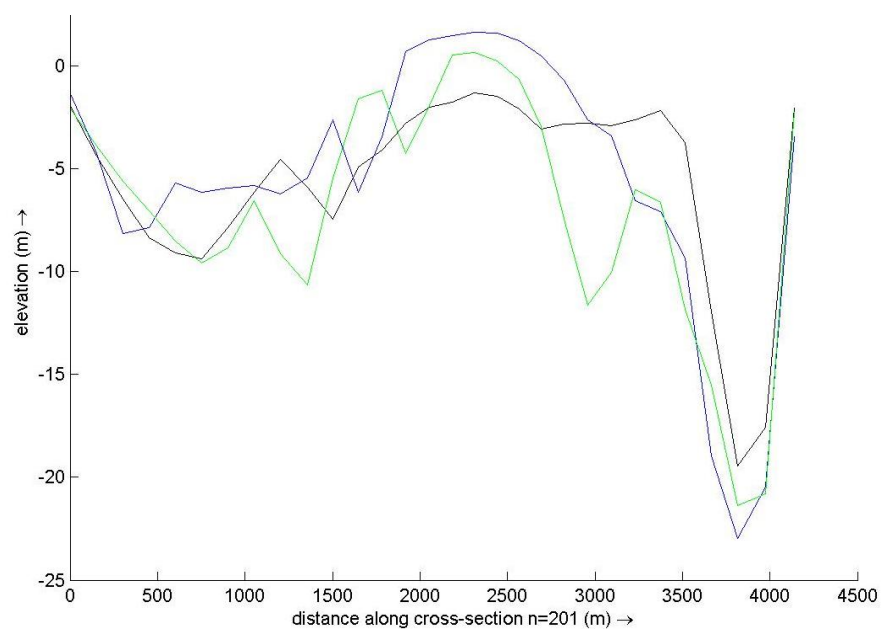


Figure A.7-50: Cross-sections of the bathymetry at location N201 for the years 1970, 1983 and 2002.

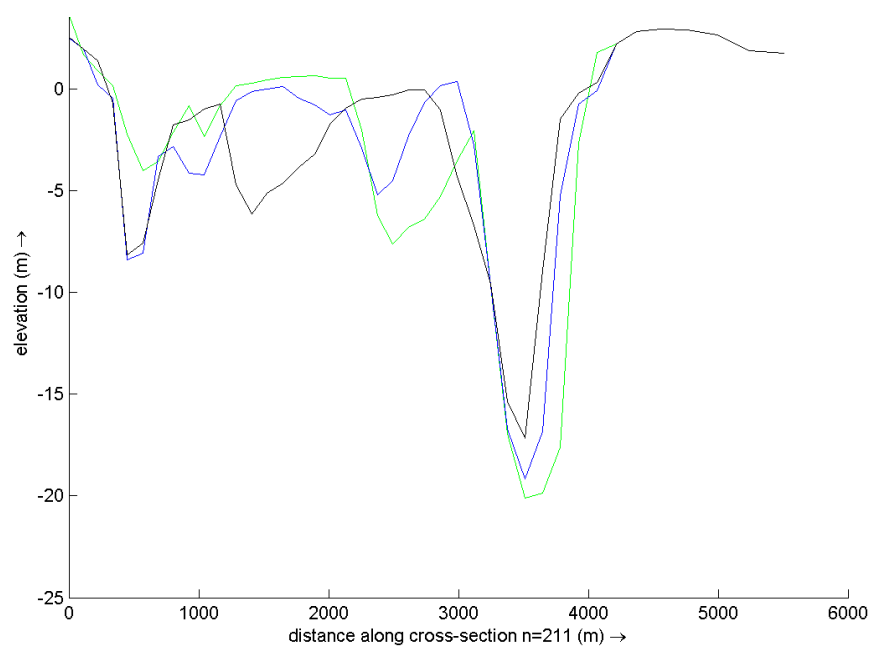


Figure A.7-51: Cross-sections of the bathymetry at location N211 for the years 1970, 1983 and 2002.

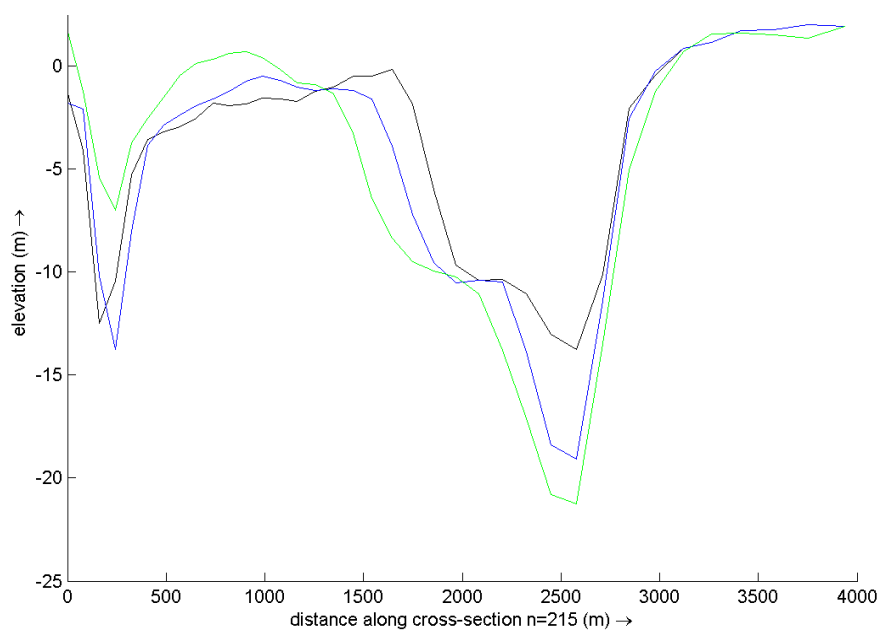


Figure A.7-52: Cross-sections of the bathymetry at location N215 for the years 1970, 1983 and 2002.

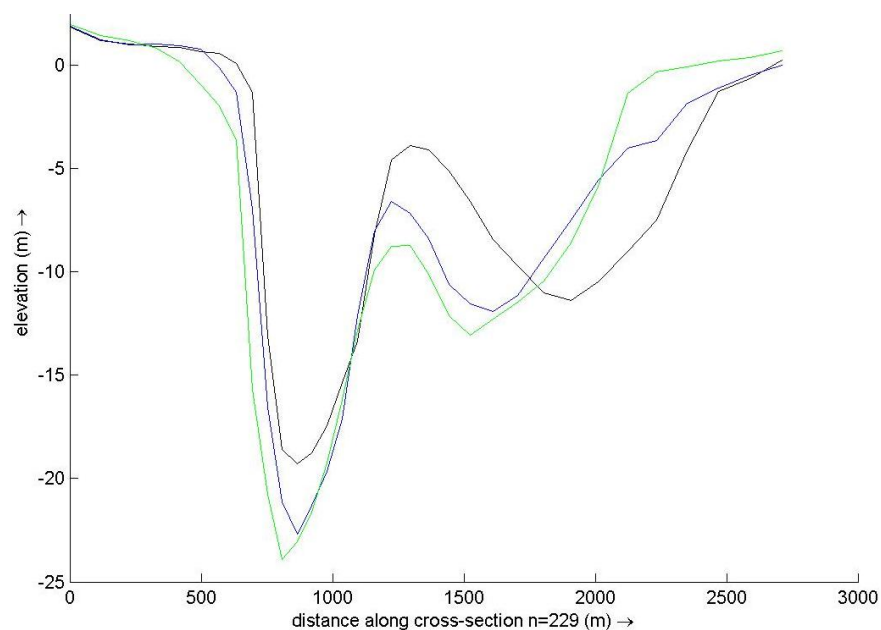


Figure A.7-53: Cross-sections of the bathymetry at location N229 for the years 1970, 1983 and 2002.

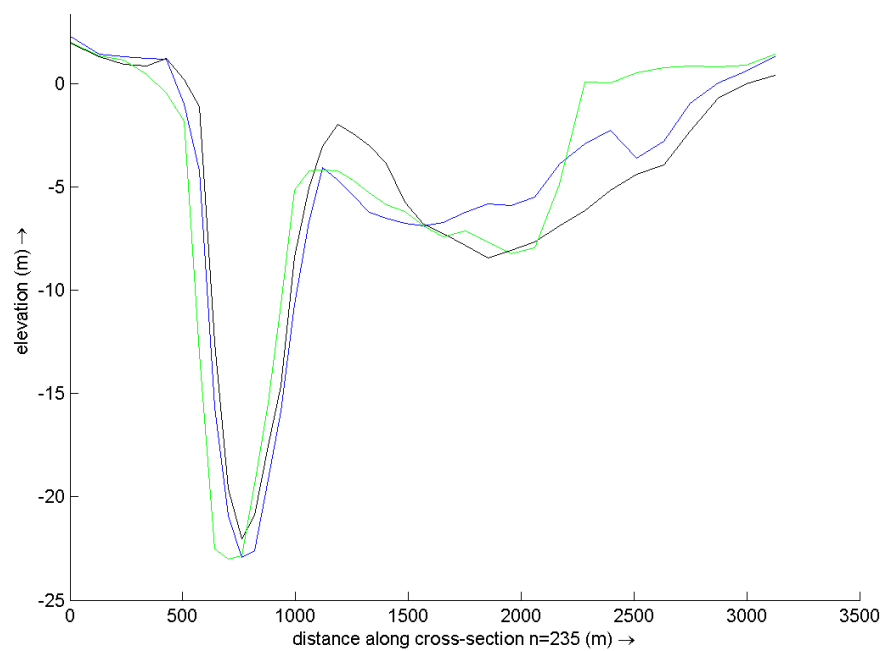


Figure A.7-54: Cross-sections of the bathymetry at location N235 for the years 1970, 1983 and 2002.

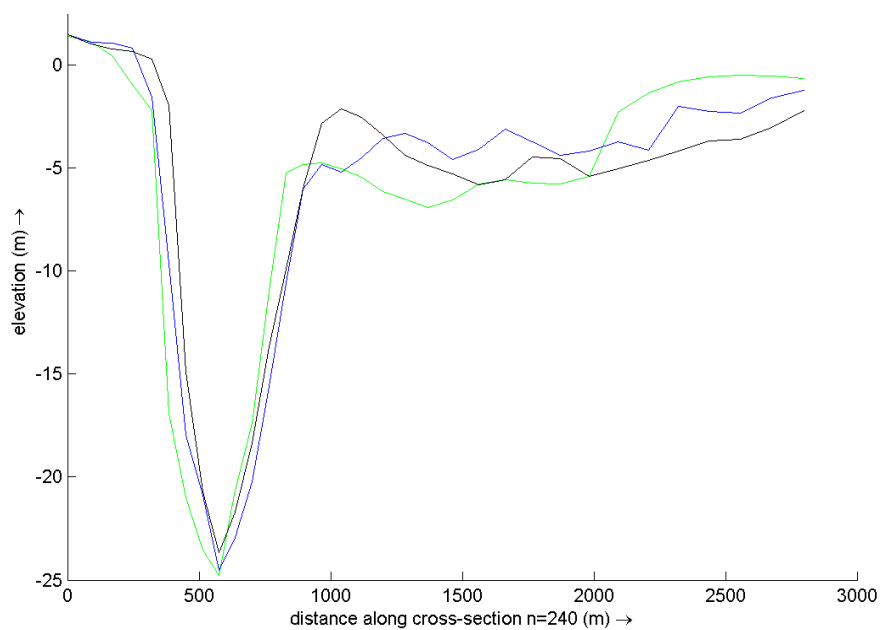


Figure A.7-55: Cross-sections of the bathymetry at location N240 for the years 1970, 1983 and 2002.

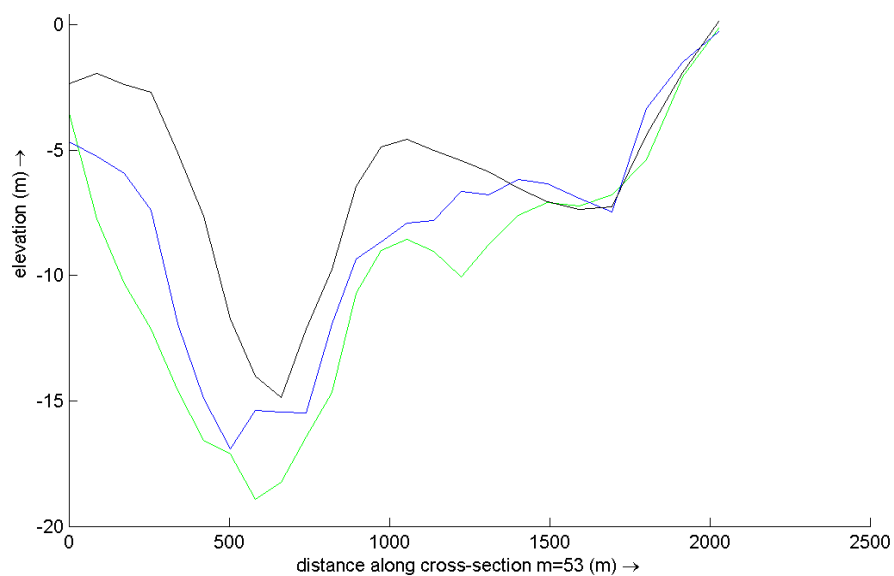


Figure A.7-56: Cross-sections of the bathymetry at location M53 for the years 1970, 1983 and 2002.

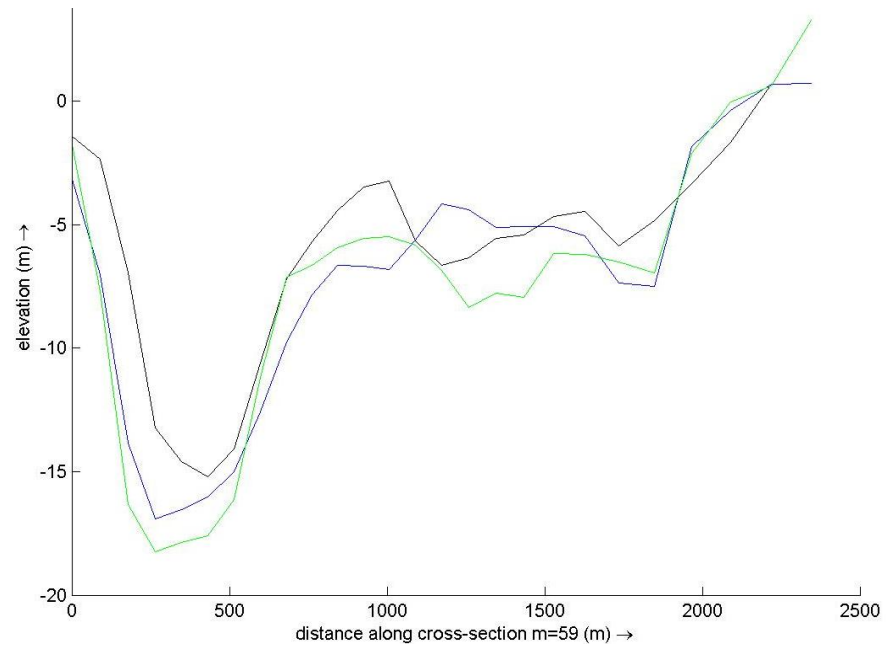


Figure A.7-57: Cross-sections of the bathymetry at location M59 for the years 1970, 1983 and 2002.

A.7.6 Comparison with Previous Studies

Whereas sufficient data are available on the tidal constituents of the vertical tide at various stations along the Western Scheldt, this information is scarce for the horizontal tide (Wang et al., 1999). The derivation of tidal constituents requires long-term observations which are much more difficult to obtain for the horizontal tide. Only a few studies based on limited field data have been reported in the past.

Wang et al. (1999) described the results of 4 weeks long velocity observations at two (single-point) locations in the western part of the estuary near Terneuzen. Tidal ellipses for the M_2 , M_4 and M_6 constituents were constructed. Their analysis showed the effect of secondary flow due to curvature, which isn't present in the recent model. As a result, no comparison could be made.

Wang and Jeuken (2000) also described the results of a discharge measurement from 1996 carried out with an Acoustic Doppler Current meter in the central part of Terneuzen during strong spring tidal conditions.

Due to the specific location and the limited amount of the observation points and the lack of data in general, no detailed comparison of model results with field measurements could be made. However some general findings from previous studies are confirmed with the recent model results.

Concerning the velocities it comes out that the main ebb channel is characterised by strongly ebb-dominant residual currents (Jeuken, 2000; Wang and Jeuken, 2000). The direction of residual sand transport is determined by the effect of the relatively small residual current. The contribution of the overtides to the residual transport is several times smaller (Wang and Jeuken, 2000).

The analysis of the discharges and velocities shows an approximately equal contribution of the M_4 and M_6 overtides in the horizontal tide. This was also found by Wang and Jeuken (2000).

The magnitude of the asymmetry in the horizontal tide, indicated by the amplitude ratio, is larger than that of the vertical tide: the asymmetry in the discharges and velocities can be up to two to three times larger than in the water levels. The vertical tide at Bath is shown in

Figure A.7-58; the horizontal tide in macro cell 6 is presented in Figures 5-25 and 5-26 (See main text). The other graphs for the vertical tide can be found in Appendix A.7.8. This agrees with the findings of Wang et al. (1999) and Wang and Jeuken (2000), and the 1D model results of Schoeman (2000).

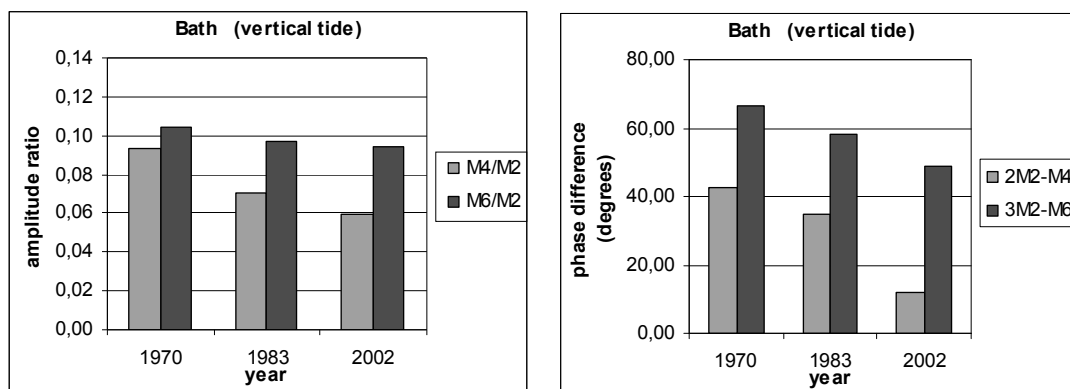


Figure A.7-58: Amplitude ratio M_4/M_2 and M_6/M_2 , and phase differences $2\varphi_2-\varphi_4$ and $3\varphi_2-\varphi_6$ for the vertical tide at the station of Bath derived from the model results for the years 1970, 1983 and 2002.

A.7.7 Graphical Representation of the Amplitude Ratios and Phase Differences of the Vertical Tide

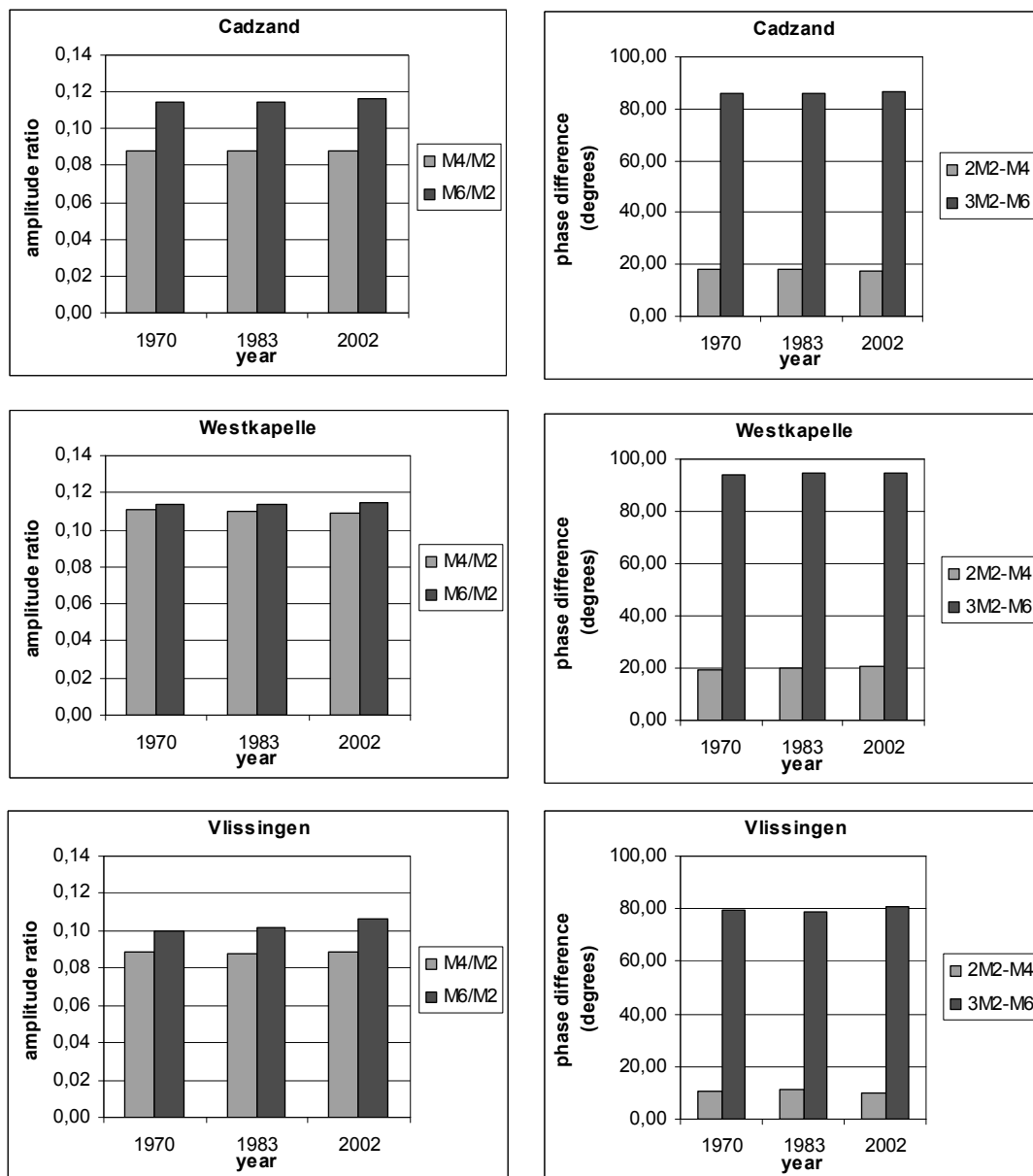


Figure A.7-59: Amplitude ratios and phase differences for the vertical tide at the stations Cadzand, Westkapelle and Vlissingen derived from the model results for the years 1970, 1983 and 2002.

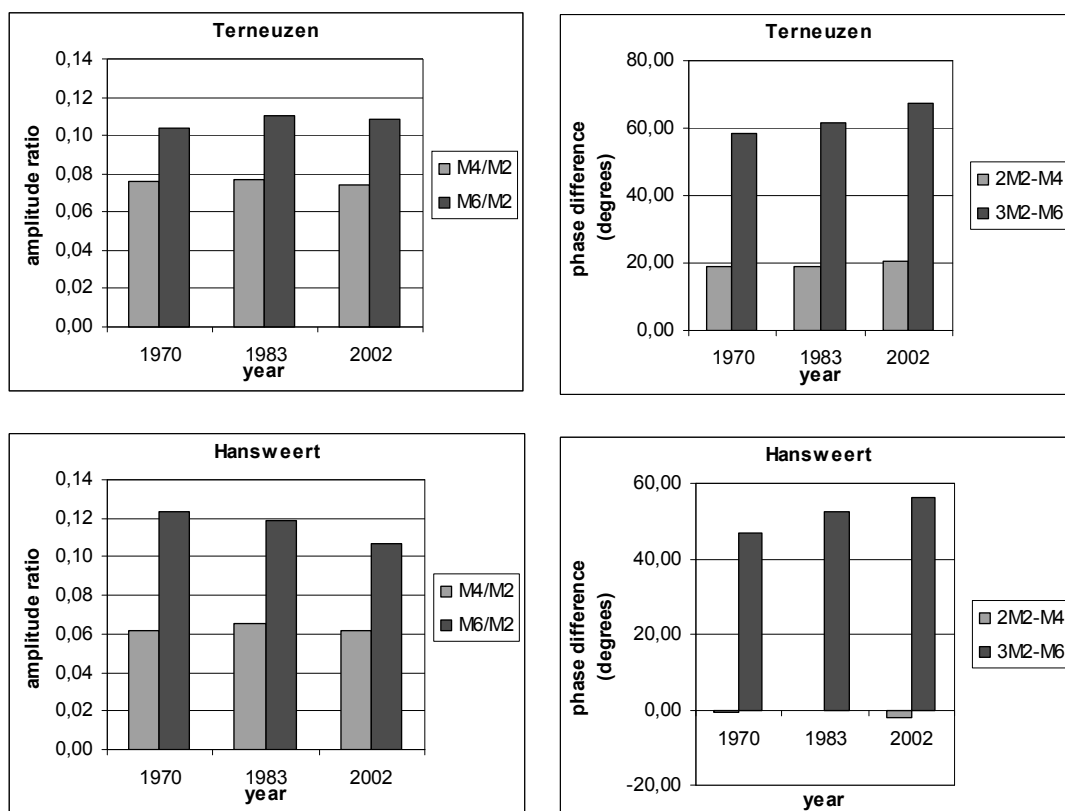


Figure A.7-60: Amplitude ratios and phase differences for the vertical tide at the stations Terneuzen and Hansweert derived from the model results for the years 1970, 1983 and 2002.

A.8 Horizontal Tidal Asymmetry

A.8.1 Location of the Cross-sections and Observation Points

Table A.8-1: Overview of the cross-sections and observation points in the model per macro cell.

Macro Cell	Ebb Channel		Flood Channel	
	Observation Point	Cross-section	Observation Point	Cross-section
1	N103_20	<i>De Honte</i> E11	N103_33	<i>Schaar van de Spijkerplaat</i> / V11
3	N135_46	<i>Pas van Terneuzen</i> E32	N135_19	<i>Everingen</i> V32
4	N163_20	<i>Middelgat</i> r6O middelgat	N163_47	<i>Gat van Ossenissee</i> r6O gat van osse
5	N201_55	<i>Zuidergat</i> Zuidergat	N201_33	<i>Schaar van Waarde</i> Schaar van Waarde
6	N229_33	<i>Nauw van Bath</i> E61	N229_46	<i>Schaar van Noord</i> V61
7	M59_249	<i>Vaarwater boven Bath</i> /E71	M59_264	<i>Appelzak</i> V71
Note: the names of the observation points and cross-sections in the Table are according to the naming in the model. The words in italics are the names of the different channels.				

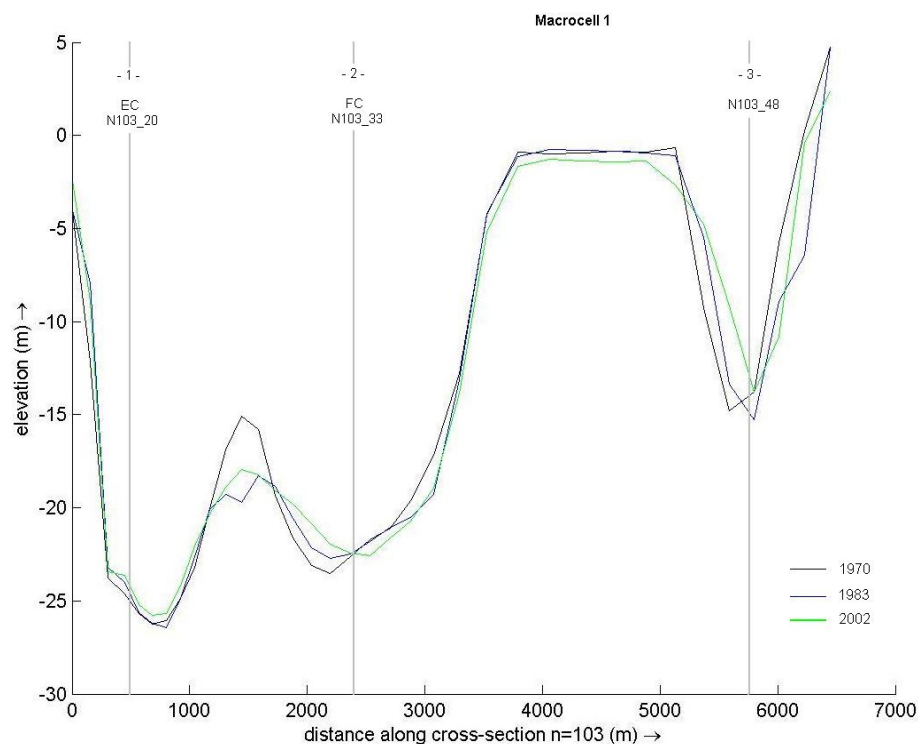


Figure A.8-1: The profile of the cross-section in macro cell 1. The vertical lines indicate the position of the observation points in the flood and ebb channel (respectively FC and EC).

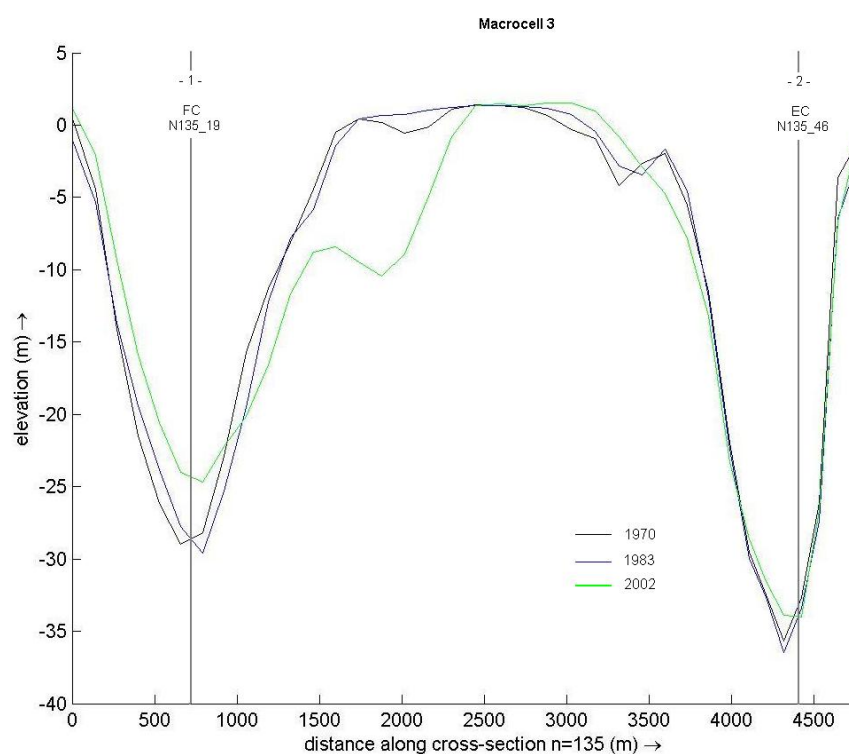


Figure A.8-2: The profile of the cross-section in macro cell 3. The vertical lines indicate the position of the observation points in the flood and ebb channel (respectively FC and EC).

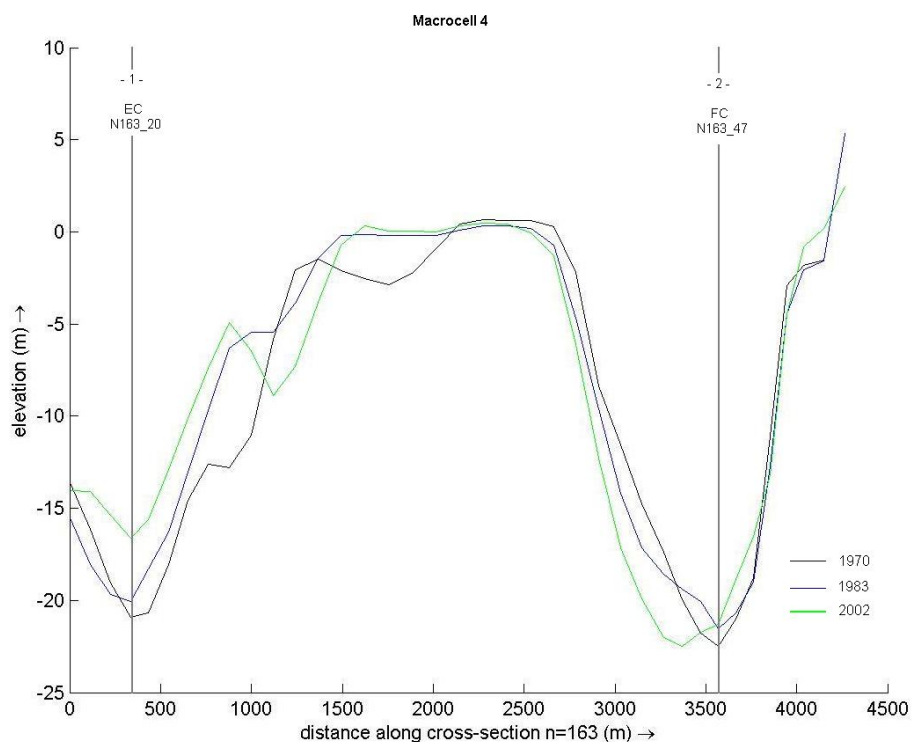


Figure A.8-3: The profile of the cross-section in macro cell 4. The vertical lines indicate the position of the observation points in the flood and ebb channel (respectively FC and EC).

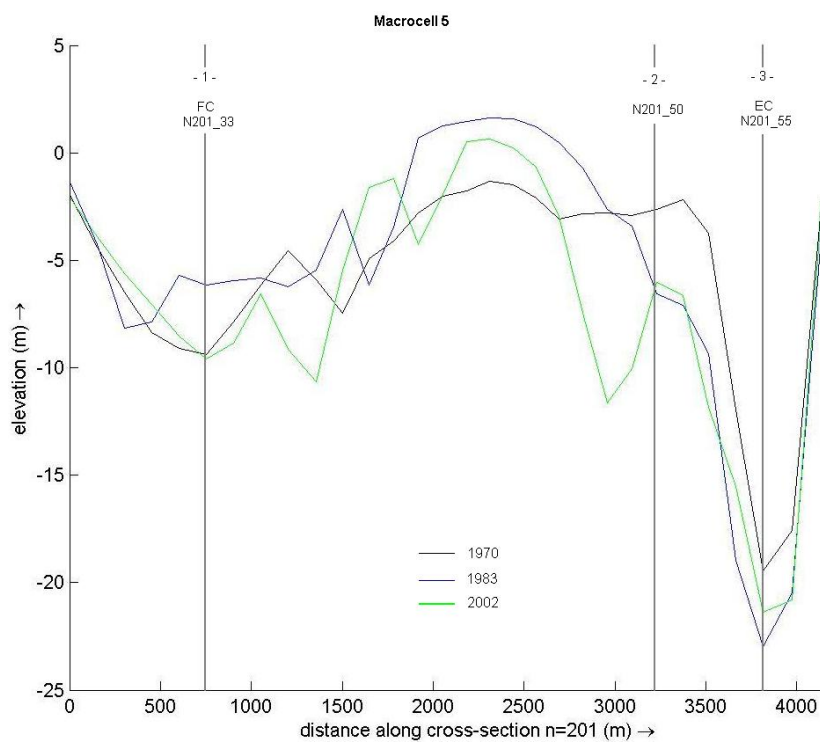


Figure A.8-4: The profile of the cross-section in macro cell 5. The vertical lines indicate the position of the observation points in the flood and ebb channel (respectively FC and EC).

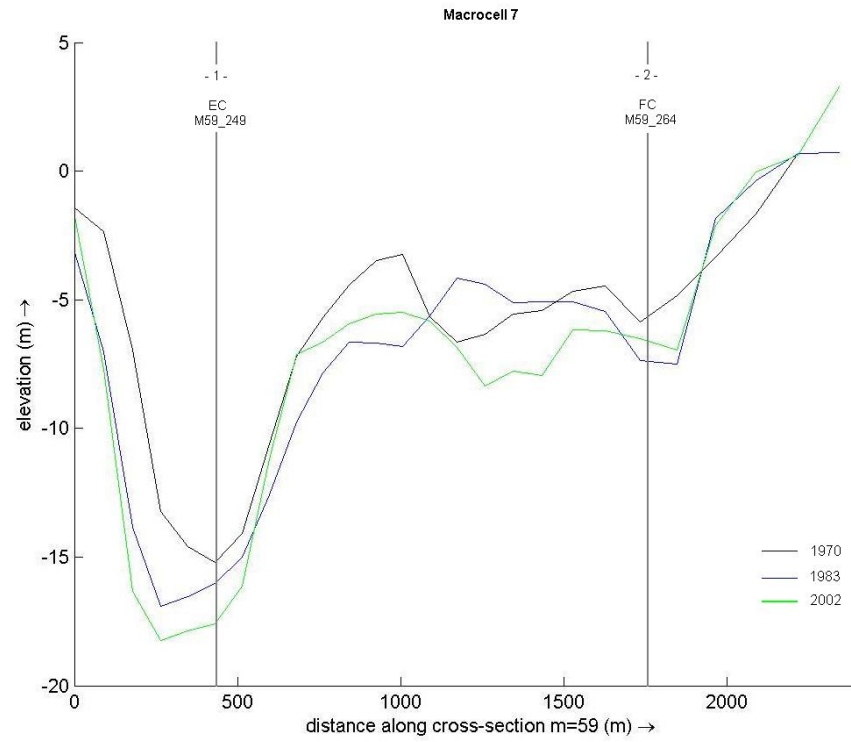


Figure A.8-5: The profile of the cross-section in macro cell 7. The vertical lines indicate the position of the observation points in the flood and ebb channel (respectively FC and EC).

A.8.2 Results per Macro Cell

A.8.2.1 Macro Cell I

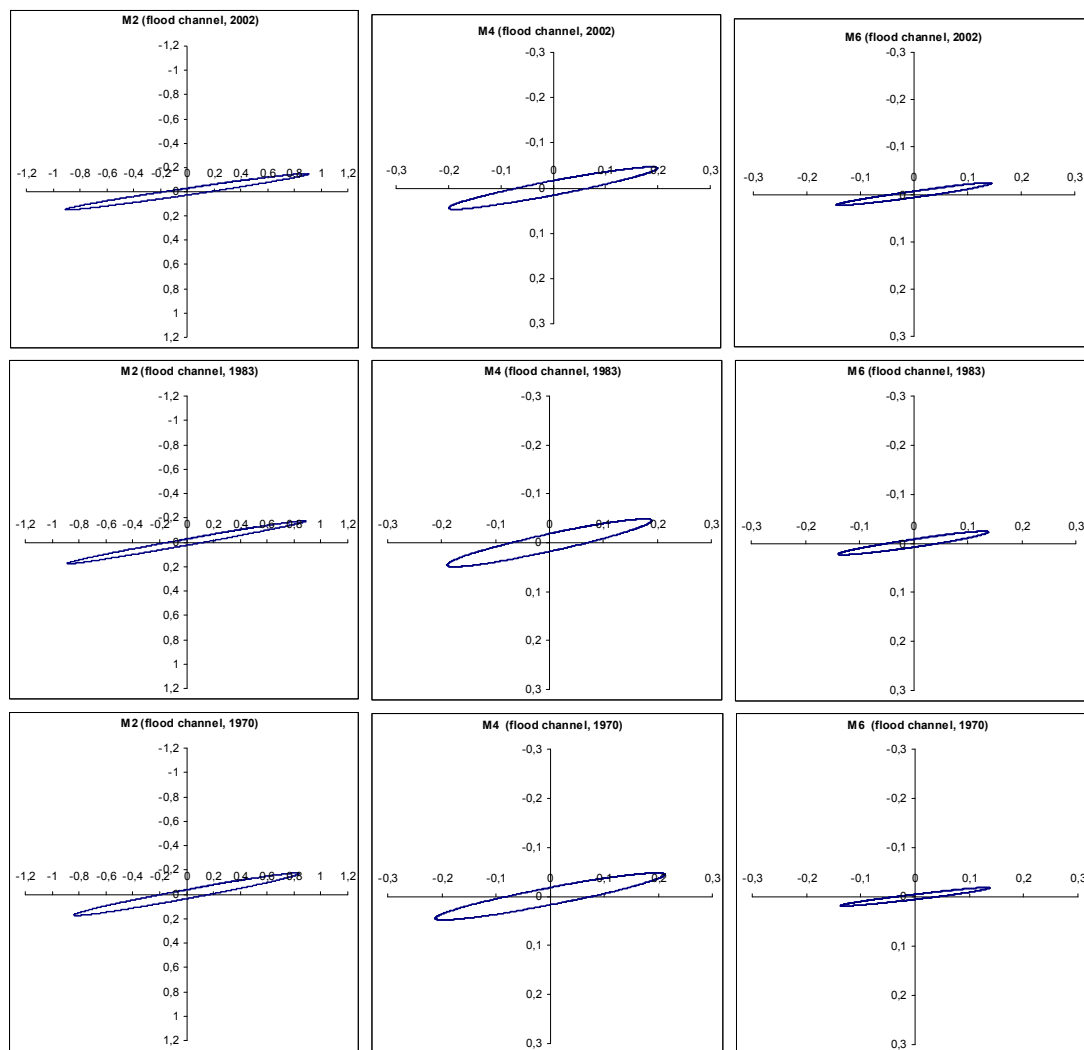


Figure A.8-6: Tidal ellipses for the M_2 , M_4 and M_6 tidal constituents derived from the model results for the velocity in the years 1970, 1983 and 2002 for the observation point in the flood channel of macro cell 1 (velocities in m/s).

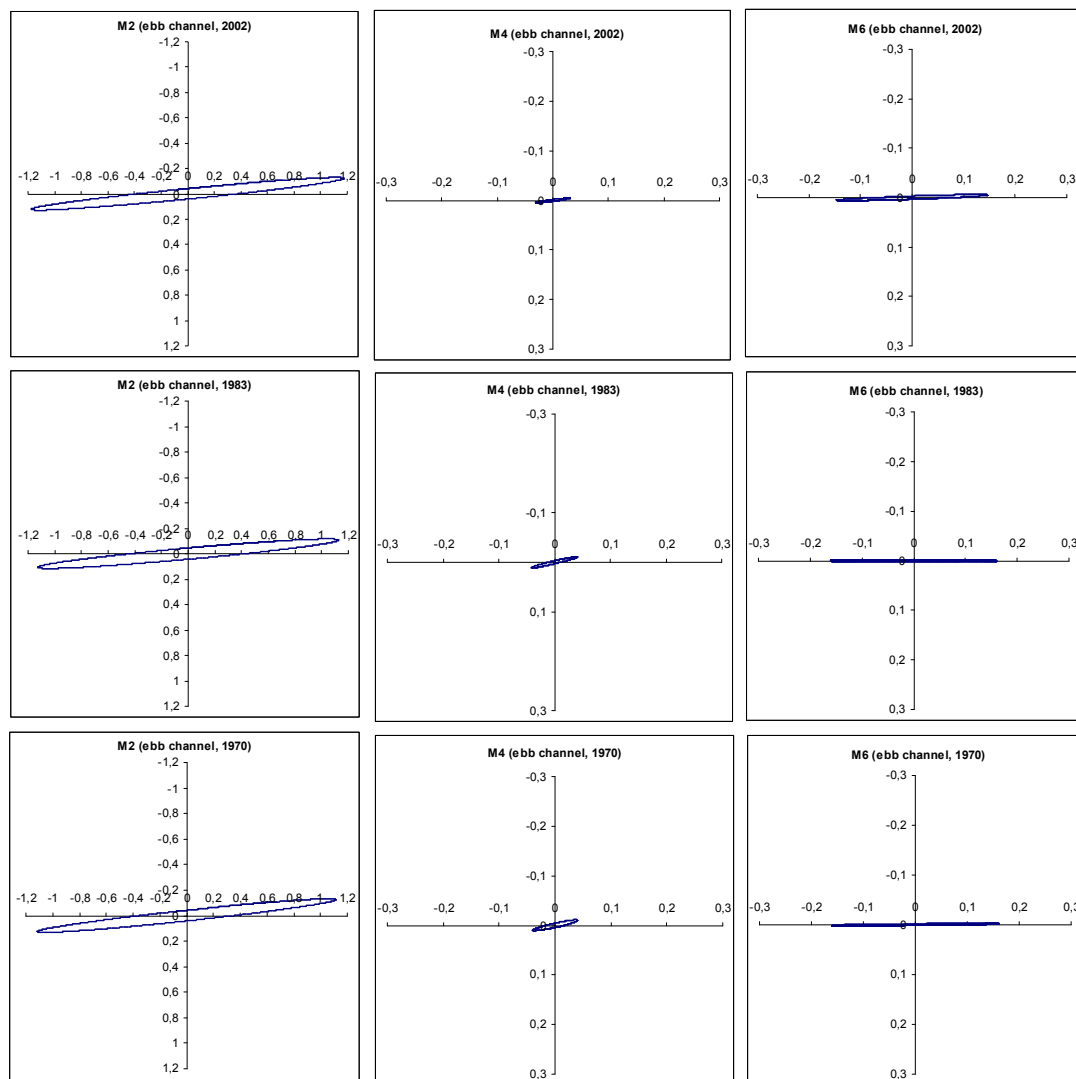


Figure A.8-7: Tidal ellipses for the M₂, M₄ and M₆ tidal constituents derived from the model for 1970, 1983 and 2002 for the observation point in the ebb channel of macro cell 1 (velocities in m/s).

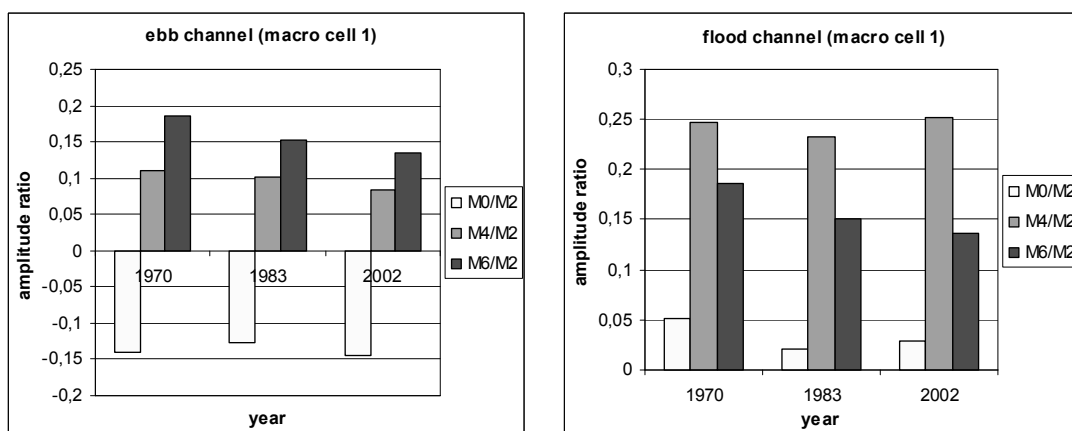


Figure A.8-8: The amplitude ratios M₀/M₂, M₄/M₂ and M₆/M₂ for the discharge through the ebb and flood channel of macro cell 1 derived from the model for 1970, 1983 and 2002.

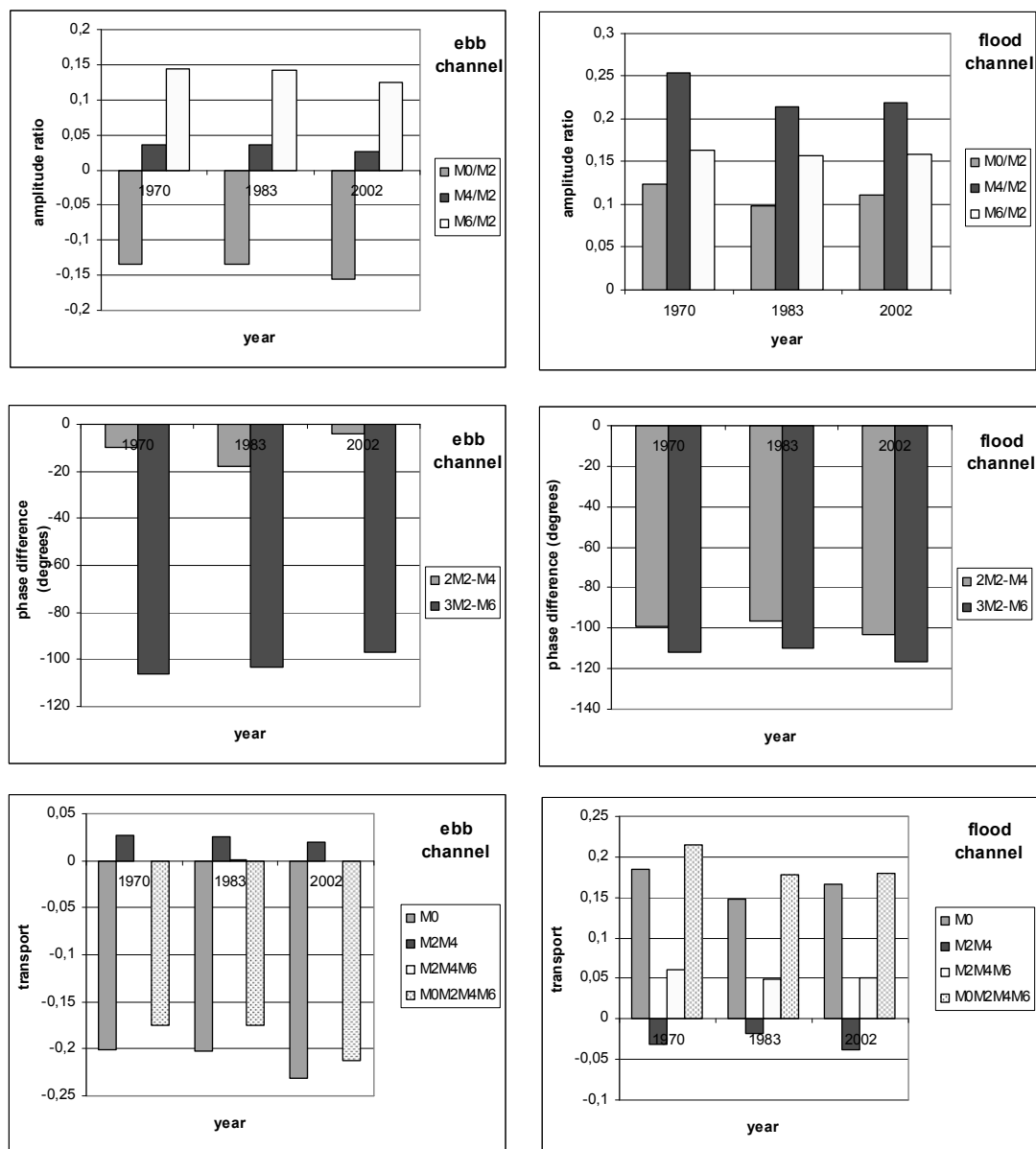


Figure A.8-9: The amplitude ratios M_0/M_2 , M_4/M_2 and M_6/M_2 , and the phase differences $2\phi_2-\phi_4$ and $3\phi_2-\phi_6$ of the velocity component in the mainstream direction at the observation points in the ebb and flood channel of macro cell 1 derived from the model results for the years 1970, 1983 and 2002, together with the contribution to the bedload transport.

A.8.2.2 Macro Cell 3

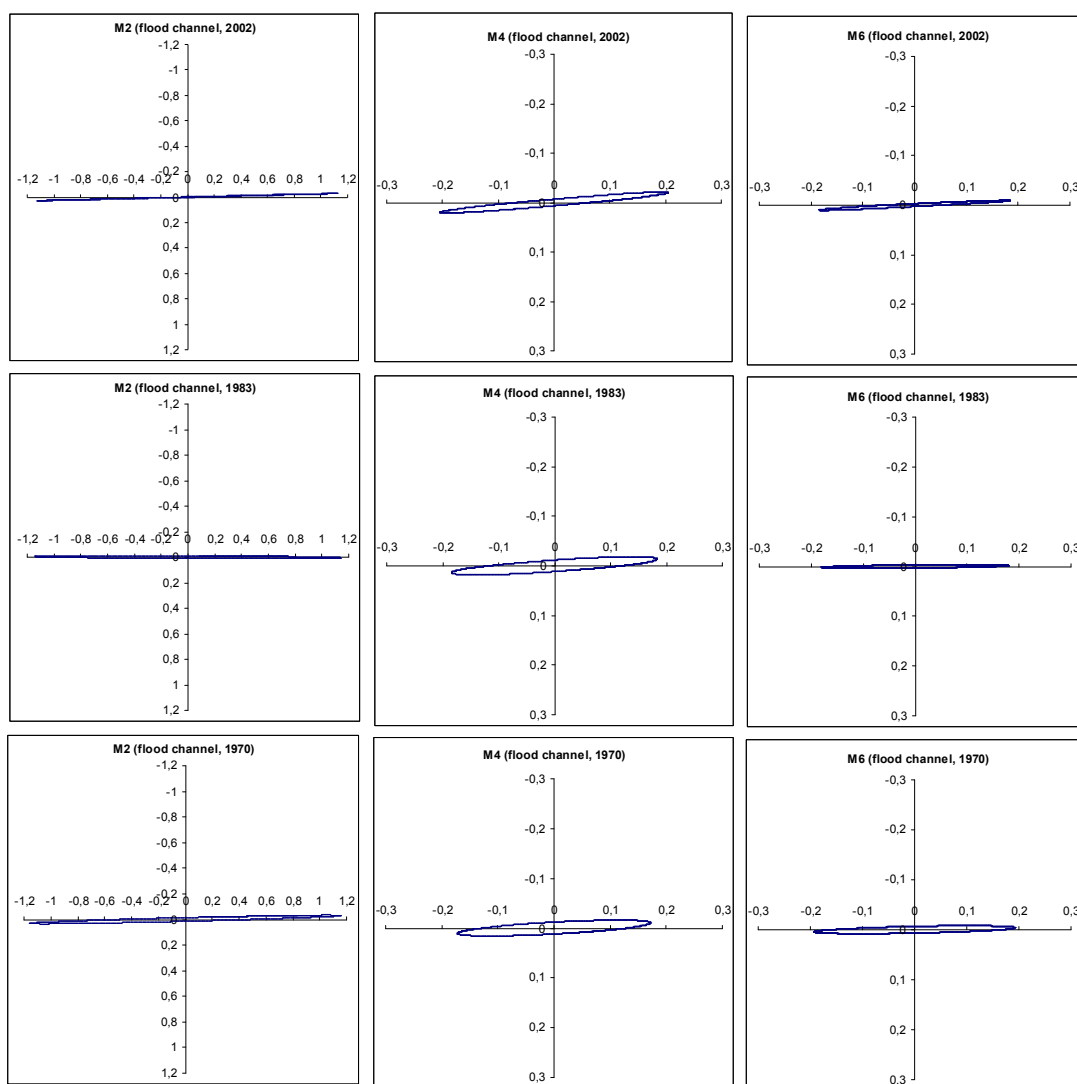


Figure A.8-10: Tidal ellipses for the M₂, M₄ and M₆ tidal constituents derived from the model results for the velocity in the years 1970, 1983 and 2002 for the observation point in the flood channel of macro cell 3 (velocities in m/s).

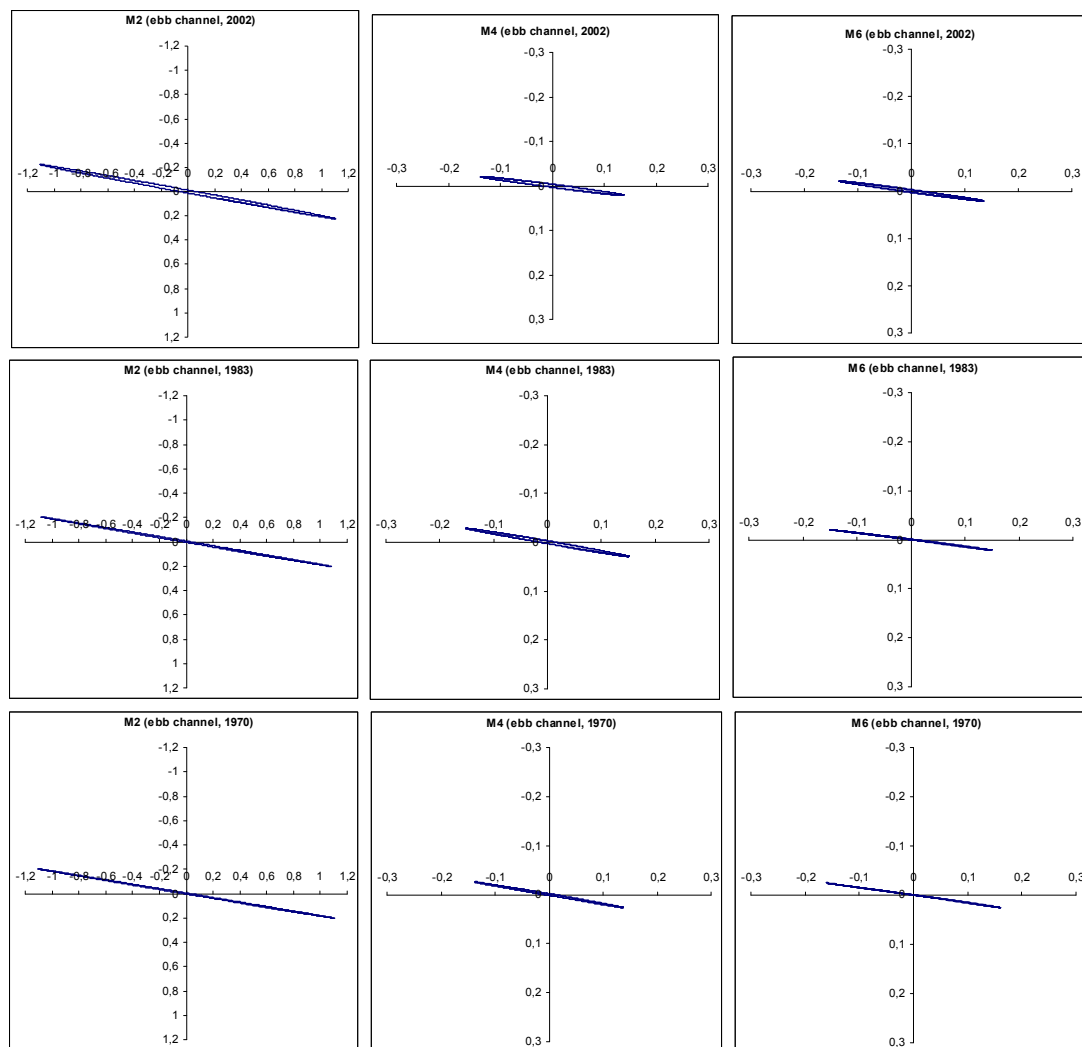


Figure A.8-11: Tidal ellipses for the M_2 , M_4 and M_6 tidal constituents derived from the model for 1970, 1983 and 2002 for the observation point in the ebb channel of macro cell 3 (velocities in m/s).

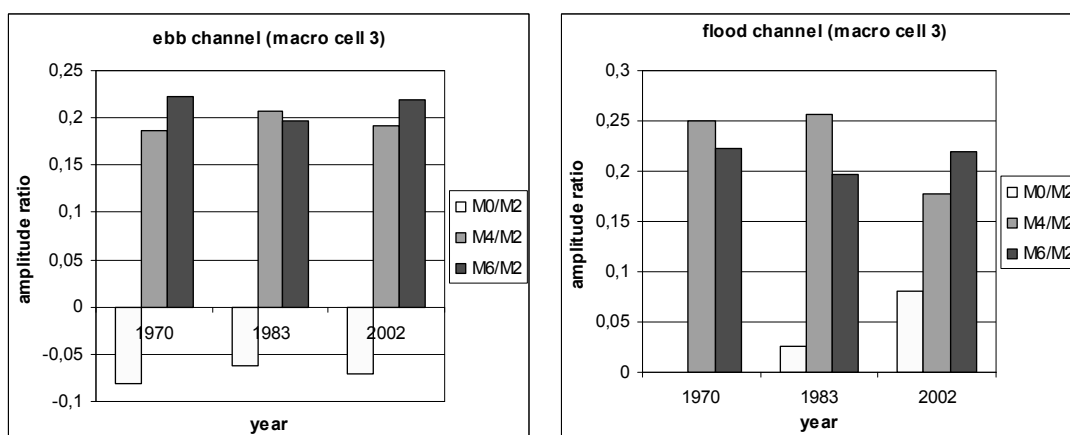


Figure A.8-12: The amplitude ratios M_0/M_2 , M_4/M_2 and M_6/M_2 for the discharge through the ebb and flood channel of macro cell 3 derived from the model for 1970, 1983 and 2002.

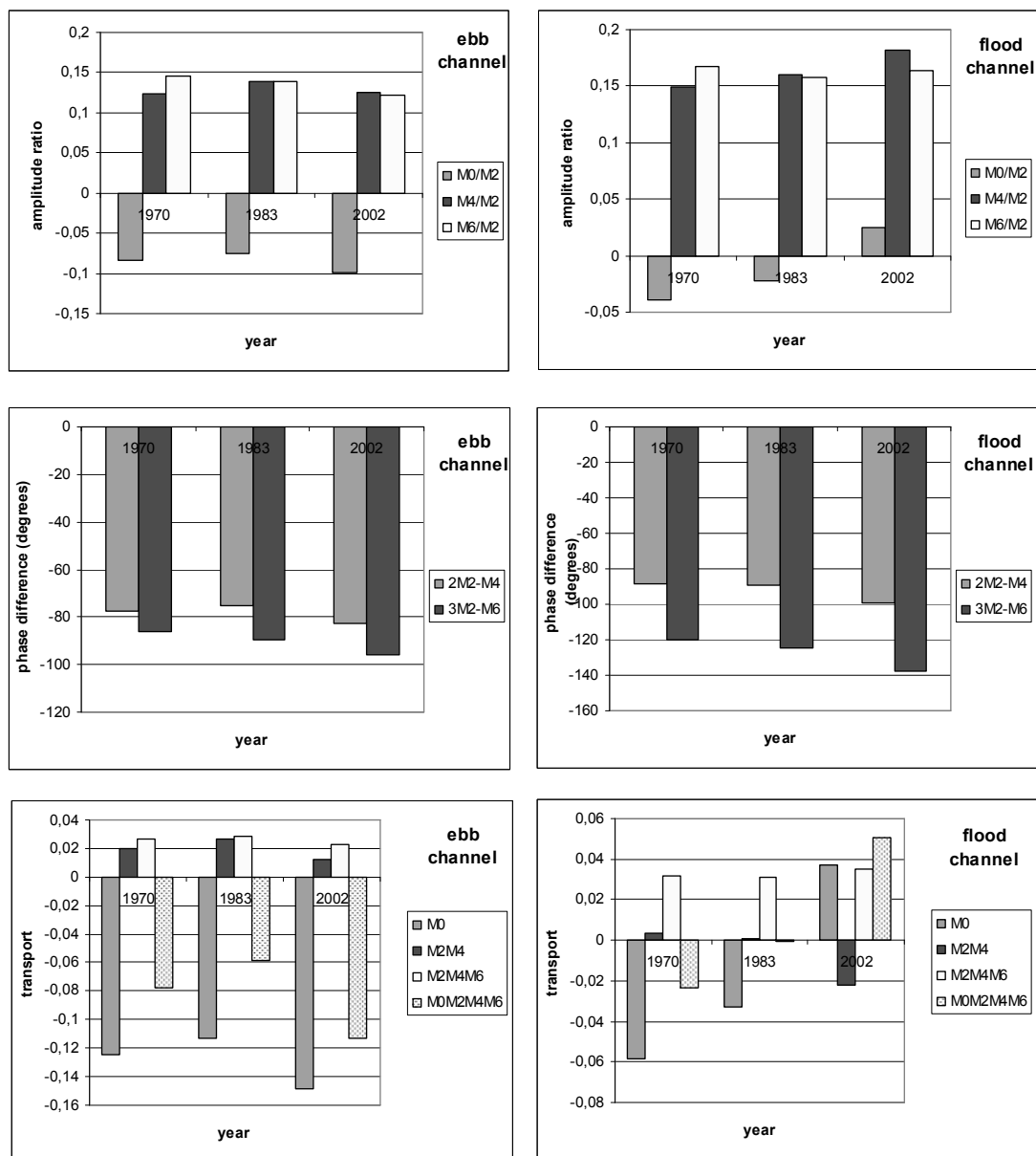


Figure A.8-13: The amplitude ratios M_0/M_2 , M_4/M_2 and M_6/M_2 , and the phase differences $2\phi_2-\phi_4$ and $3\phi_2-\phi_6$ of the velocity component in the mainstream direction at the observation points in the ebb and flood channel of macro cell 3 derived from the model results for the years 1970, 1983 and 2002, together with the contribution to the bedload transport.

A.8.2.3 Macro Cell 4

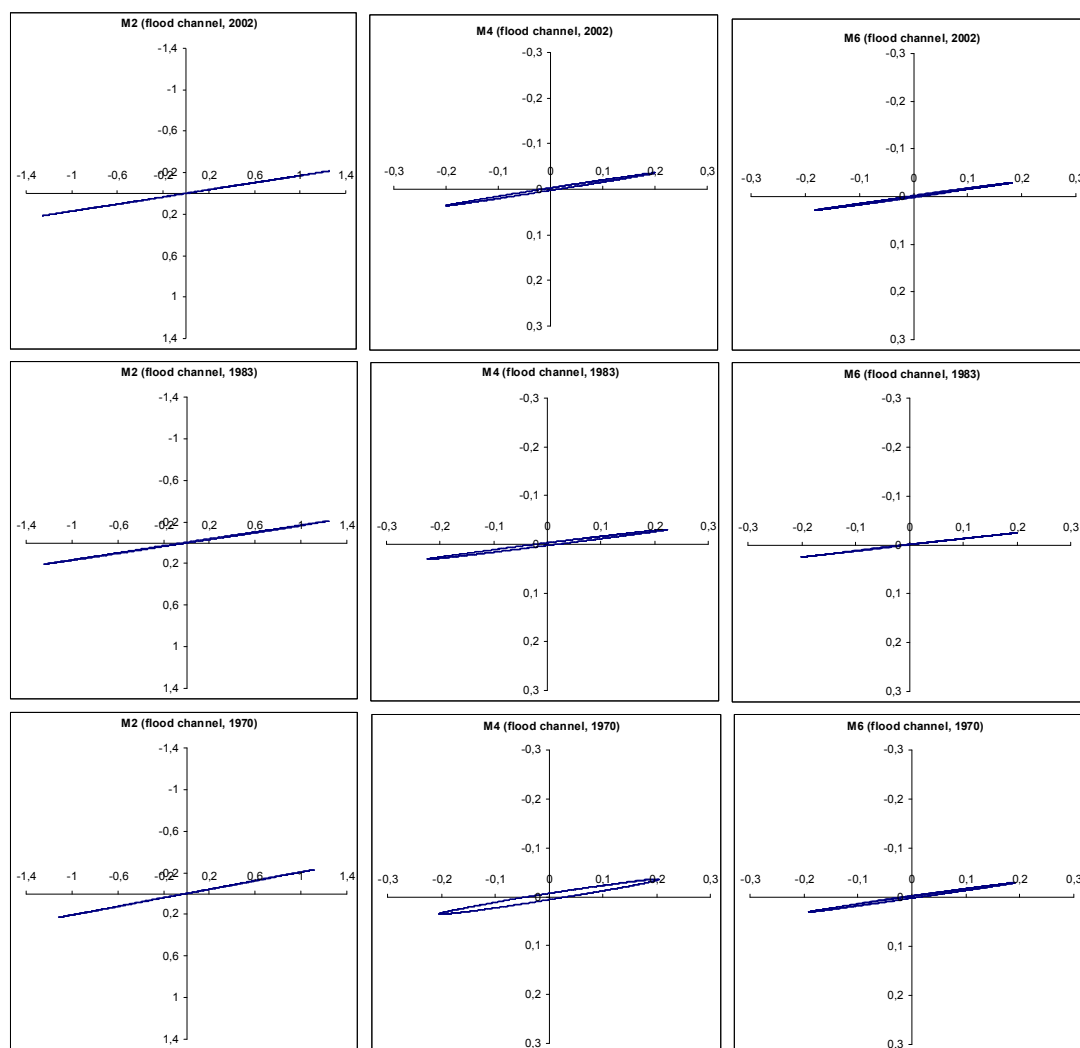


Figure A.8-14: Tidal ellipses for the M_2 , M_4 and M_6 tidal constituents derived from the model results for the velocity in the years 1970, 1983 and 2002 for the observation point in the flood channel of macro cell 4 (velocities in m/s).

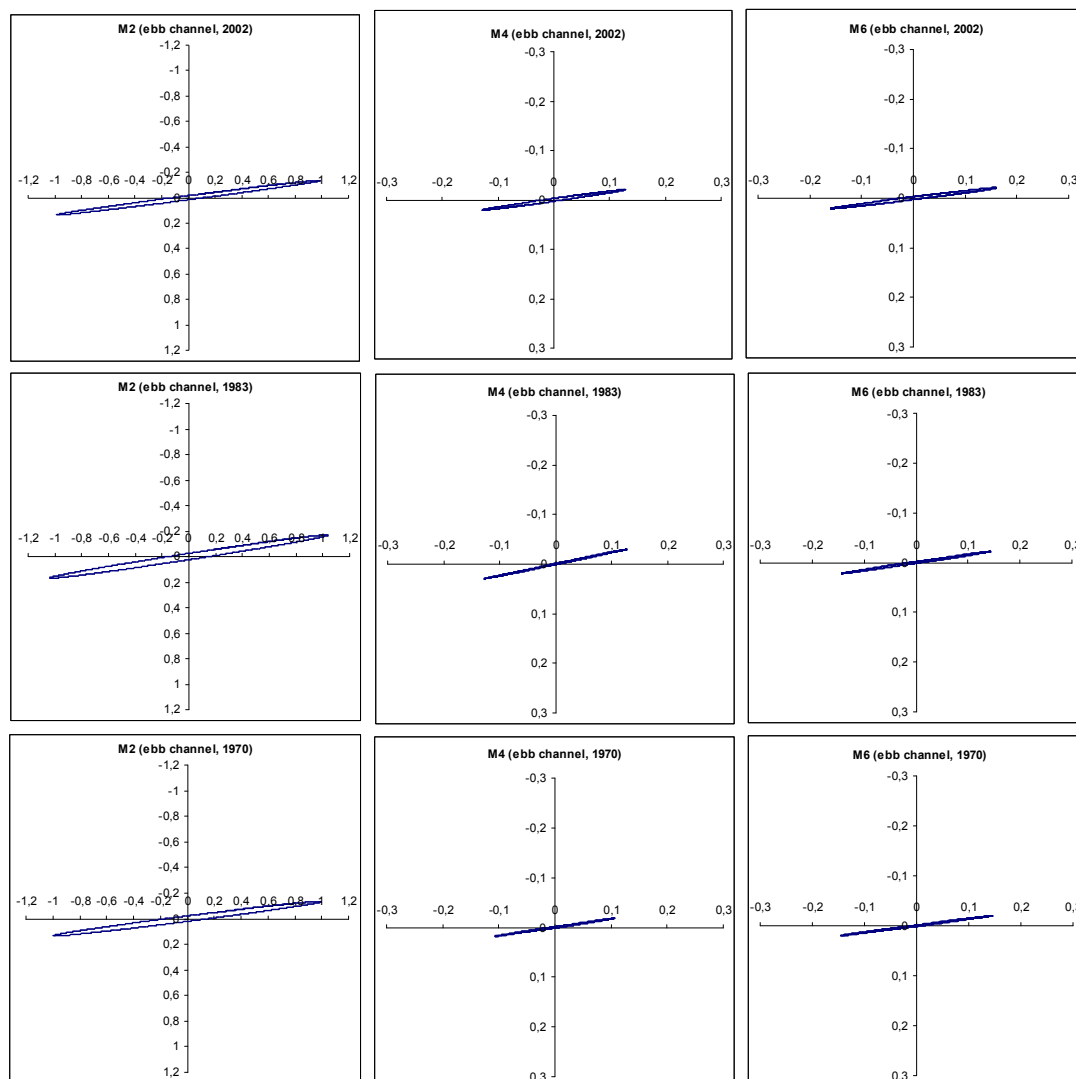


Figure A.8-15: Tidal ellipses for the M_2 , M_4 and M_6 tidal constituents derived from the model for 1983 and 2002 for the observation point in the ebb channel of macro cell 4 (velocities in m/s).

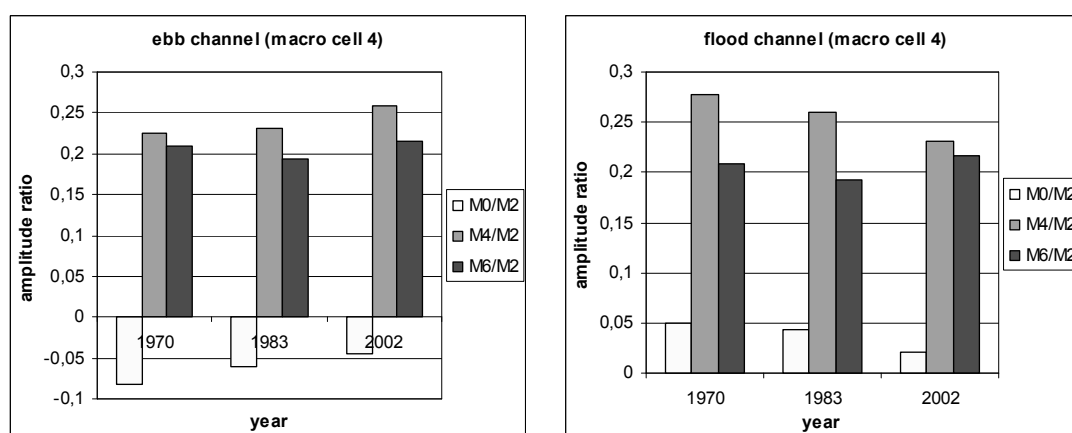


Figure A.8-16: The amplitude ratios M_0/M_2 , M_4/M_2 and M_6/M_2 for the discharge through the ebb and flood channel of macro cell 4 derived from the model for 1970, 1983 and 2002.

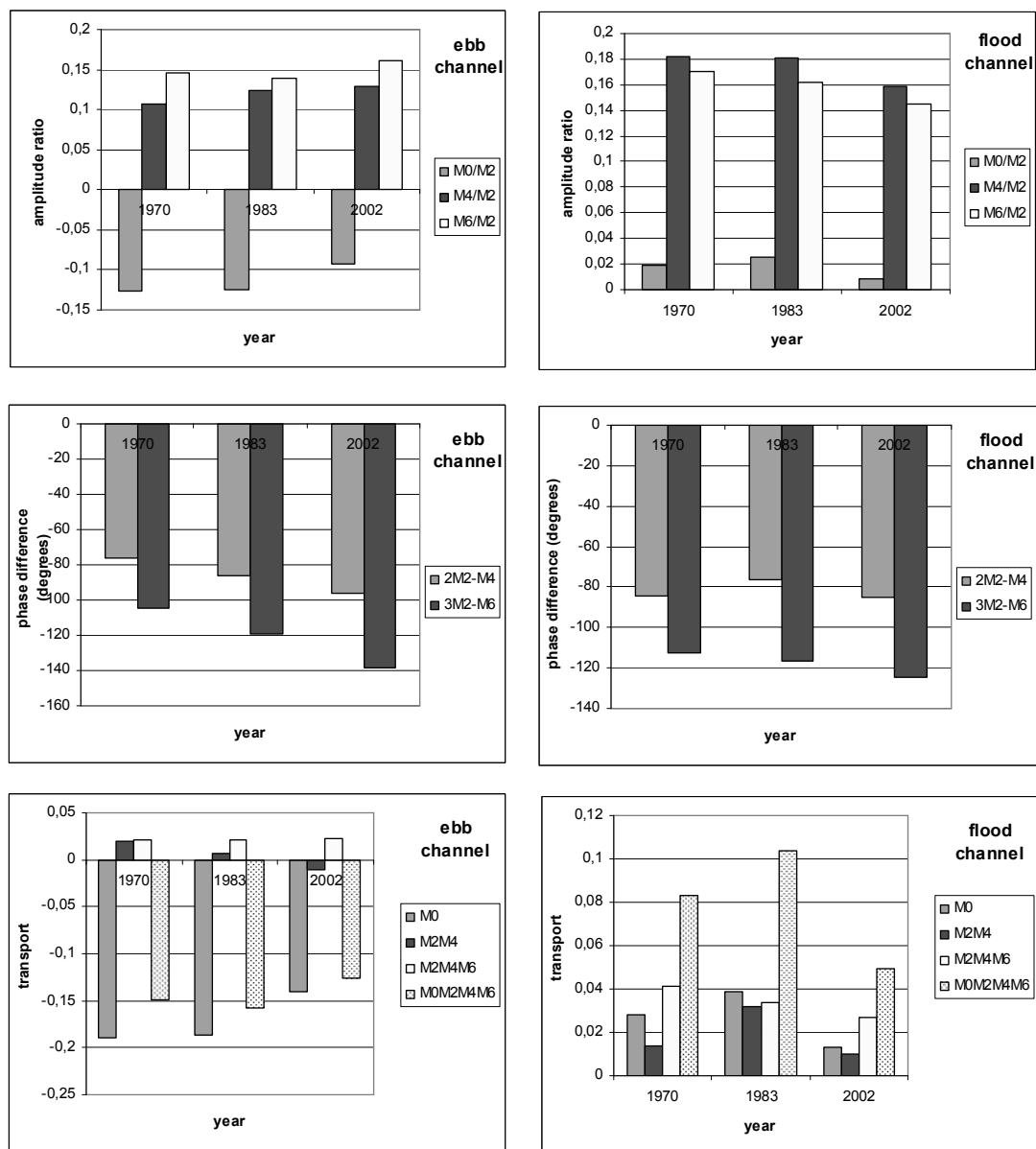


Figure A.8-17: The amplitude ratios M_0/M_2 , M_4/M_2 and M_6/M_2 , and the phase differences $2\varphi_2-\varphi_4$ and $3\varphi_2-\varphi_6$ of the velocity component in the mainstream direction at the observation points in the ebb and flood channel of macro cell 4 derived from the model results for the years 1970, 1983 and 2002, together with the contribution to the bedload transport.

A.8.2.4 Macro Cell 5

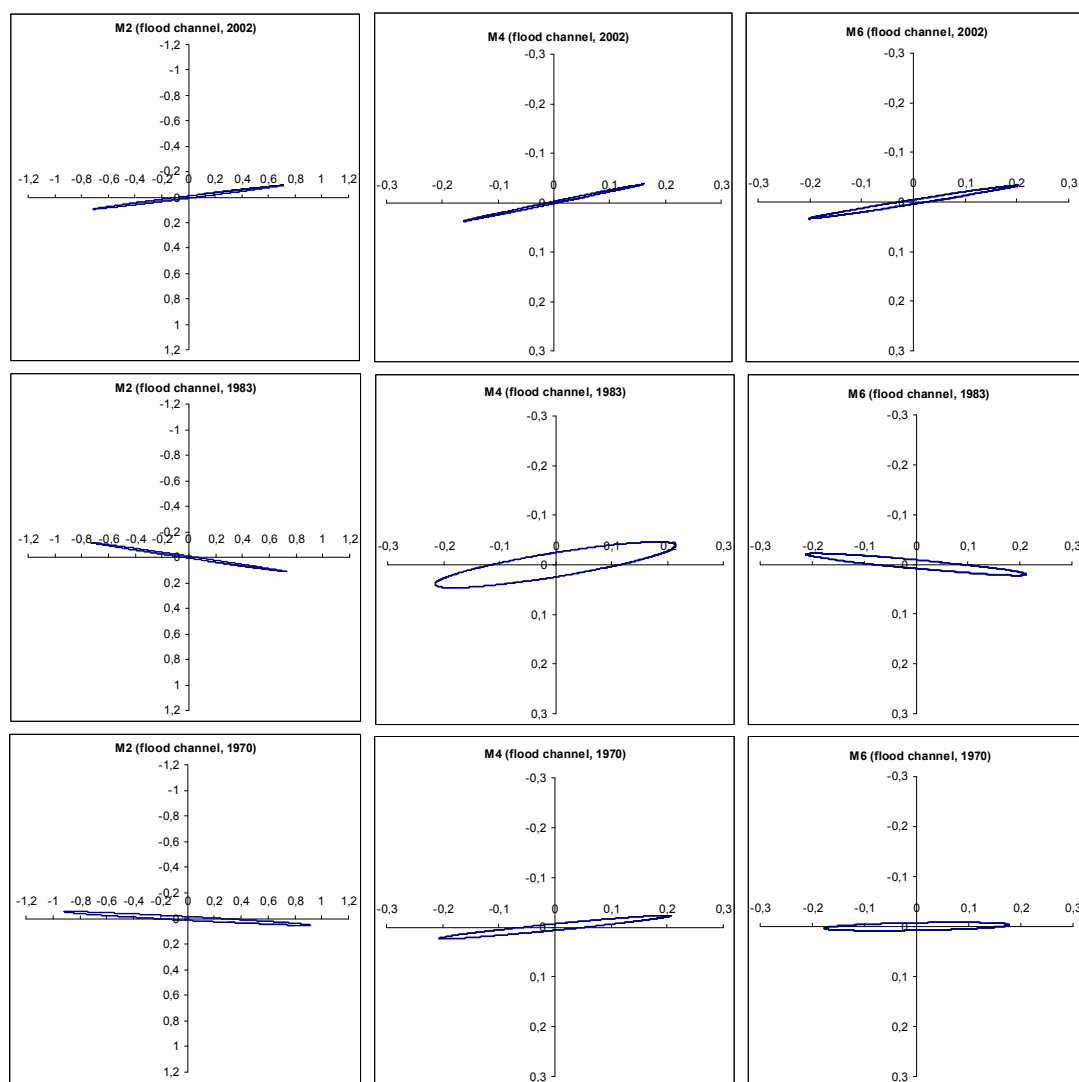


Figure A.8-18: Tidal ellipses for the M_2 , M_4 and M_6 tidal constituents derived from the model results for the velocity in the years 1970, 1983 and 2002 for the observation point in the flood channel of macro cell 5 (velocities in m/s).

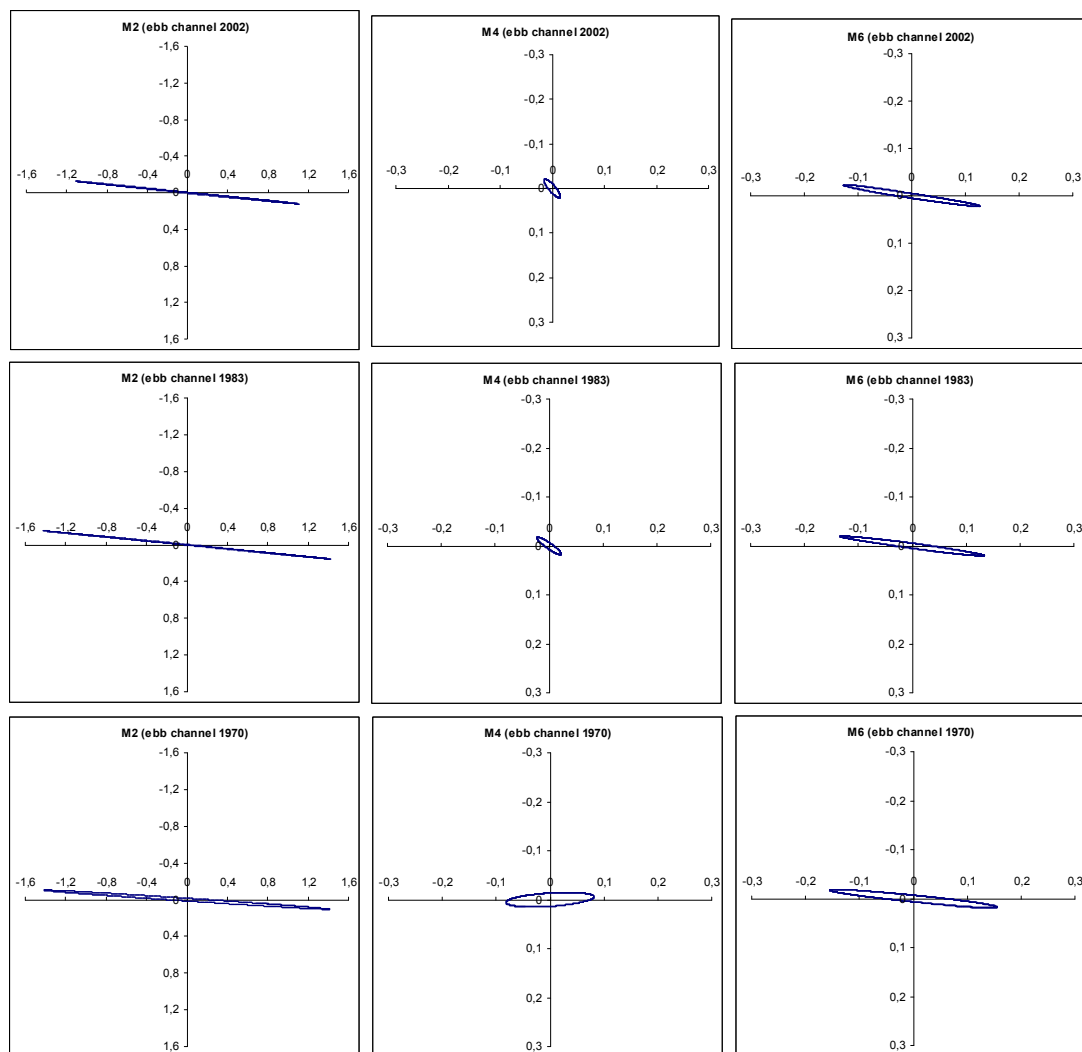


Figure A.8-19: Tidal ellipses for the M_2 , M_4 and M_6 tidal constituents derived from the model for 1970, 1983 and 2002 for the observation point in the ebb channel of macro cell 5 (velocities in m/s).

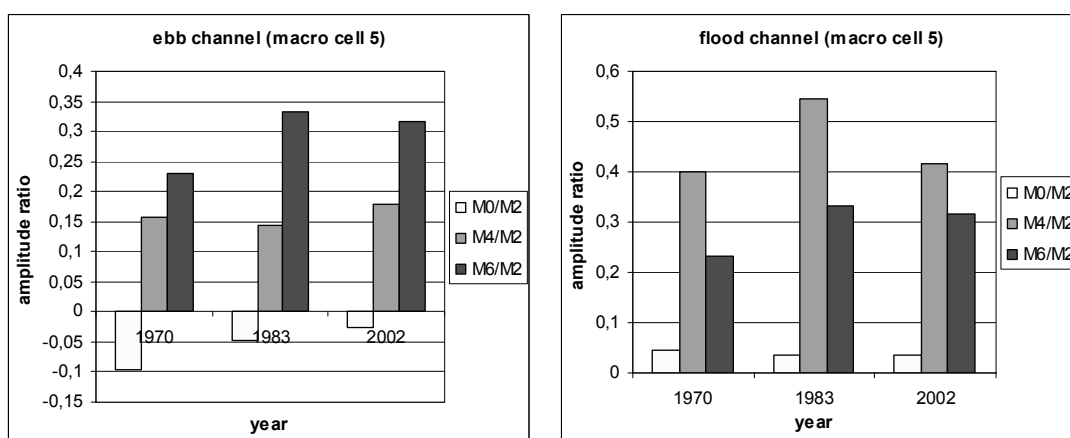


Figure A.8-20: The amplitude ratios M_0/M_2 , M_4/M_2 and M_6/M_2 for the discharge through the ebb and flood channel of macro cell 5 derived from the model results for 1970, 1983 and 2002.

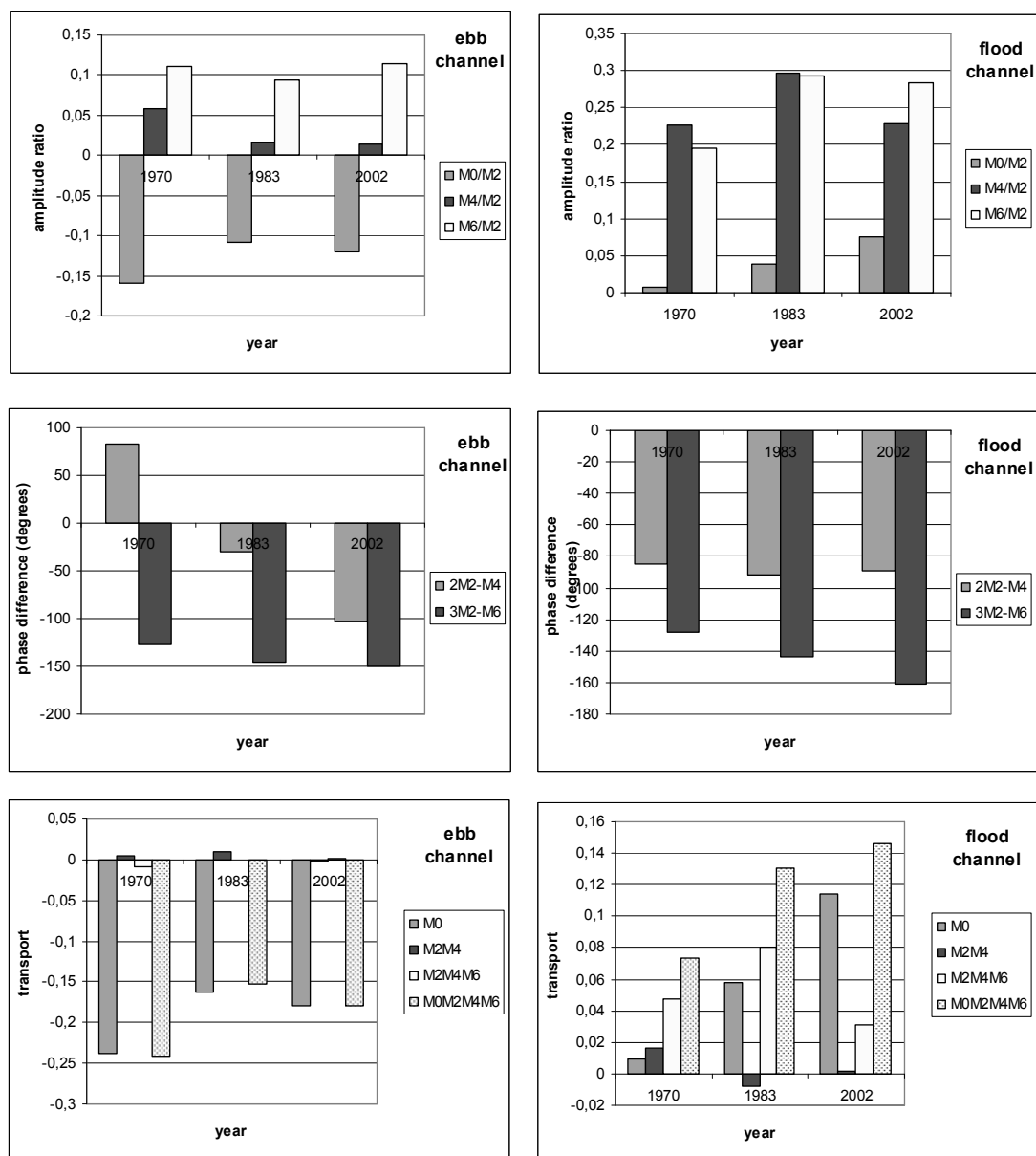


Figure A.8-21: The amplitude ratios M_0/M_2 , M_4/M_2 and M_6/M_2 , and the phase differences $2\phi_2-\phi_4$ and $3\phi_2-\phi_6$ of the velocity component in the mainstream direction at the observation points in the ebb and flood channel of macro cell 5 derived from the model results for the years 1970, 1983 and 2002, together with the contribution to the bedload transport.

A.8.2.5 Macro Cell 7

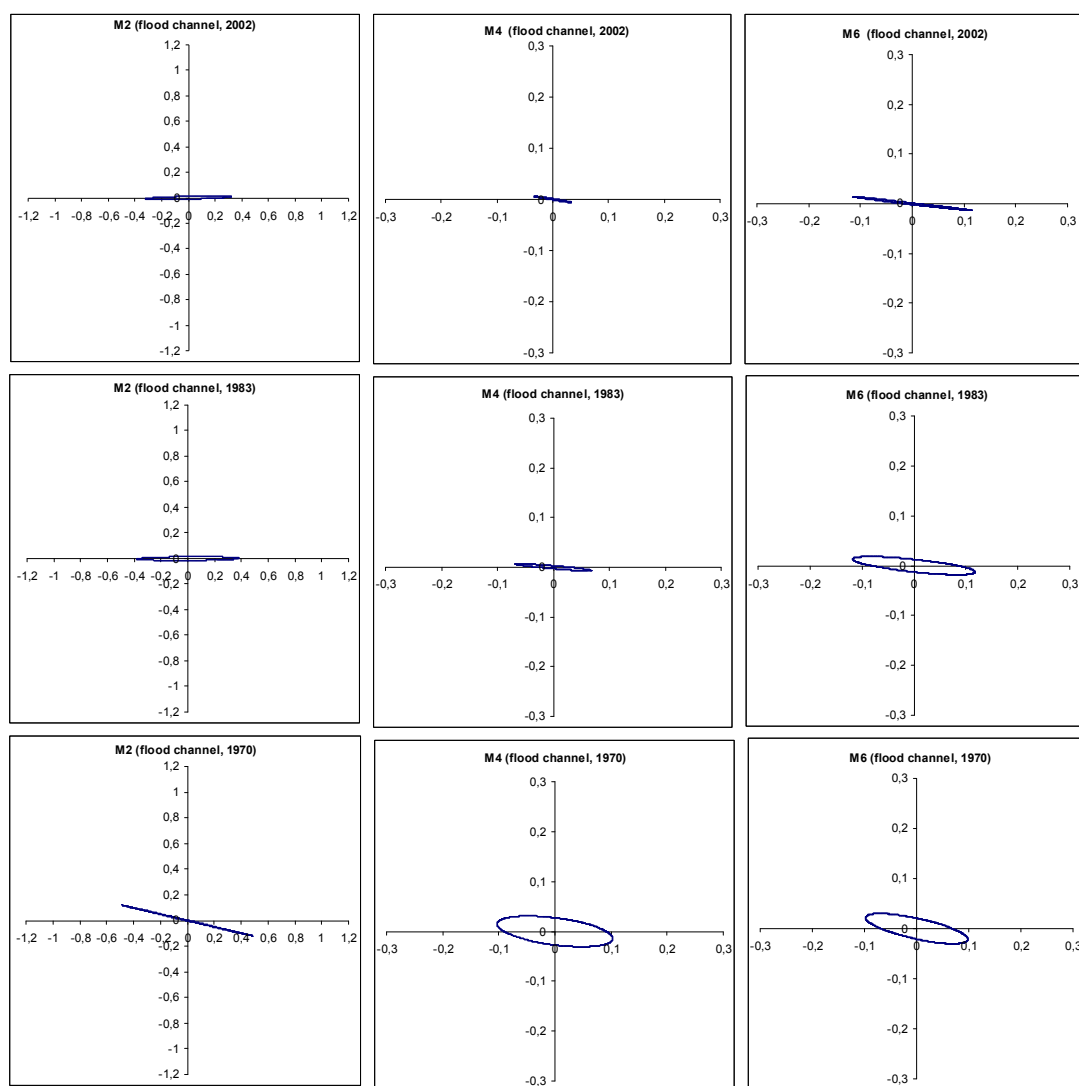


Figure A.8-22: Tidal ellipses for the M_2 , M_4 and M_6 tidal constituents derived from the model results for the velocity in the years 1970, 1983 and 2002 for the observation point in the flood channel of macro cell 7 (velocities in m/s).

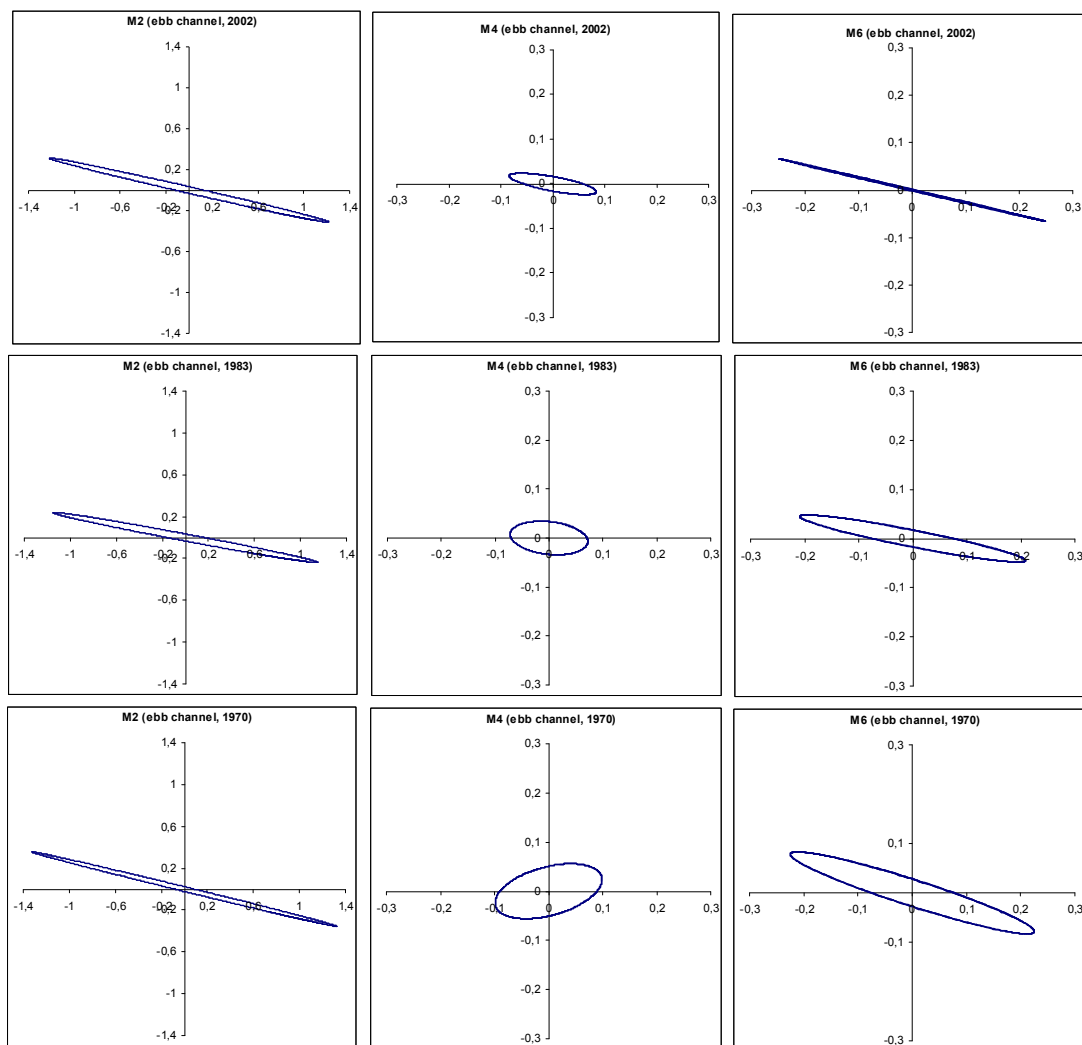


Figure A.8-23: Tidal ellipses for the M_2 , M_4 and M_6 tidal constituents derived from the model for 1970, 1983 and 2002 for the observation point in the ebb channel of macro cell 7 (velocities in m/s).

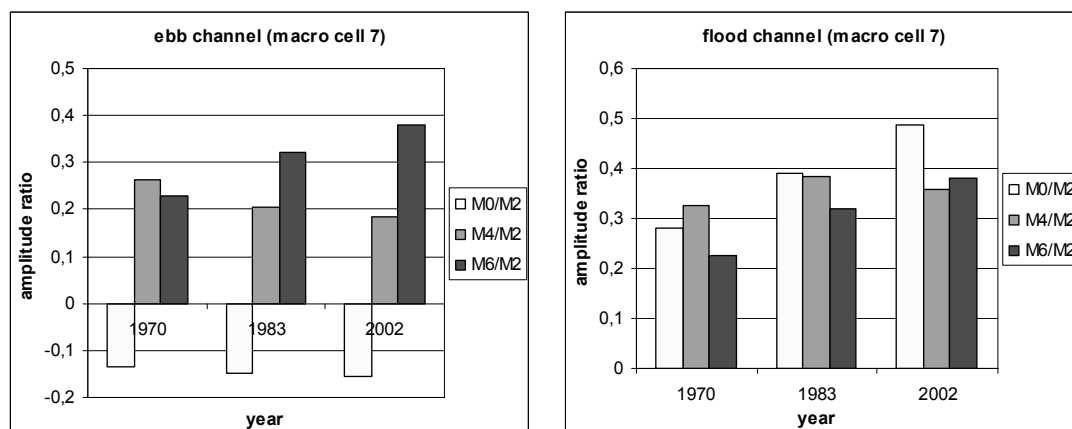


Figure A.8-24: The amplitude ratios M_0/M_2 , M_4/M_2 and M_6/M_2 for the discharge through the ebb and flood channel of macro cell 7 derived from the model for 1970, 1983 and 2002.

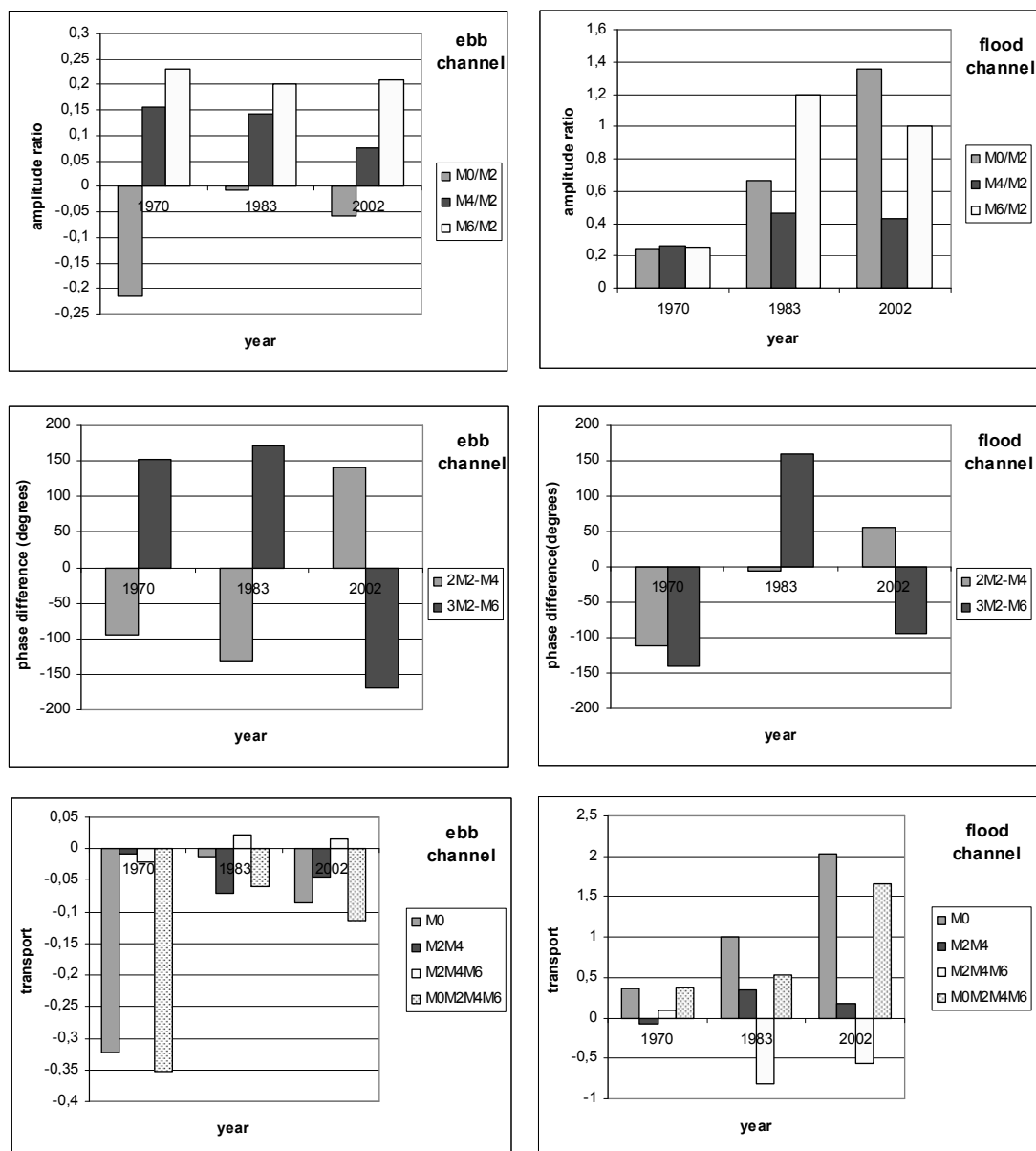


Figure A.8-25: The amplitude ratios M_0/M_2 , M_4/M_2 and M_6/M_2 , and the phase differences $2\phi_2-\phi_4$ and $3\phi_2-\phi_6$ of the velocity component in the mainstream direction at the observation points in the ebb and flood channel of macro cell 7 derived from the model results for the years 1970, 1983 and 2002, together with the contribution to the bedload transport.

A.8.3 Values of the Amplitude and Phase of the Velocity and the Direction of the Principal Axis Relative to the Mainstream Direction in Every Observation Point

Table A.8-2: Values of the amplitude of the velocity in the observation points.

amplitude (m/s) (for cells 1-6: n = the main stream direction, m = perpendicular to the main stream, cell 7: the other way around)		M0		M2		M4		M6		
		m	n	m	n	m	n	m	n	
cell 1	ebb channel	2002	0.02	0.18	0.13	1.18	0.01	0.03	0.01	0.15
		1983	0.02	0.15	0.12	1.13	0.01	0.04	0.00	0.16
		1970	0.02	0.15	0.13	1.12	0.01	0.04	0.00	0.16
	flood channel	2002	0.03	0.10	0.15	0.91	0.05	0.20	0.02	0.15
		1983	0.02	0.09	0.18	0.89	0.05	0.19	0.02	0.14
		1970	0.02	0.10	0.17	0.84	0.05	0.21	0.02	0.14
cell 3	ebb channel	2002	0.02	0.11	0.22	1.10	0.02	0.14	0.02	0.14
		1983	0.01	0.08	0.20	1.08	0.03	0.15	0.02	0.15
		1970	0.01	0.09	0.20	1.11	0.03	0.14	0.03	0.16
	flood channel	2002	0.01	0.03	0.03	1.13	0.02	0.21	0.01	0.19
		1983	0.01	0.03	0.01	1.15	0.02	0.18	0.00	0.18
		1970	0.01	0.05	0.03	1.16	0.02	0.17	0.01	0.19
cell 4	ebb channel	2002	0.01	0.09	0.14	0.99	0.02	0.13	0.02	0.16
		1983	0.00	0.13	0.17	1.04	0.03	0.13	0.02	0.14
		1970	0.00	0.13	0.14	1.00	0.02	0.11	0.02	0.15
	flood channel	2002	0.01	0.01	0.22	1.26	0.04	0.20	0.03	0.18
		1983	0.01	0.03	0.21	1.25	0.03	0.23	0.03	0.20
		1970	0.01	0.02	0.23	1.12	0.04	0.20	0.03	0.19
cell 5	ebb channel	2002	0.01	0.13	0.13	1.11	0.02	0.02	0.02	0.13
		1983	0.00	0.15	0.15	1.42	0.02	0.02	0.02	0.13
		1970	0.02	0.23	0.11	1.41	0.02	0.08	0.02	0.16
	flood channel	2002	0.02	0.05	0.10	0.71	0.04	0.16	0.03	0.20
		1983	0.04	0.03	0.11	0.73	0.05	0.22	0.02	0.21
		1970	0.02	0.01	0.05	0.92	0.02	0.21	0.01	0.18
cell 6	ebb channel	2002	0.06	0.25	0.33	1.07	0.00	0.01	0.03	0.14
		1983	0.06	0.24	0.33	1.10	0.01	0.05	0.03	0.14
		1970	0.08	0.29	0.32	1.04	0.03	0.06	0.03	0.13
	flood channel	2002	0.03	0.17	0.01	0.75	0.02	0.18	0.01	0.27
		1983	0.04	0.16	0.02	0.77	0.01	0.20	0.01	0.22
		1970	0.02	0.11	0.14	0.86	0.02	0.23	0.01	0.14
cell 7	ebb channel	2002	0.21	0.02	1.22	0.31	0.08	0.02	0.25	0.07
		1983	0.21	0.00	1.15	0.24	0.07	0.03	0.21	0.05
		1970	0.26	0.08	1.33	0.36	0.10	0.06	0.23	0.08
	flood channel	2002	0.18	0.02	0.32	0.01	0.03	0.01	0.12	0.01
		1983	0.20	0.01	0.38	0.02	0.07	0.01	0.12	0.02
		1970	0.19	0.03	0.49	0.12	0.10	0.03	0.10	0.03

Table A.8-3: Values of the phase of the velocity in the observation points.

phase (degrees) (for cells 1-6: n = the main stream direction, m = perpendicular to the main stream, cell 7: the other way around)	M0		M2		M4		M6	
	m	n	m	n	m	n	m	n
cell 1 ebb channel	2002	0,0	180,0	145,7	100,0	-102,1	87,4	-61,8
	1983	0,0	180,0	149,1	75,0	-88,9	26,0	-56,6
	1970	0,0	180,0	145,6	59,7	-95,7	102,8	-52,1
flood channel	2002	180,0	0,0	134,1	-170,1	-10,1	142,3	-54,0
	1983	180,0	0,0	134,9	-168,9	-10,7	148,6	-51,3
	1970	180,0	0,0	137,3	-169,4	-11,0	143,0	-53,4
cell 3 ebb channel	2002	180,0	180,0	-33,6	18,2	8,8	-22,0	-14,7
	1983	180,0	180,0	-34,2	9,6	4,0	-19,2	-17,6
	1970	180,0	180,0	-33,5	12,0	8,4	-16,9	-17,5
flood channel	2002	180,0	0,0	132,9	161,1	0,0	-174,4	-11,3
	1983	180,0	180,0	-106,5	139,4	-0,4	-130,3	-10,0
	1970	180,0	180,0	161,2	133,1	1,5	-132,3	-10,3
cell 4 ebb channel	2002	180,0	180,0	143,2	-163,7	8,4	-165,1	7,0
	1983	180,0	180,0	150,0	-168,3	9,3	-171,6	3,9
	1970	180,0	180,0	153,1	-171,3	4,3	-179,4	-3,3
flood channel	2002	0,0	180,0	144,7	-161,6	14,0	-159,0	17,9
	1983	0,0	0,0	145,0	-165,7	9,1	-164,8	15,3
	1970	0,0	0,0	146,8	-152,8	16,9	-163,8	12,0
cell 5 ebb channel	2002	0,0	180,0	-29,4	18,2	49,2	56,3	69,1
	1983	180,0	180,0	-23,5	8,1	-14,6	64,2	78,9
	1970	0,0	180,0	-28,4	-10,4	-123,3	45,4	67,1
flood channel	2002	180,0	0,0	142,4	-179,4	3,6	-155,7	31,9
	1983	180,0	0,0	-34,0	164,2	16,3	53,6	30,1
	1970	180,0	0,0	-13,7	-170,1	25,4	154,5	39,7
cell 6 ebb channel	2002	0,0	180,0	164,2	-54,9	175,9	-57,4	105,3
	1983	0,0	180,0	163,8	110,2	-73,6	-48,5	121,2
	1970	0,0	180,0	168,8	109,7	-70,9	-7,4	141,8
flood channel	2002	180,0	0,0	109,7	-157,6	9,8	-110,9	69,9
	1983	180,0	0,0	-50,5	31,8	22,1	-114,6	76,5
	1970	180,0	0,0	155,5	28,7	27,2	-20,3	87,7
cell 7 ebb channel	2002	180,0	180,0	-24,6	45,9	-177,2	113,3	-65,4
	1983	180,0	0,0	-20,8	4,6	106,6	130,6	-28,4
	1970	180,0	0,0	-16,0	4,3	69,6	150,4	-9,9
flood channel	2002	0,0	180,0	-23,9	-23,6	145,8	43,9	-142,4
	1983	0,0	180,0	-13,5	-24,8	179,9	56,2	-79,1
	1970	0,0	180,0	-8,7	-19,3	98,4	74,5	-61,2

Table A.8-4: Direction of the principal axis of the tidal ellipse in the observation points, relative to the mainstream direction.

theta (degrees)				M2	M4	M6
cell 1	ebb channel	De Honte	2002	0,7	1,4	0,1
			1983	0,6	4,2	0,0
			1970	0,8	4,2	0,0
	flood channel	Schaar van Spijkerplaat	2002	1,6	3,1	1,5
			1983	2,3	3,8	1,7
			1970	2,5	2,9	1,1
cell 3	ebb channel	Pas van Terneuzen	2002	-2,4	-1,3	-1,4
			1983	-2,1	-2,2	-1,1
			1970	-2,0	-2,1	-1,4
	flood channel	Everingen	2002	0,0	0,6	0,2
			1983	0,0	0,4	0,0
			1970	0,0	0,3	0,1
cell 4	ebb channel	Gat van Ossensisse	2002	1,1	1,6	1,0
			1983	1,6	3,3	1,4
			1970	1,1	1,7	1,1
	flood channel	Middelgat	2002	1,8	1,9	1,5
			1983	1,6	1,1	0,9
			1970	2,5	1,8	1,4
cell 5	ebb channel	Zuidergat	2002	-0,7	38,1	-1,9
			1983	-0,7	-35,5	-1,3
			1970	-0,3	0,8	-0,8
	flood channel	Schaar van Waarde	2002	1,0	3,3	1,7
			1983	-1,4	2,3	-0,6
			1970	-0,2	0,8	0,0
cell 6	ebb channel	Nauw van bath	2002	5,8	7,9	3,5
			1983	5,7	4,3	2,7
			1970	5,7	21,7	2,5
	flood channel	Schaar van Noord	2002	0,0	0,6	0,2
			1983	0,0	-0,2	0,1
			1970	1,5	-0,3	0,2
cell 7	ebb channel	Vaarwater boven Bath	2002	4,0	3,7	4,3
			1983	2,6	3,4	3,0
			1970	4,4	-10,7	8,3
	flood channel	Appelzak	2002	-0,1	1,8	0,9
			1983	0,0	0,6	1,0
			1970	3,7	2,6	4,2

A.8.4 Values of the Amplitude and Phase of the Discharge through the Cross-sections in the Ebb and Flood Channel in Every Macro Cell

Table A.8-5: Amplitude and amplitude ratio of the discharge through the cross-sections in the ebb and flood channel in every macro cell.

discharges through channel cross sections			amplitude (m ³ /s)				amplitude ratio		
		year	M0	M2	M4	M6	M0/M2	M4/M2	M6/M2
macro cell 1	ebb channel	2002	-3809	26301	2179	3572	-0,14	0,08	0,14
		1983	-3324	26434	2699	4007	-0,13	0,10	0,15
		1970	-3604	25664	2842	4771	-0,14	0,11	0,19
	flood channel	2002	1300	46159	11645	7495	0,03	0,25	0,16
		1983	914	43530	10106	5368	0,02	0,23	0,12
		1970	2259	43340	10689	6660	0,05	0,25	0,15
macro cell 3	ebb channel	2002	-1615	22678	4337	3557	-0,07	0,19	0,16
		1983	-1382	22325	4627	3826	-0,06	0,21	0,17
		1970	-1783	22028	4121	3903	-0,08	0,19	0,18
	flood channel	2002	2327	29055	5145	6359	0,08	0,18	0,22
		1983	652	25311	6477	4966	0,03	0,26	0,20
		1970	17	22331	5577	4981	0,00	0,25	0,22
macro cell 4	ebb channel	2002	-623	13723	3544	2965	-0,05	0,26	0,22
		1983	-1013	16535	3825	3186	-0,06	0,23	0,19
		1970	-1448	17618	3982	3683	-0,08	0,23	0,21
	flood channel	2002	506	24368	5620	4495	0,02	0,23	0,18
		1983	906	20620	5356	4054	0,04	0,26	0,20
		1970	850	17270	4794	3816	0,05	0,28	0,22
macro cell 5	ebb channel	2002	-407	16426	2928	2752	-0,02	0,18	0,17
		1983	-770	16282	2354	2717	-0,05	0,14	0,17
		1970	-1175	12317	1927	1629	-0,10	0,16	0,13
	flood channel	2002	309	8807	3675	2789	0,04	0,42	0,32
		1983	256	7357	4015	2445	0,03	0,55	0,33
		1970	454	9839	3938	2272	0,05	0,40	0,23
macro cell 6	ebb channel	2002	-373	10433	1599	1960	-0,04	0,15	0,19
		1983	-508	10728	1333	1775	-0,05	0,12	0,17
		1970	-1084	8581	1062	1096	-0,13	0,12	0,13
	flood channel	2002	699	5446	1893	1906	0,13	0,35	0,35
		1983	802	5177	2345	1615	0,15	0,45	0,31
		1970	1093	6382	2868	1676	0,17	0,45	0,26
macro cell 7	ebb channel	2002	-1753	11223	2076	2603	-0,16	0,18	0,23
		1983	-1572	10529	2144	2187	-0,15	0,20	0,21
		1970	-1277	9511	2518	1927	-0,13	0,26	0,20
	flood channel	2002	1739	3573	1277	1359	0,49	0,36	0,38
		1983	1509	3878	1483	1244	0,39	0,38	0,32
		1970	1098	3923	1277	892	0,28	0,33	0,23

Table A.8-6: Phase and phase difference of the discharge through the cross-sections in the ebb and flood channel in every macro cell.

discharges through channel cross sections		year	phase (degrees)			phase difference (degrees)	
			phase M2	phase M4	phase M6	$2\varphi_2 - \varphi_4$	$3\varphi_2 - \varphi_6$
macro cell 1	ebb channel	2002	-55	-40	-70	-70	-94
		1983	-55	-46	-71	-63	-92
		1970	-53	-21	-51	-85	-109
	flood channel	2002	-53	-15	-53	-92	-107
		1983	-53	-22	-63	-83	-95
		1970	-52	-25	-57	-78	-99
macro cell 3	ebb channel	2002	-43	-10	-19	-76	-110
		1983	-42	-11	-20	-73	-104
		1970	-42	-2	-12	-81	-112
	flood channel	2002	-52	-2	-4	-103	-153
		1983	-47	-5	-19	-88	-121
		1970	-48	2	-12	-98	-131
macro cell 4	ebb channel	2002	-46	-6	3	-86	-141
		1983	-41	-4	1	-77	-122
		1970	-39	-1	1	-76	-117
	flood channel	2002	-38	4	14	-81	-130
		1983	-37	4	13	-77	-123
		1970	-36	13	15	-86	-123
macro cell 5	ebb channel	2002	-31	16	56	-77	-148
		1983	-27	19	69	-73	-150
		1970	-24	1	62	-50	-135
	flood channel	2002	-42	5	33	-89	-160
		1983	-38	12	34	-88	-148
		1970	-34	22	41	-89	-142
macro cell 6	ebb channel	2002	-26	26	92	-77	-170
		1983	-20	14	104	-53	-163
		1970	-15	14	124	-45	-170
	flood channel	2002	-32	16	67	-81	-165
		1983	-27	24	75	-78	-157
		1970	-21	29	82	-71	-144
macro cell 7	ebb channel	2002	-30	32	103	-91	-192
		1983	-25	28	113	-78	-188
		1970	-19	34	122	-71	-179
	flood channel	2002	-20	14	60	-53	-118
		1983	-11	18	74	-39	-107
		1970	-9	18	84	-35	-111

A.9 Residual Sediment Transport Patterns

In this Appendix the sediment transport patterns for the years 1970, 1983 and 2002 are given for the western, central and eastern part of the Western Scheldt. Two different transport formulations have been applied: the Van Rijn formulation which distinguishes between suspended load and bedload, and the Engelund Hansen formula for the total load.

The second part shows maps with the differences in direction and magnitude for some situations.

The depth scale for all the maps in the first part of the appendix is shown in Figure A.9-1. The vectors for the Engelund Hansen transport formulation have the same scale when the same area (western, central or eastern part of the Western Scheldt) is considered. The vectors of the suspended load and the bedload derived with the Van Rijn formulation are scaled differently. This is done to make the patterns of the bedload visible, since the calculated bedload is only 3% of the total load. When one transport mode is considered, vectors for the same area have the identical scales.

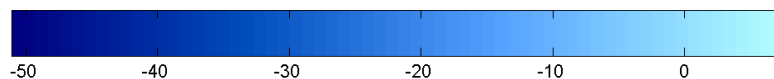


Figure A.9-1: Depth scale (in metres) applicable for all the maps in this appendix.

A.9.1 Residual Sediment Transport Patterns

A.9.1.1 Engelund Hansen Formula

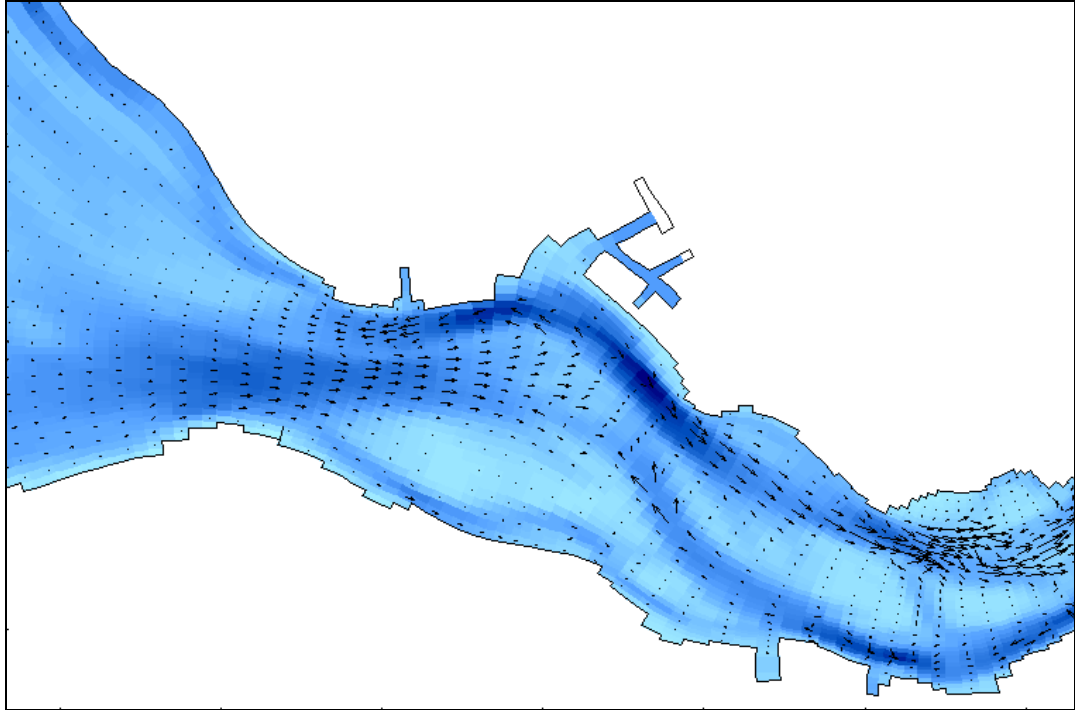


Figure A.9-2: Residual transport patterns in the western part of the Western Scheldt for 1970 as calculated with the Engelund Hansen formulation for the total load.

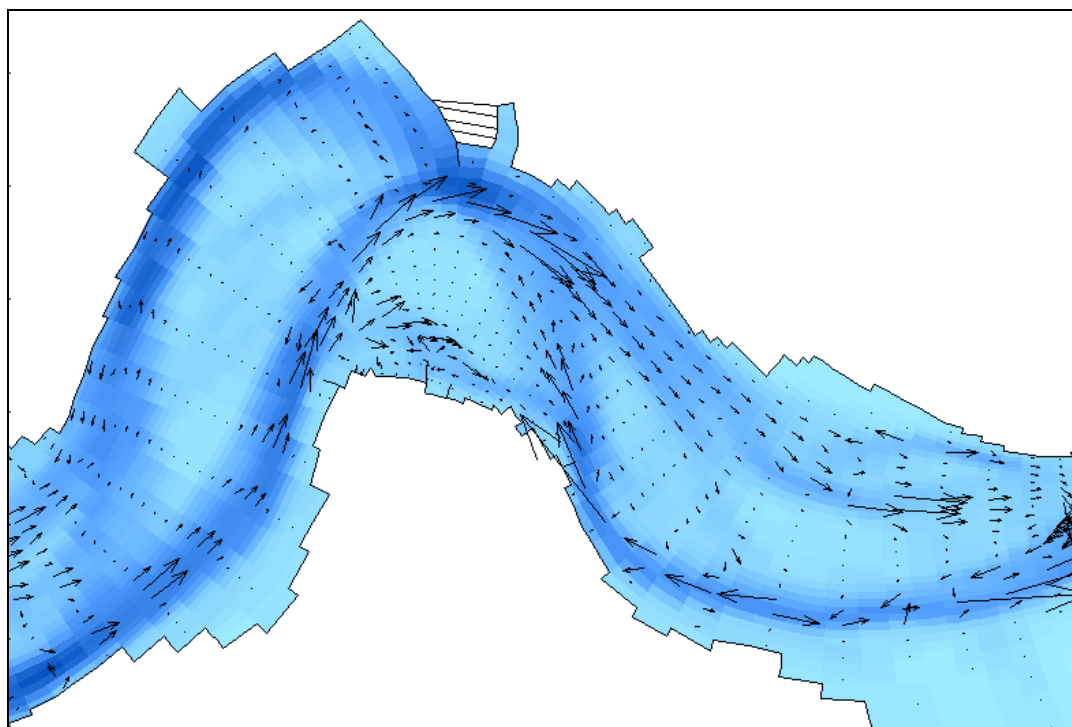


Figure A.9-3: Residual transport patterns in the central part of the Western Scheldt for 1970 as calculated with the Engelund Hansen formulation for the total load.

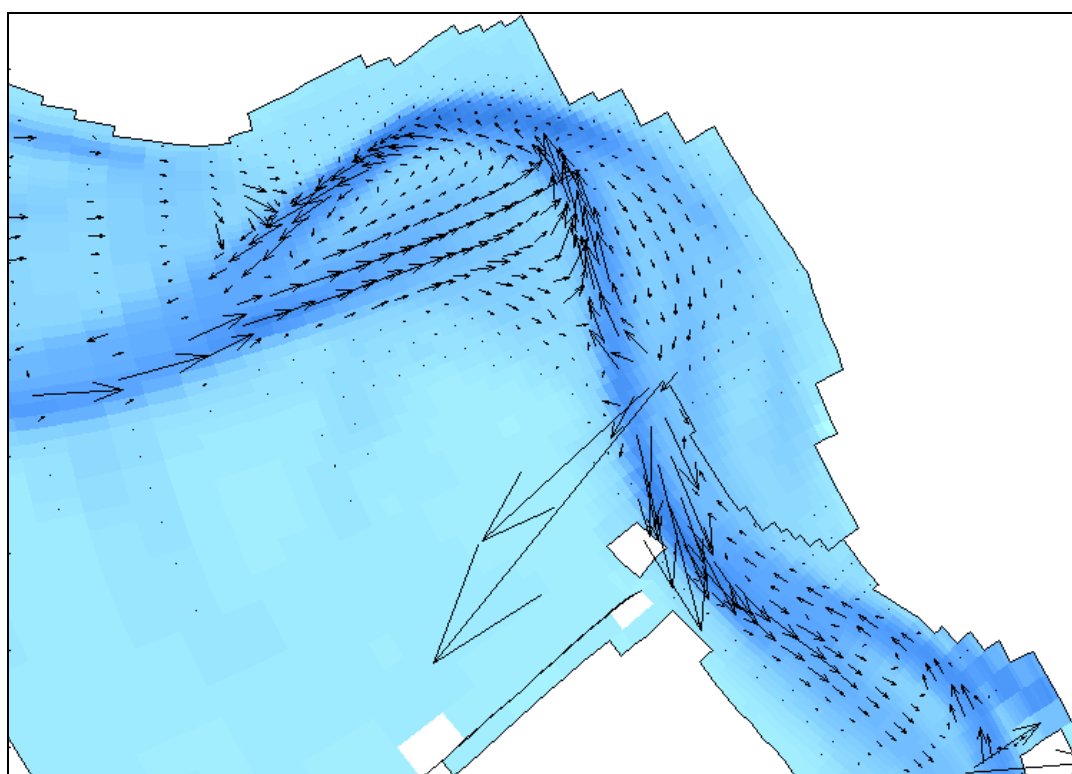


Figure A.9-4: Residual transport patterns in the eastern part of the Western Scheldt for 1970 as calculated with the Engelund Hansen formulation for the total load.

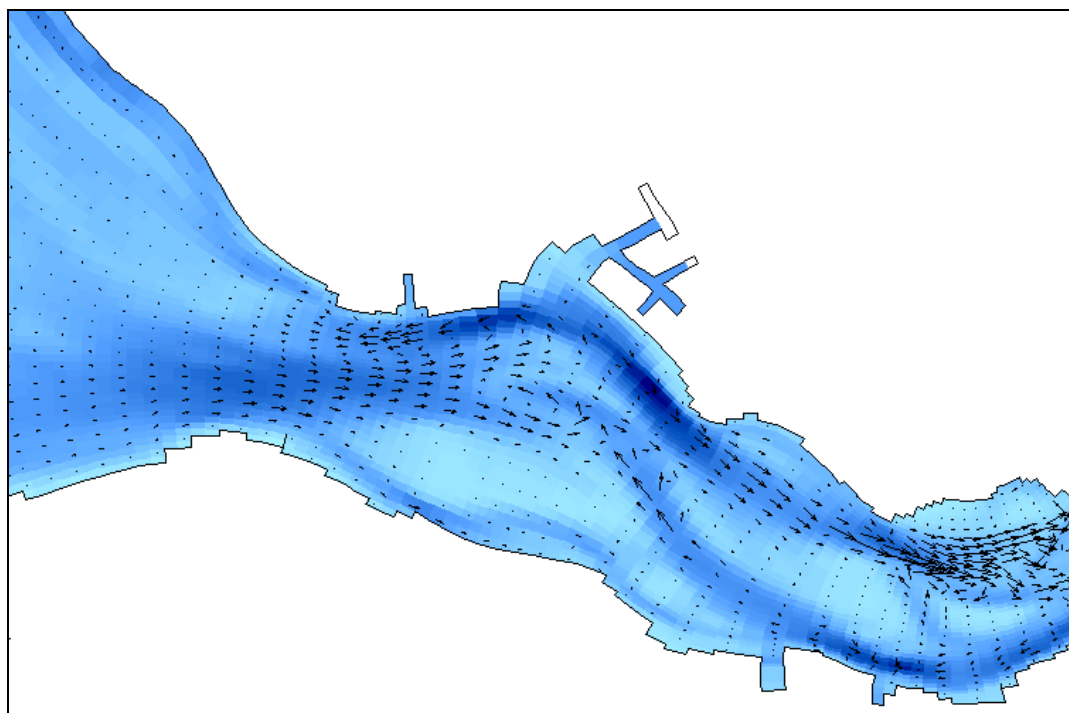


Figure A.9-5: Residual transport patterns in the western part of the Western Scheldt for 1983 as calculated with the Engelund Hansen formulation for the total load.

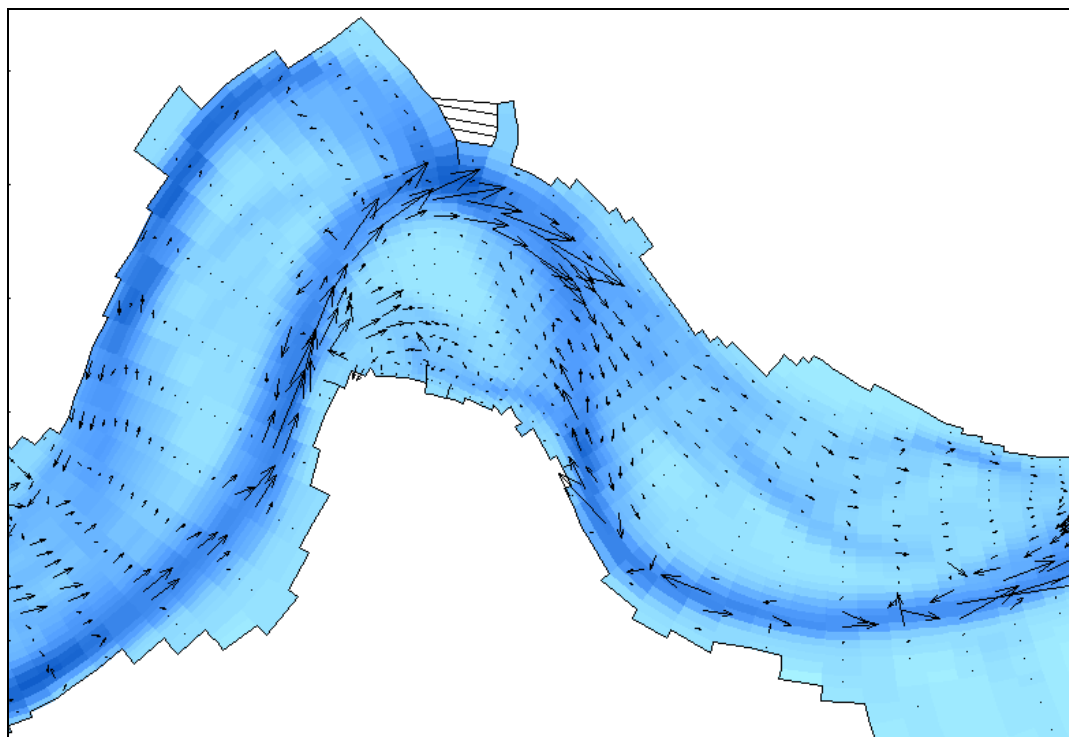


Figure A.9-6: Residual transport patterns in the central part of the Western Scheldt for 1983 as calculated with the Engelund Hansen formulation for the total load.

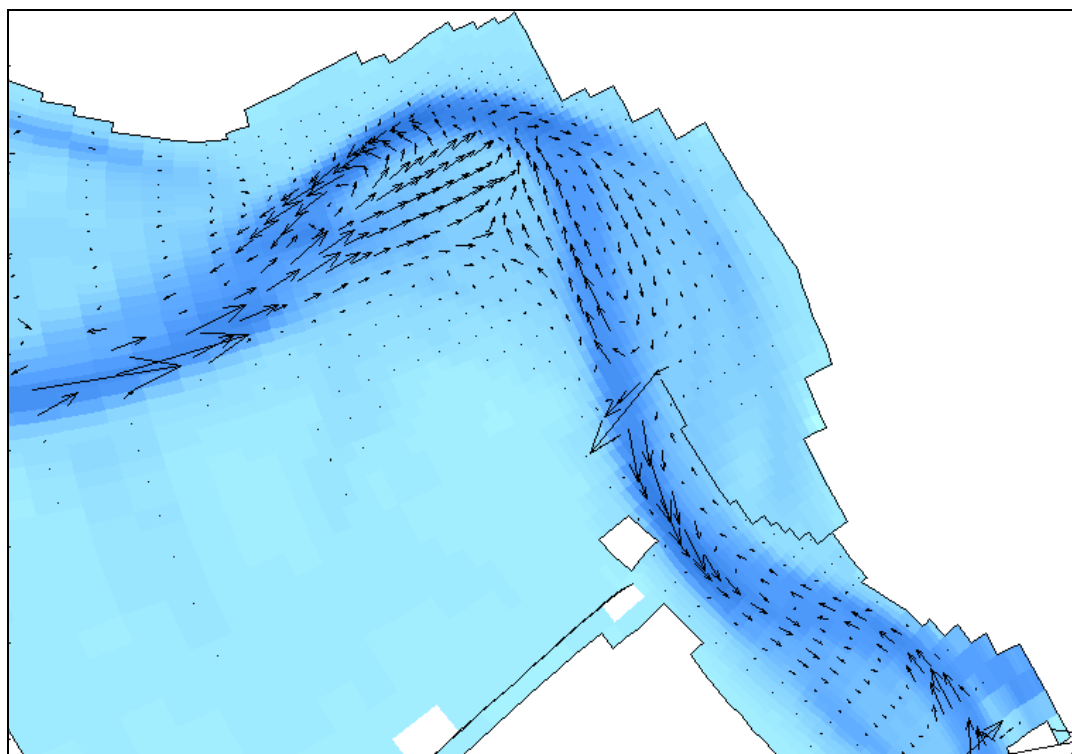


Figure A.9-7: Residual transport patterns in the eastern part of the Western Scheldt for 1983 as calculated with the Engelund Hansen formulation for the total load.

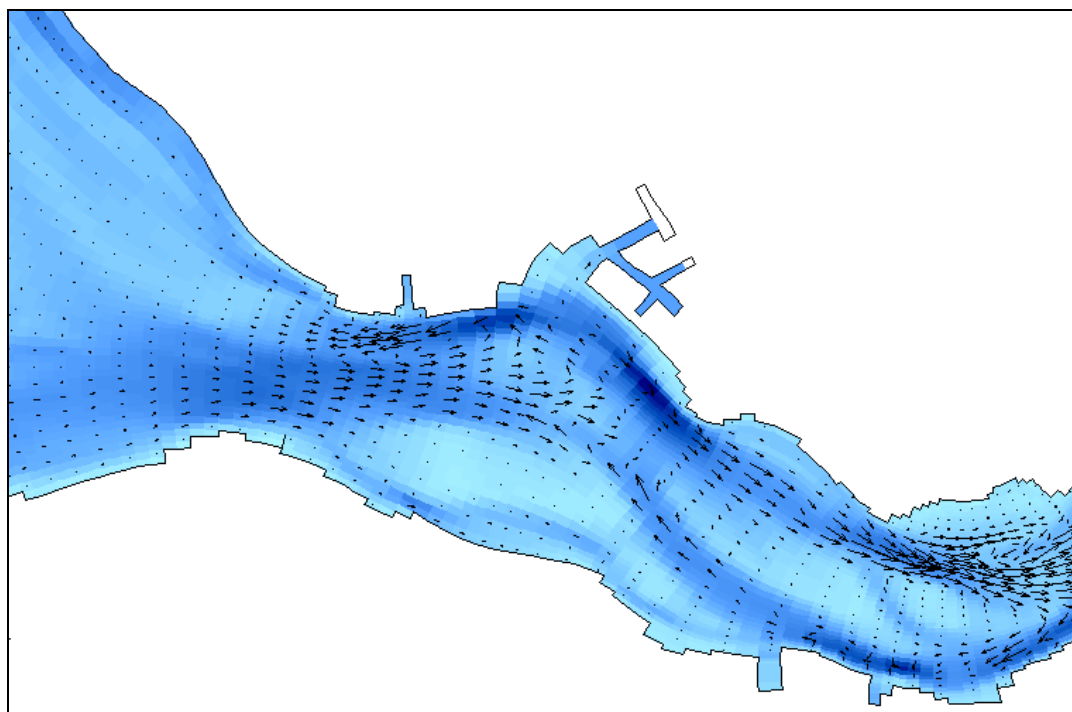


Figure A.9-8: Residual transport patterns in the western part of the Western Scheldt for 2002 as calculated with the Engelund Hansen formulation for the total load.

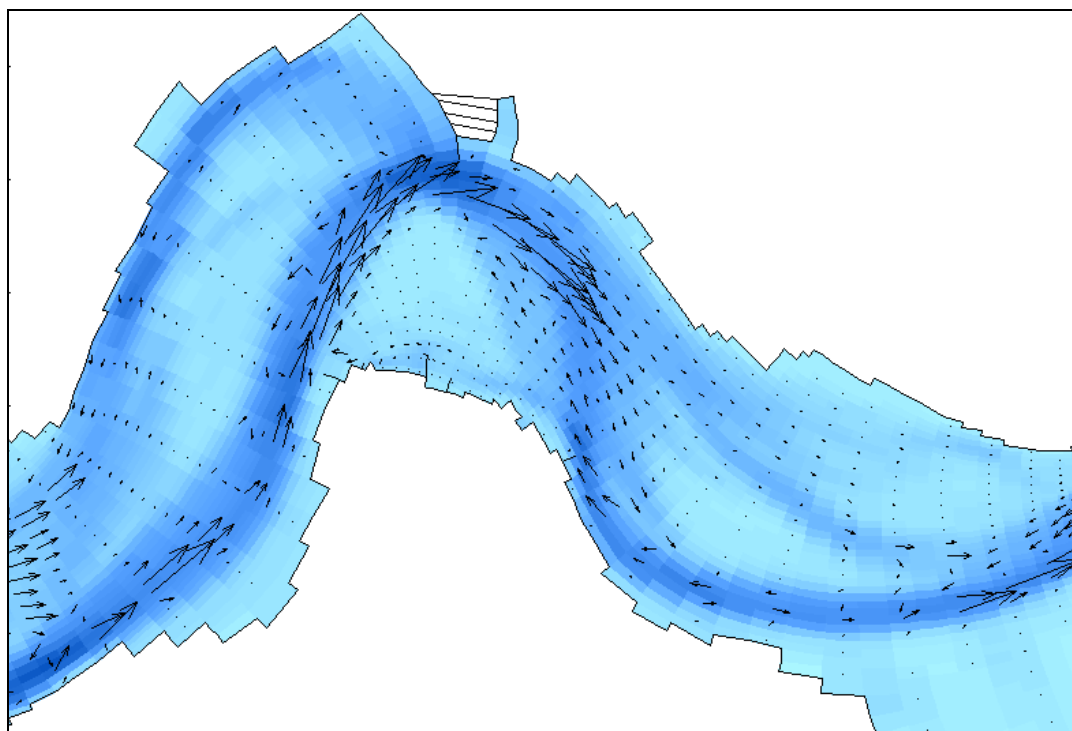


Figure A.9-9: Residual transport patterns in the central part of the Western Scheldt for 2002 as calculated with the Engelund Hansen formulation for the total load.

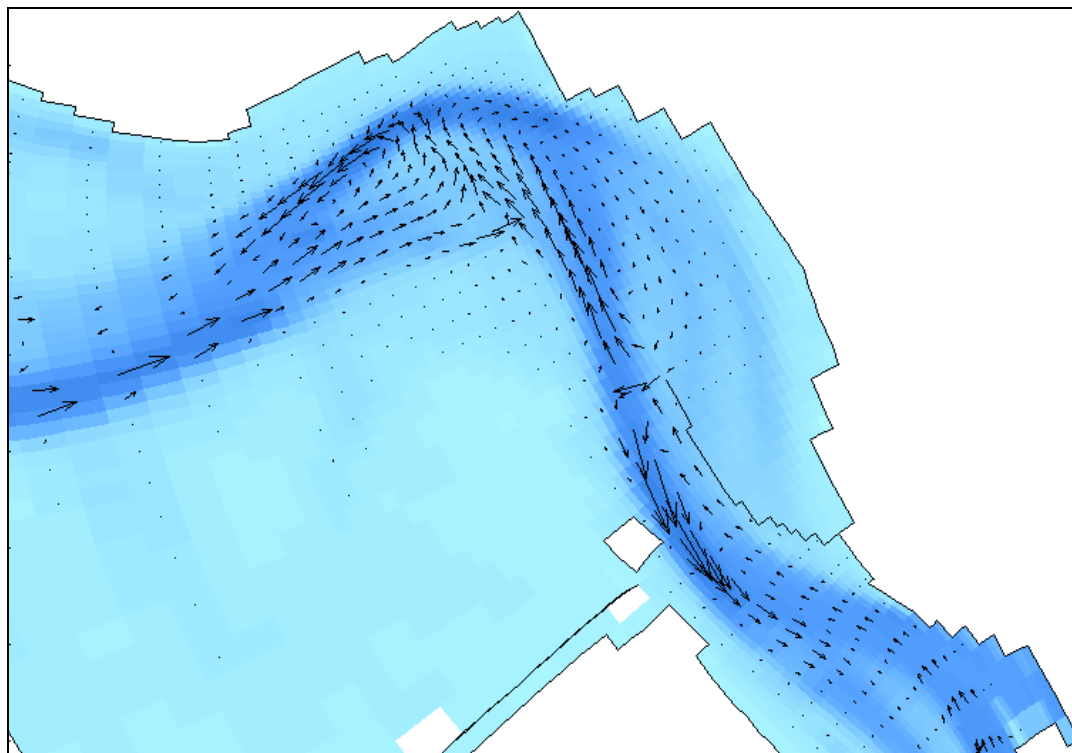


Figure A.9-10: Residual transport patterns in the eastern part of the Western Scheldt for 2002 as calculated with the Engelund Hansen formulation for the total load.

A.9.1.2 Van Rijn Formulation

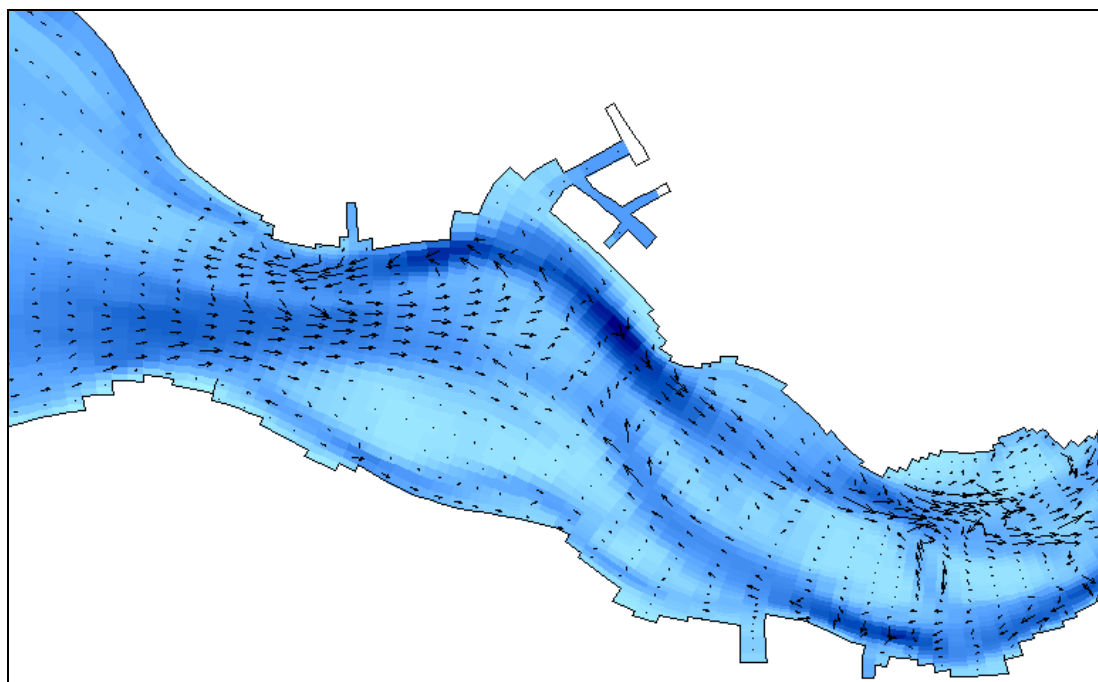


Figure A.9-11: Residual transport patterns in the western part of the Western Scheldt for 1970 as calculated with the Van Rijn formulation for the bedload.

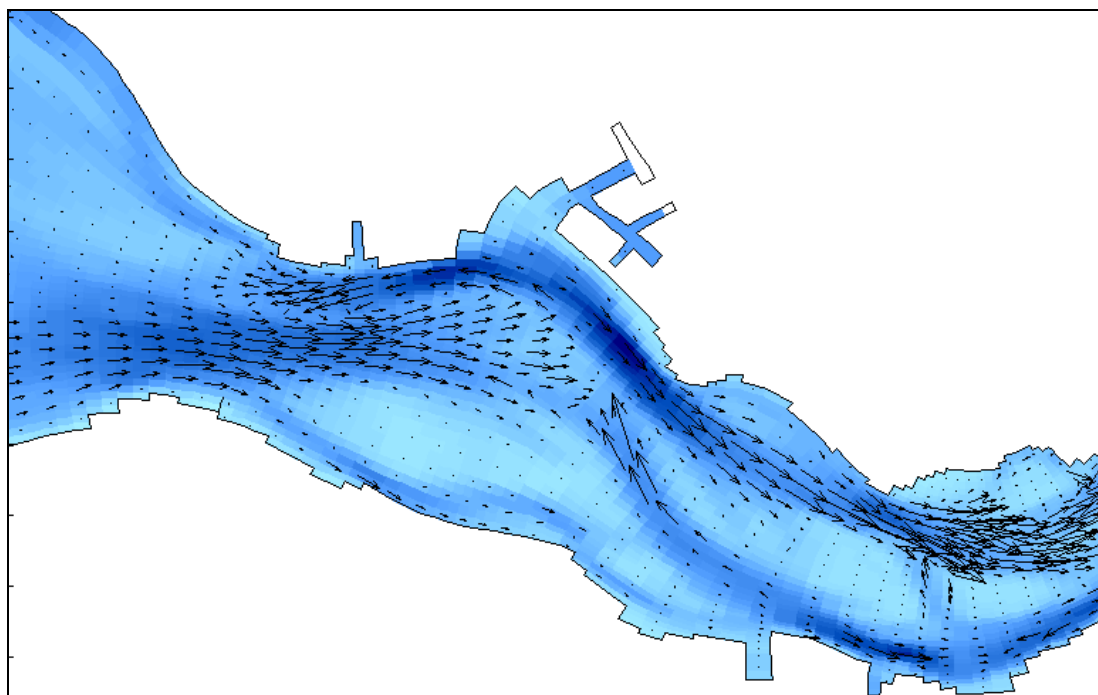


Figure A.9-12: Residual transport patterns in the western part of the Western Scheldt for 1970 as calculated with the Van Rijn formulation for the suspended load.

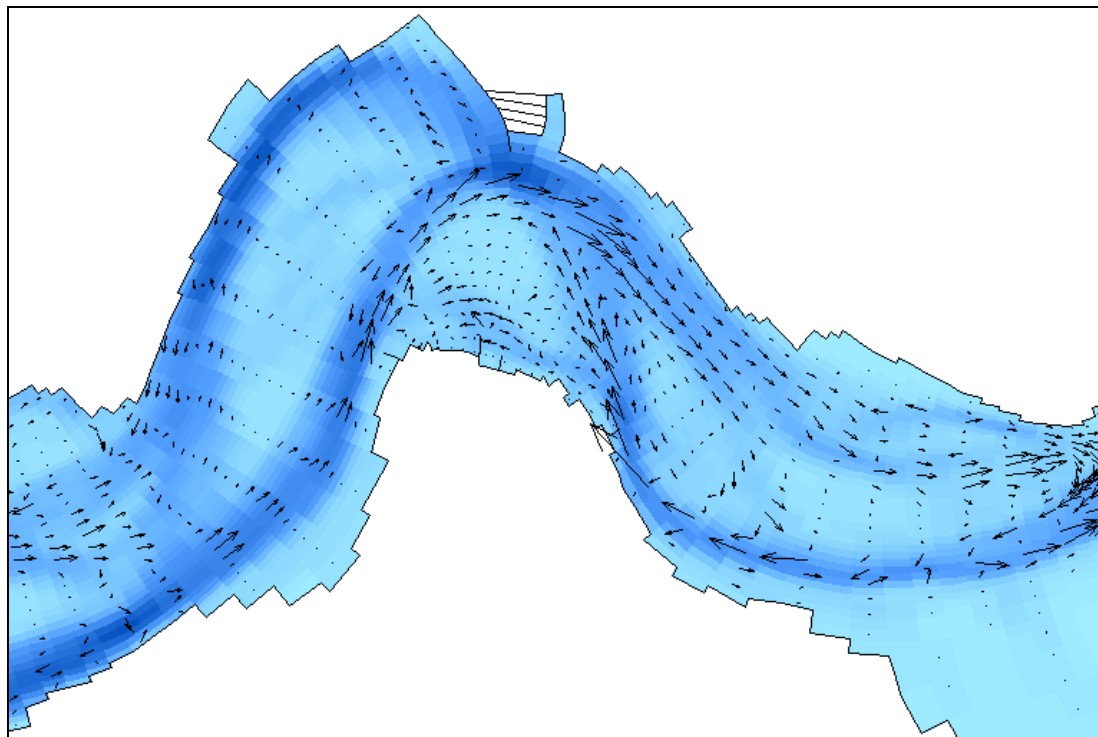


Figure A.9-13: Residual transport patterns in the central part of the Western Scheldt for 1970 as calculated with the Van Rijn formulation for the bedload.

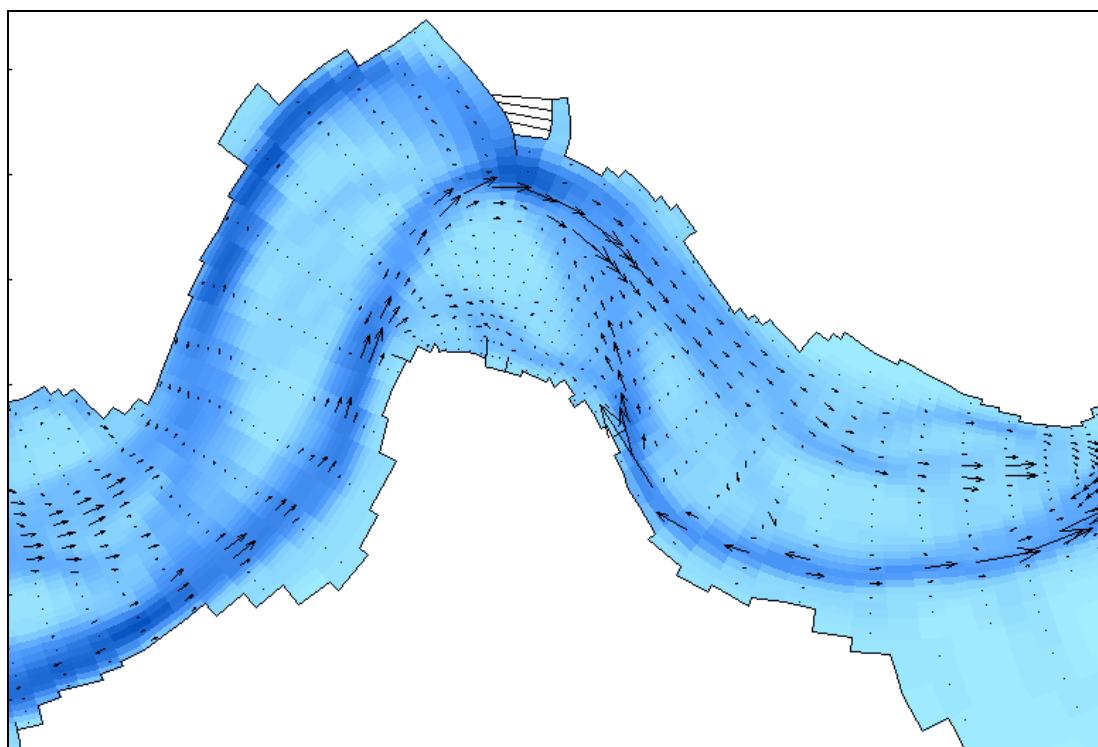


Figure A.9-14: Residual transport patterns in the central part of the Western Scheldt for 1970 as calculated with the Van Rijn formulation for the suspended load.

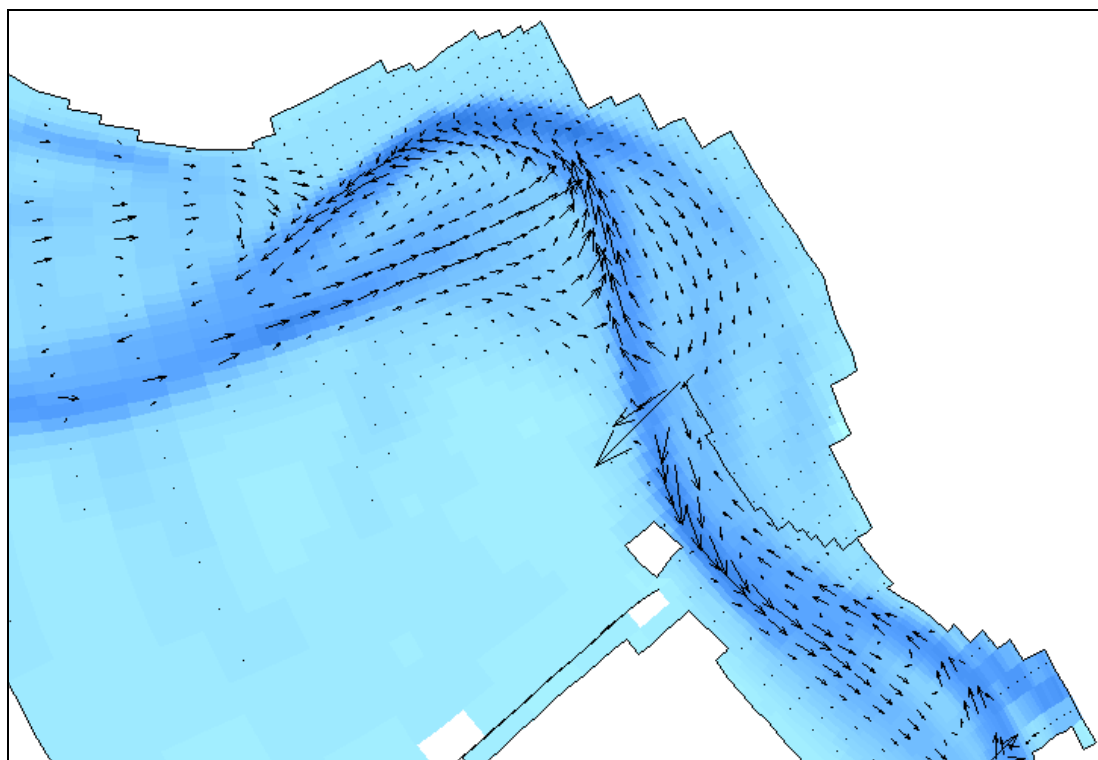


Figure A.9-15: Residual transport patterns in the eastern part of the Western Scheldt for 1970 as calculated with the Van Rijn formulation for the bedload.

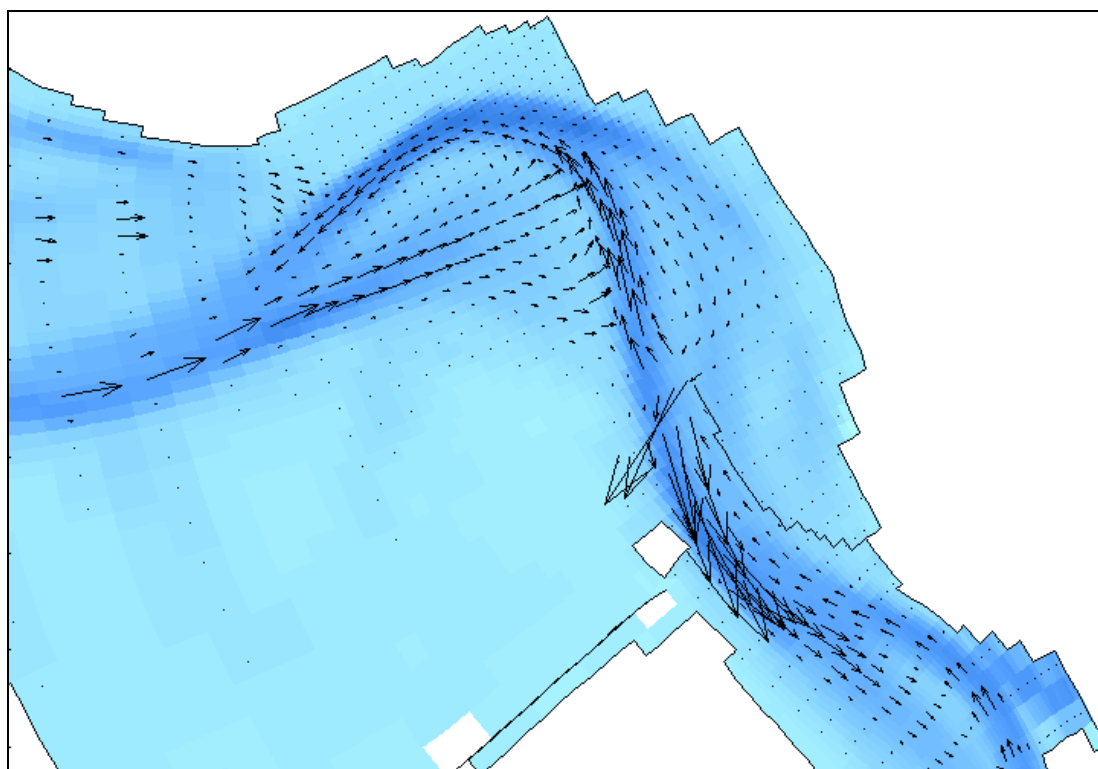


Figure A.9-16: Residual transport patterns in the eastern part of the Western Scheldt for 1970 as calculated with the Van Rijn formulation for the suspended load.

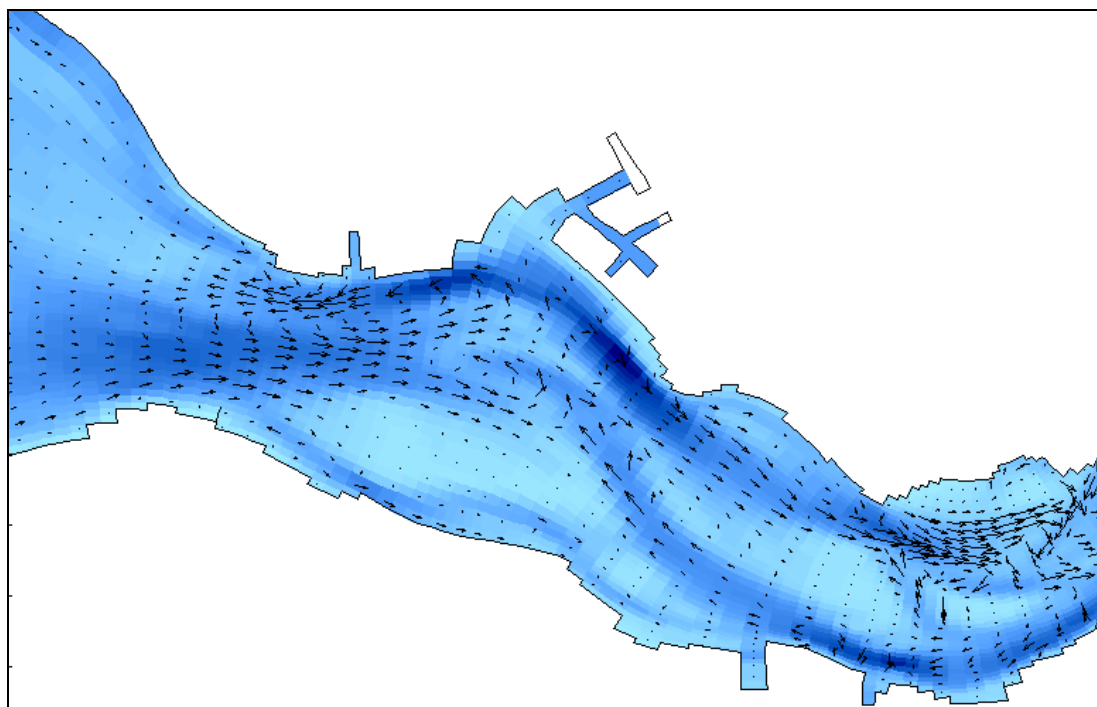


Figure A.9-17: Residual transport patterns in the western part of the Western Scheldt for 1983 as calculated with the Van Rijn formulation for the bedload.

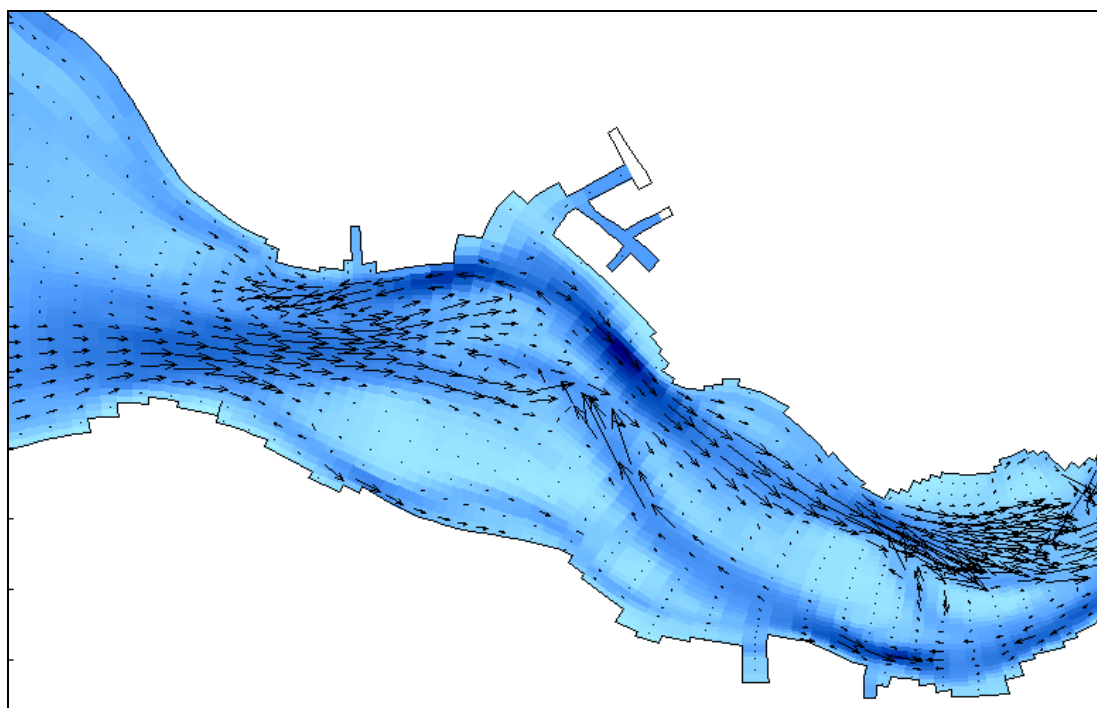


Figure A.9-18: Residual transport patterns in the western part of the Western Scheldt for 1983 as calculated with the Van Rijn formulation for the suspended load.

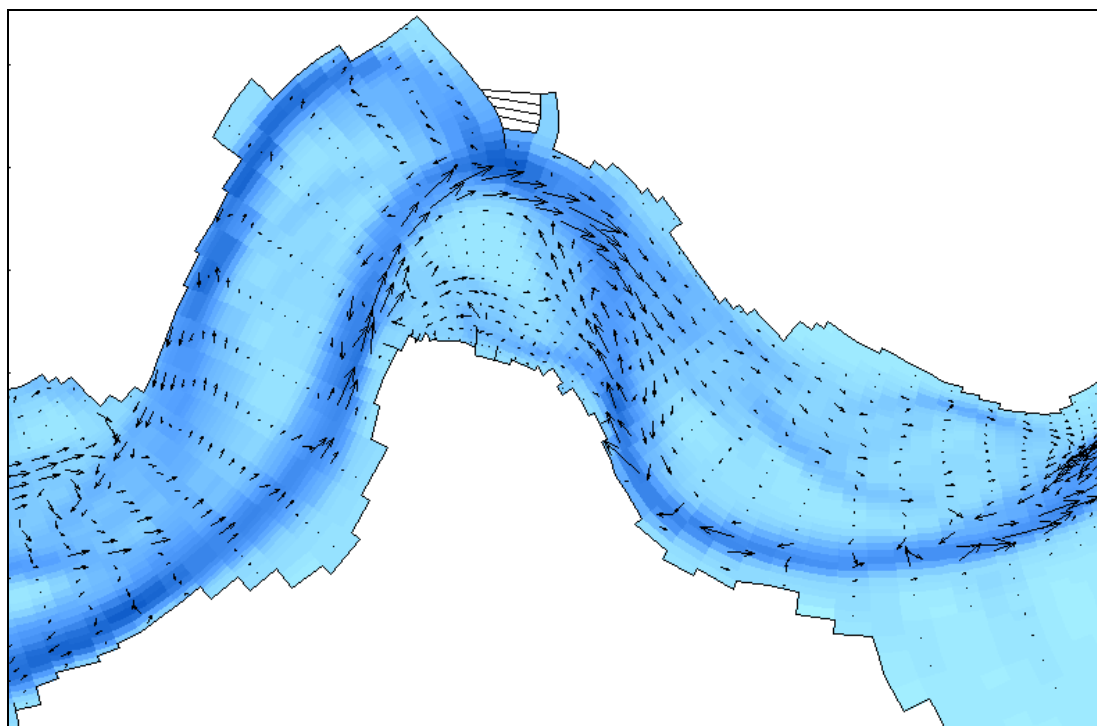


Figure A.9-19: Residual transport patterns in the central part of the Western Scheldt for 1983 as calculated with the Van Rijn formulation for the bedload.

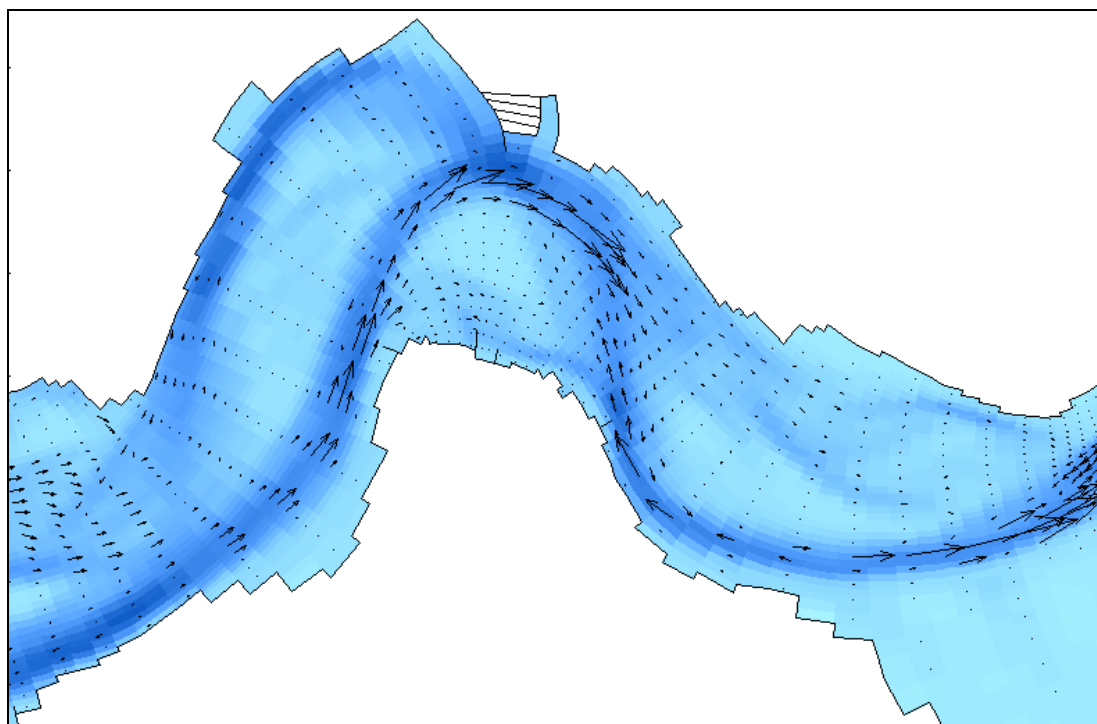


Figure A.9-20: Residual transport patterns in the central part of the Western Scheldt for 1983 as calculated with the Van Rijn formulation for the suspended load.

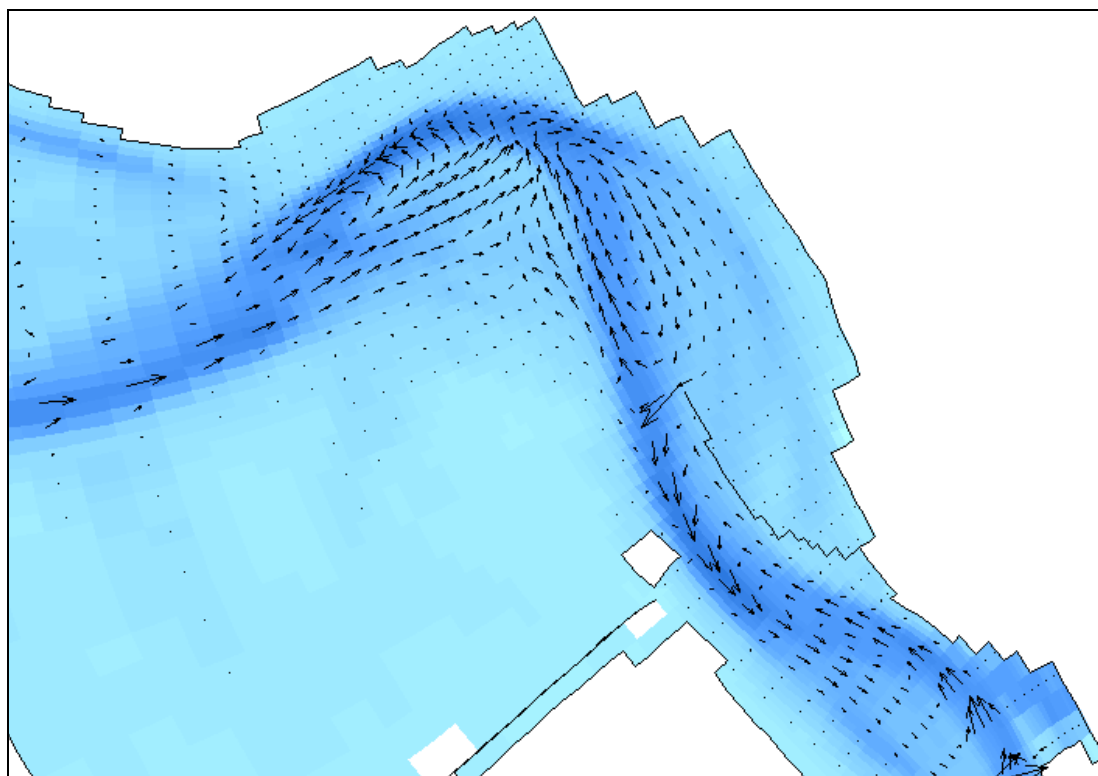


Figure A.9-21: Residual transport patterns in the eastern part of the Western Scheldt for 1983 as calculated with the Van Rijn formulation for the bedload.

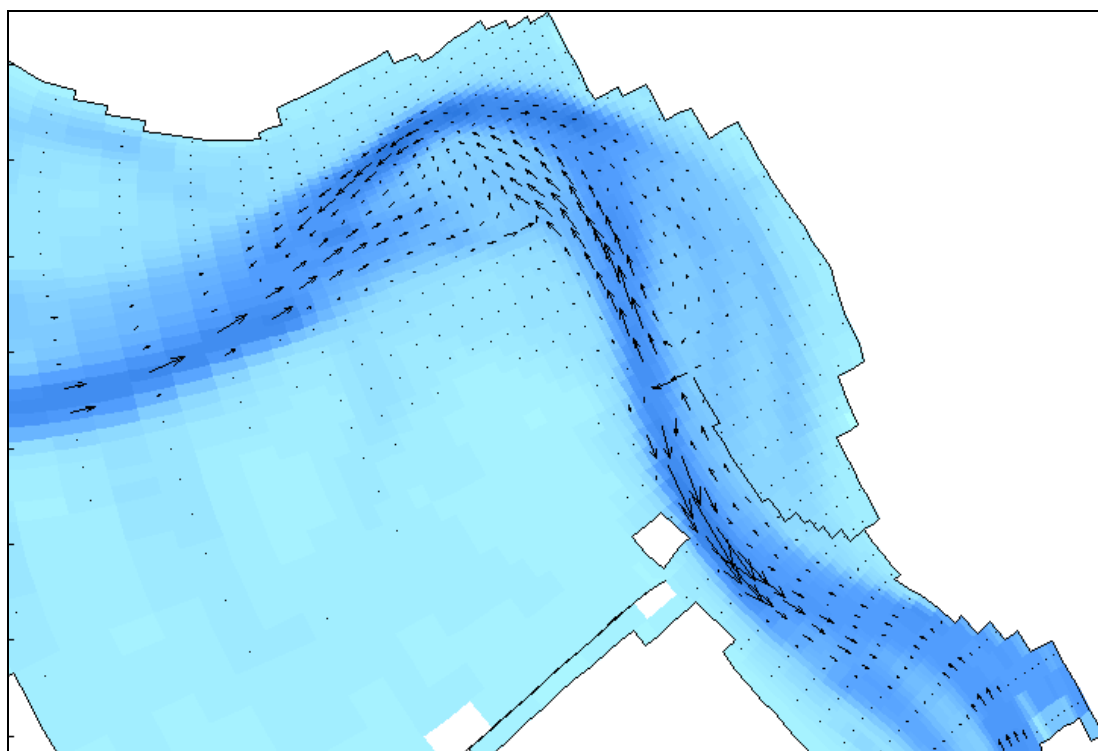


Figure A.9-22: Residual transport patterns in the eastern part of the Western Scheldt for 1983 as calculated with the Van Rijn formulation for the suspended load.

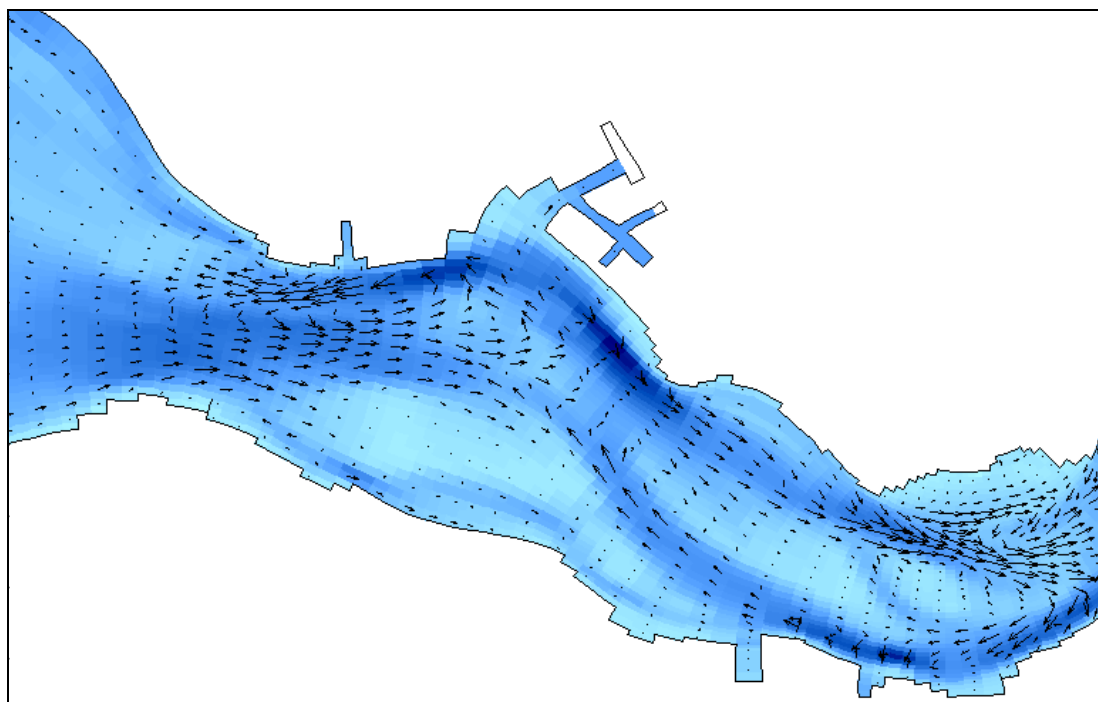


Figure A.9-23: Residual transport patterns in the western part of the Western Scheldt for 2002 as calculated with the Van Rijn formulation for the bedload.

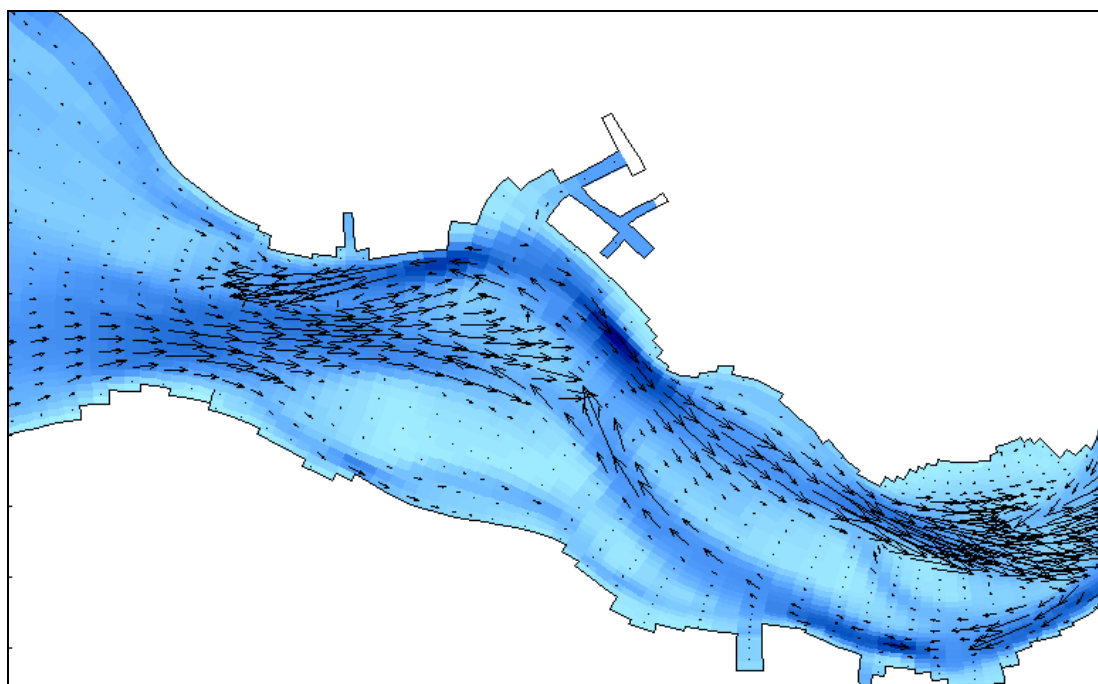


Figure A.9-24: Residual transport patterns in the western part of the Western Scheldt for 2002 as calculated with the Van Rijn formulation for the suspended load.

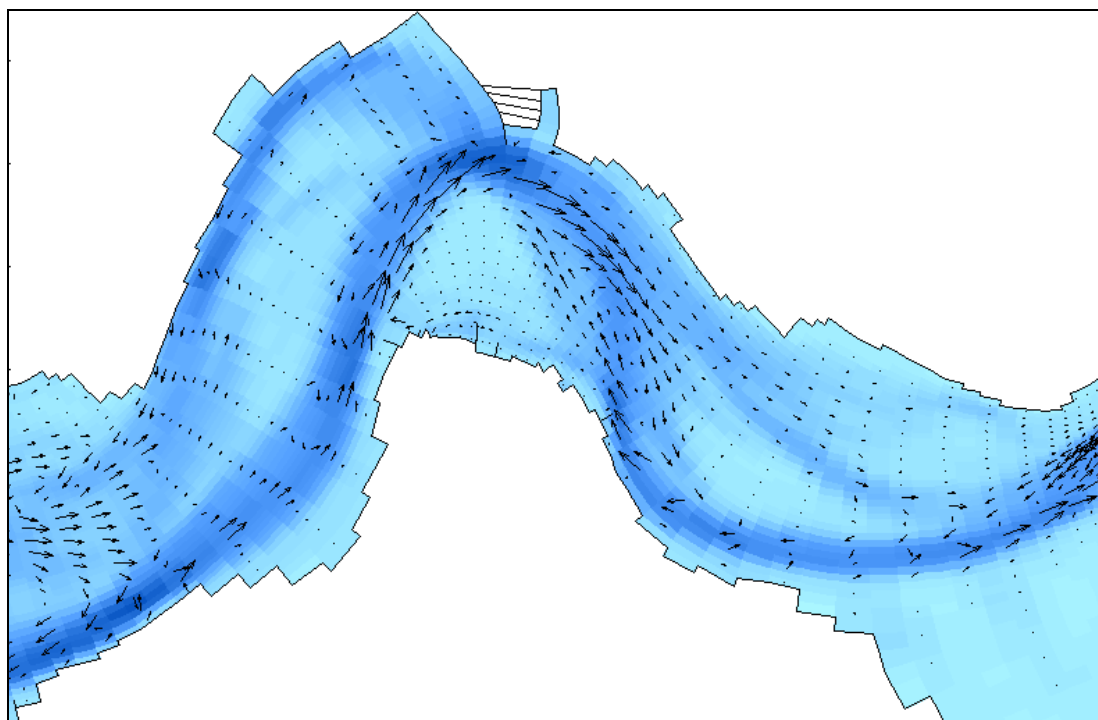


Figure A.9-25: Residual transport patterns in the central part of the Western Scheldt for 2002 as calculated with the Van Rijn formulation for the bedload.

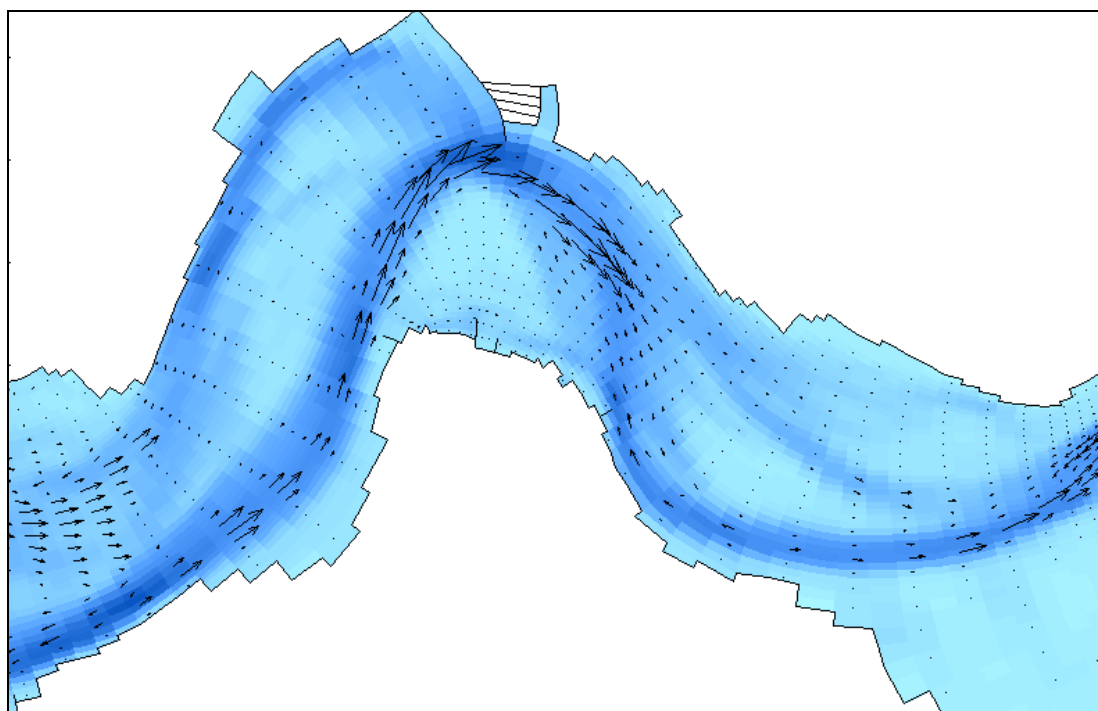


Figure A.9-26: Residual transport patterns in the central part of the Western Scheldt for 2002 as calculated with the Van Rijn formulation for the suspended load.

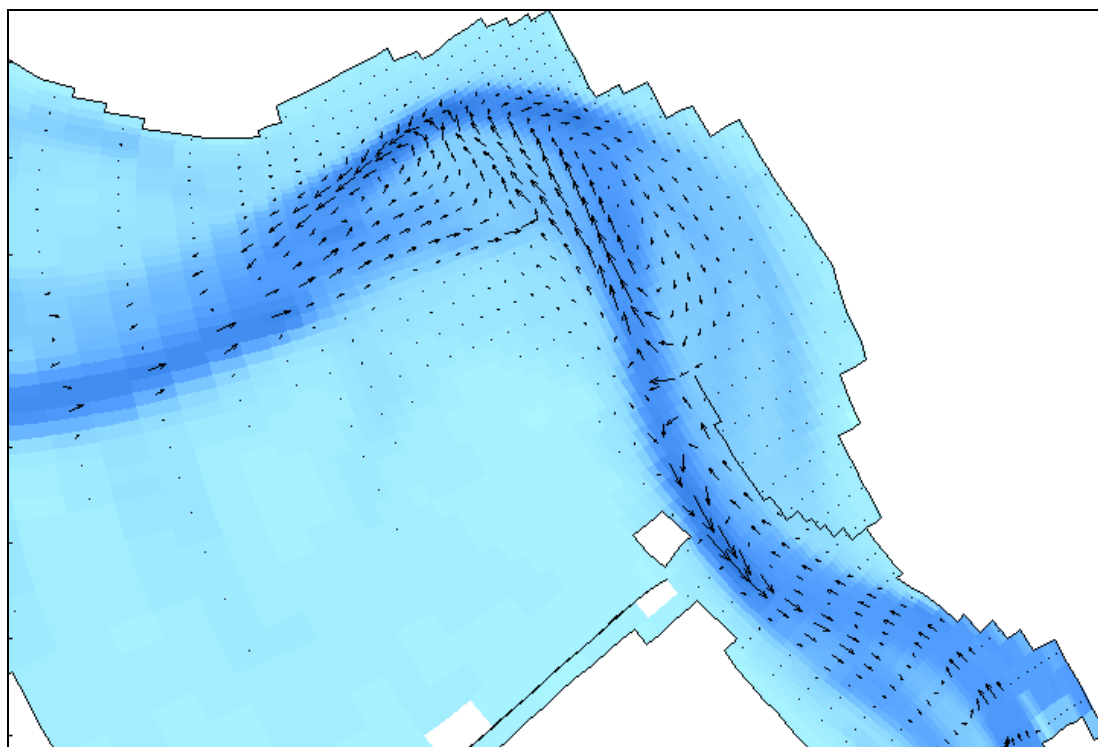


Figure A.9-27: Residual transport patterns in the eastern part of the Western Scheldt for 2002 as calculated with the Van Rijn formulation for the bedload.

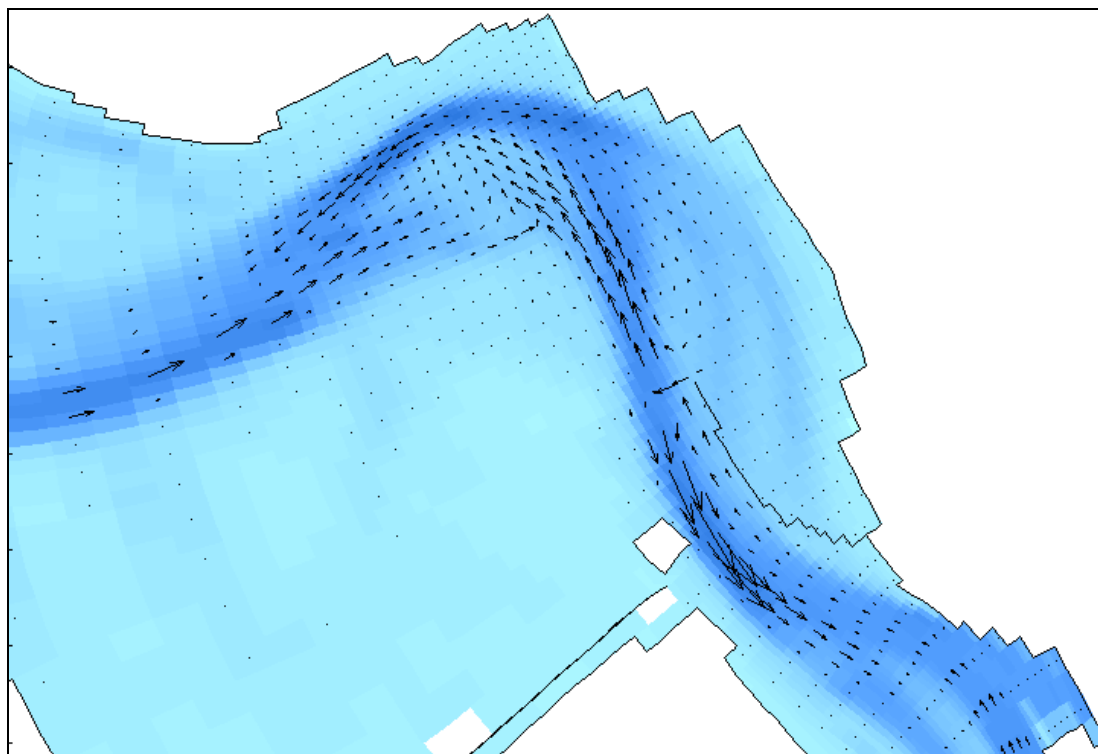


Figure A.9-28: Residual transport patterns in the eastern part of the Western Scheldt for 2002 as calculated with the Van Rijn formulation for the suspended load.

A.9.2 Differences in Direction and Magnitude of the Residual Sediment Transport

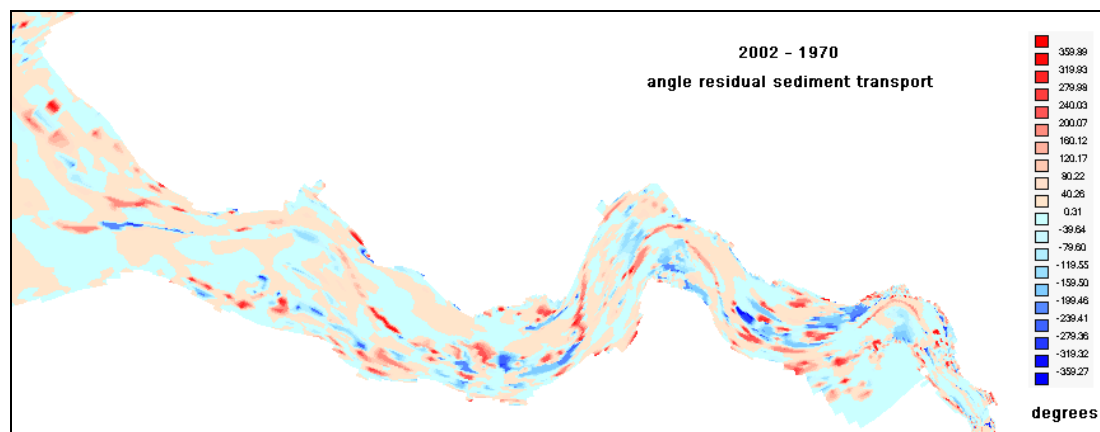


Figure A.9-29: Differences in the direction of the residual total sediment transport between the years 2002 and 1970.

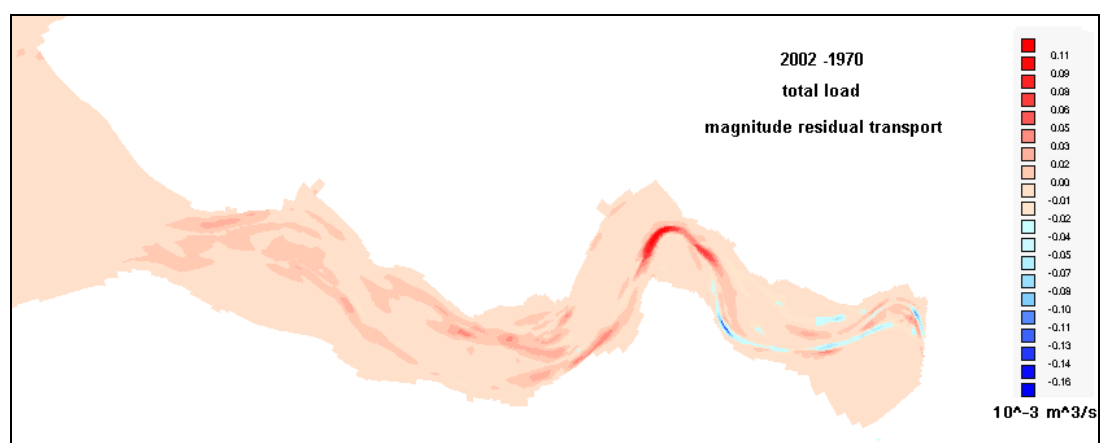


Figure A.9-30: Differences in the magnitude of the residual total sediment transport between the years 2002 and 1970.

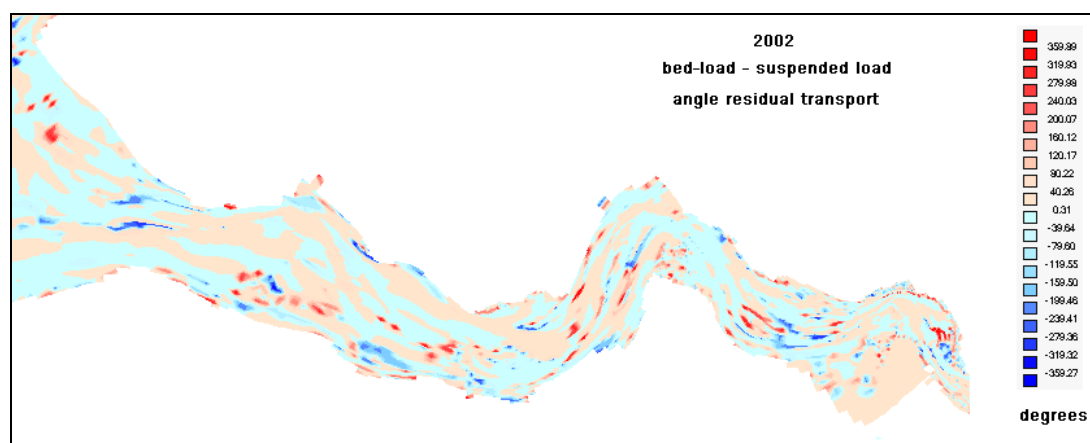


Figure A.9-31: Differences in the direction of the residual bed-load and suspended load transport as calculated according to the Van Rijn formulation in 2002.

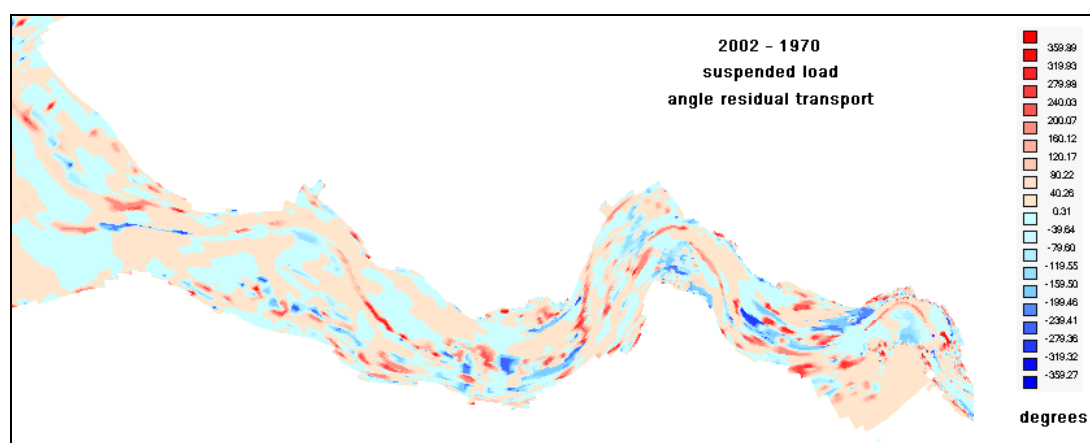


Figure A.9-32: Differences in the direction of the residual suspended load transport as calculated according to the Van Rijn formulation for 2002 and 1970.

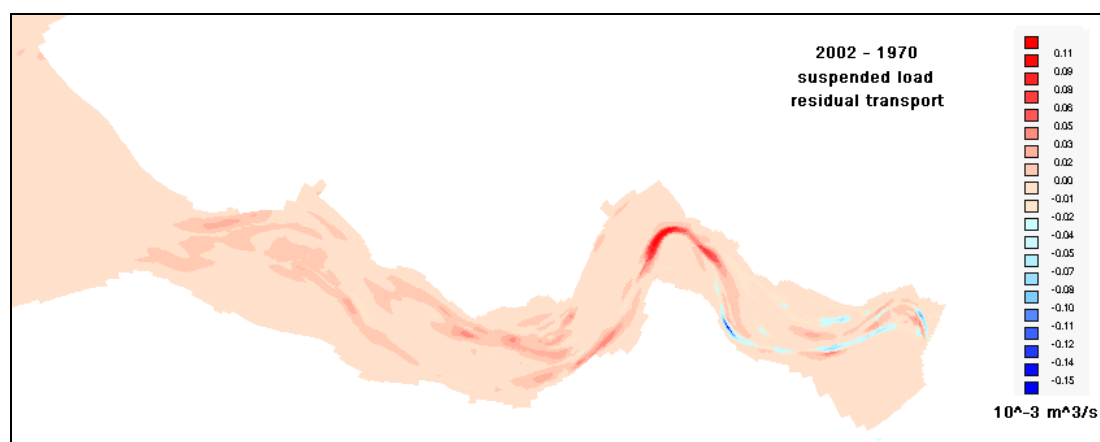


Figure A.9-33: Differences in the magnitude of the residual suspended load transport as calculated according to the Van Rijn formulation for 2002 and 1970.

A.10 Sand Balance Derived from the Model

A.10.1 Cross-sections Used for the Calculation of the Sand Balance.

Table A.10-1: Overview of the selected cross-sections for the calculation of the sand balance.

Border	Cross-sections
delta - macro cell 1	N96, N97, N91, N90, N88
macro cell 1 - 3	N120, N121, N122
macro cell 3 - 4	N157, N158, N159, N160
macro cell 4 - 5	N179, raaiCDvhansw, N180, N181
macro cell 5 - 6	N220, N223, N224, N225
macro cell 7 - upstream	M78, M79, M80, R1VwVBath

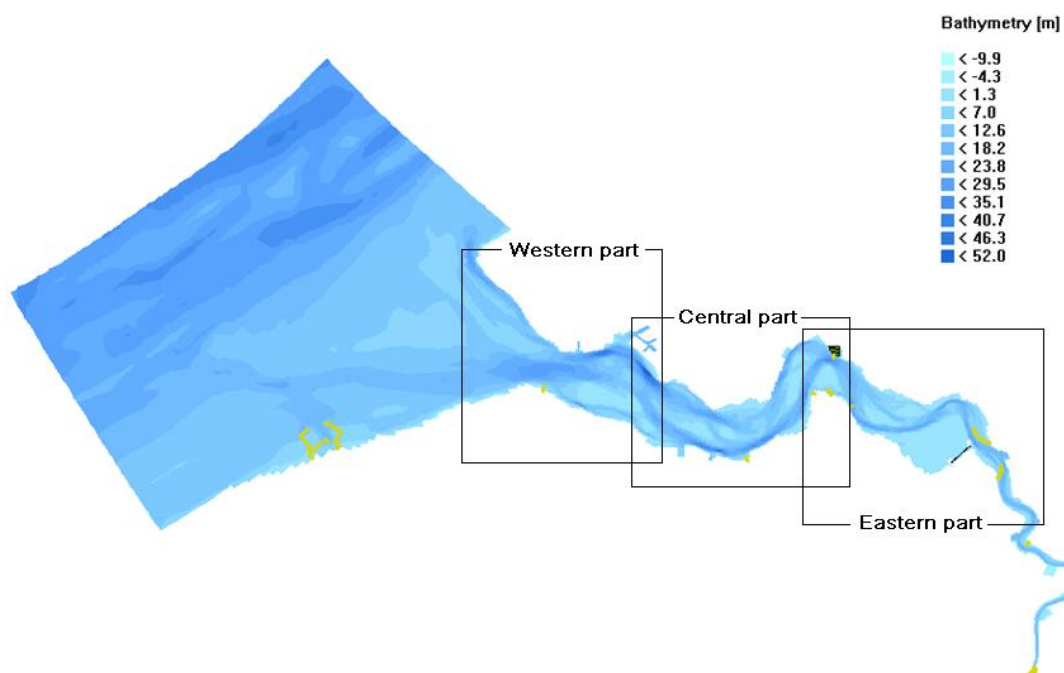


Figure A.10-1: Division of the Western Scheldt into the western, central and eastern part.

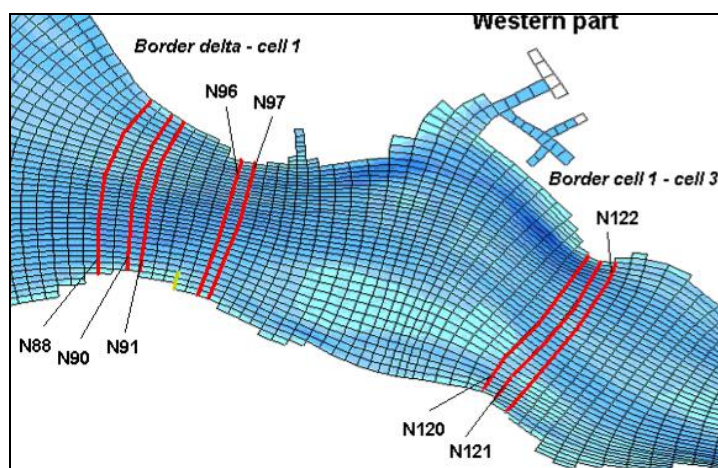


Figure A.10-2: Location of the cross-sections in the western part of the Western Scheldt.

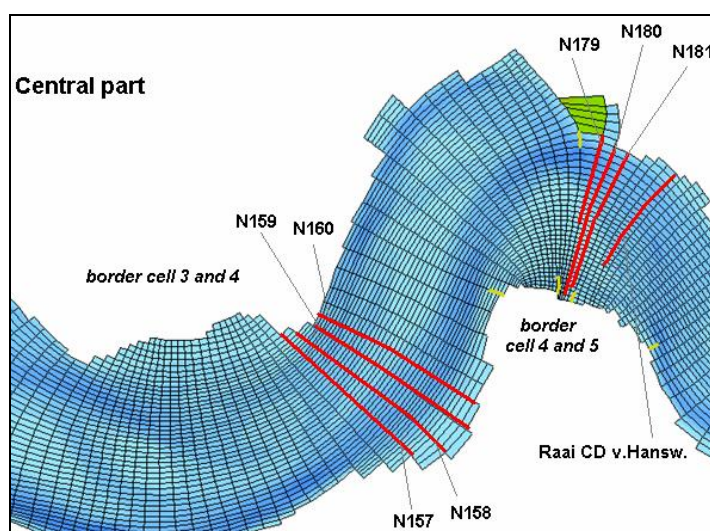


Figure A.10-3: Location of the cross-sections in the central part of the Western Scheldt.

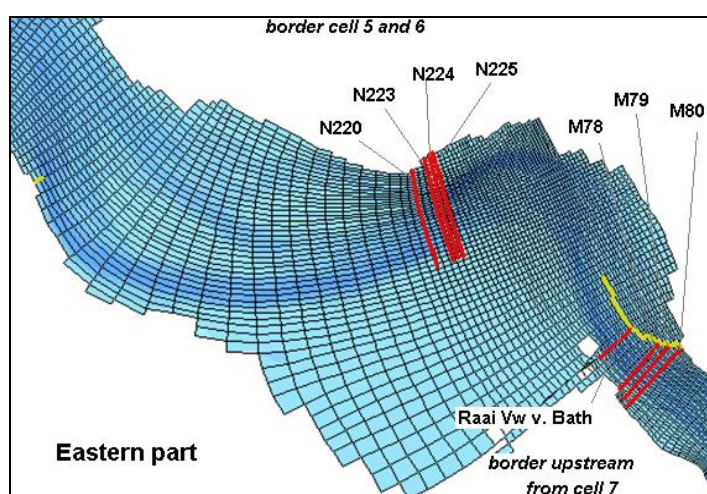


Figure A.10-4: Location of the cross-sections in the eastern part of the Western Scheldt.

A.10.2 Transport at the Seaward Border of Macro Cell I

Table A.10-2: Comparison of the transport through different cross-sections at the seaward border of macro cell 1 near Vlissingen for two transport formulations.

		Van Rijn			Engelund Hansen		
Cross-section	Transport Mode	2002	1983	1970	2002	1983	1970
N96	total load	1596	2313	1991	803	990	851
	bedload	8	45	38			
	suspended load	1930	2267	1953			
N97	total load	1119	1516	1346	515	547	517
	bedload	7	8	4			
	suspended load	1112	1508	1342			
N91	total load	3041	2834	2825	1140	1077	999
	bedload	25	42	44			
	suspended load	3017	2791	2782			
N90	total load	2344	2453	2251	868	852	756
	bedload	16	21	22			
	suspended load	2328	2432	2229			
N88	total load	1746	2114	1579	557	642	448
	bedload	-2	3	-3			
	suspended load	1748	2111	1582			
Average Value of all Cross-sections	total load	1969	2246	1998	777	822	715
	bedload	11	24	21			
	suspended load	2027	2222	1978			

A.10.3 Sand Balance Derived from the Model with the Engelund Hansen Transport Formulation

Table A.10-3: Transport across the macro cell borders in $\text{m}^3/\text{tidal cycle}$ with the Engelund Hansen transport formulation (+ = import; - = export).

		Transport across the macro cell borders in $\text{m}^3/\text{tidal cycle}$ (+ = import; - = export)					
downstream		delta	cell 1	cell 3	cell 4	cell 5	cell 7
upstream		cell 1	cell 3	cell 4	cell 5	cell 6	upstream
1970	total load	777	-143	1633	2184	290	638
1983	total load	822	-466	1333	1953	1142	474
2002	total load	715	-221	1009	1626	1376	1181

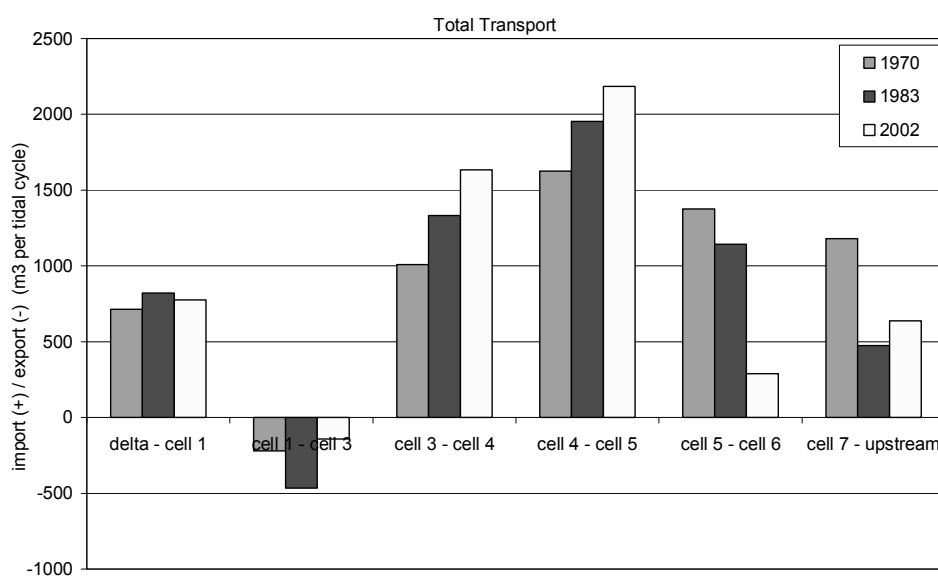


Figure A.10-5: Transport across the borders of the macro cells in the Western Scheldt in $\text{m}^3/\text{tidal cycle}$ for the total transport calculated with the Engelund Hansen formula (+ = import or transport to the east, - = export or transport to the west).

Table A.10-4: Erosion and sedimentation in the macro cells with the Engelund Hansen transport formulation (+ = sedimentation; - = erosion).

		Erosion (-) and sedimentation (+) in the macro cells (in m³/tidal cycle)				
macro cell		cell 1+2	cell 3	cell 4	cell 5	cell 6+7
1970	total load	936	-1230	-618	251	195
1983	total load	1287	-1798	-620	810	668
2002	total load	919	-1776	-551	1894	-349

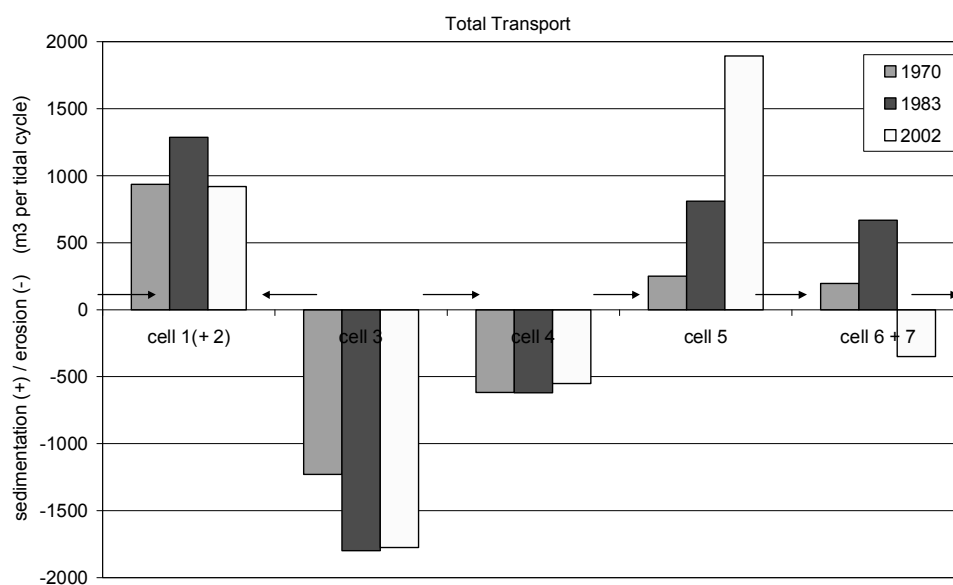


Figure A.10-6: Sedimentation (+) and erosion (-) in the macro cells in the Western Scheldt in m³/tidal cycle for the total transport calculated with the Engelund Hansen formula. The arrow gives the direction of the sediment transport between the cells.

A.10.4 Comparison with Previous Studies

Stikvoort et al. (2003) performed a data analysis for the period 1986-2000 considering the evolution of the sand transport in the Western Scheldt. They concluded that in the period 1998-2000 the transport from the west to the east was higher than before the second deepening. However they also noticed that since 1998 the transport started decreasing again. The sand balance derived from the model in this study also shows an increased transport from the west to the east in the central part of the Western Scheldt. About the decrease since 1998, no comparison with the model results could be made.

Regarding the import/export at the mouth during the same period, Stikvoort et al. (2003) couldn't reject the hypothesis that the small import (between -5 and +5 Mm³/year) would subsist. However they noticed a period of export from the Western Scheldt since 1994, with as only exception the year 1998.

Also the most recent sand balance from Haecon (2006) mentions a decrease of the sediment import at the mouth since 1994 and a change to export from 1997.

Kuijper et al. (2004) found a small landward directed annual-averaged net sediment transport for the period 1998-2001 in their final calibration run of the Western Scheldt model. This doesn't agree with the observations for this period, which show export at the mouth. However, a decrease has been noticed from 2.0 Mm³/year in 1998 to -0.2 Mm³/year in 2001. This indicates already the limited capability of the model to reproduce this process.

The results for the bed-load only are comparable with those from Groenendaal (2005), which calculated the bed-load transport with the formulation from Van der Kreeke and Robaczewska using velocities obtained from the hydrodynamic model WAQUA. The evolution between 1972 and 2002 from that study is visualised in Figure A.10-7. However, some differences were found: the sediment transport between cell 5 and 6 is directed upstream in the recent results, and doesn't change direction although the transport strongly decreases. Also at the Dutch-Belgian border another transport direction has been found: Groenendaal mentions an increase of seaward directed transport, whereas in the present model this remains directed landward.

However as mentioned before, the bed-load is only a small percentage of the total transport. To explain import or export, also the suspended load should be considered.

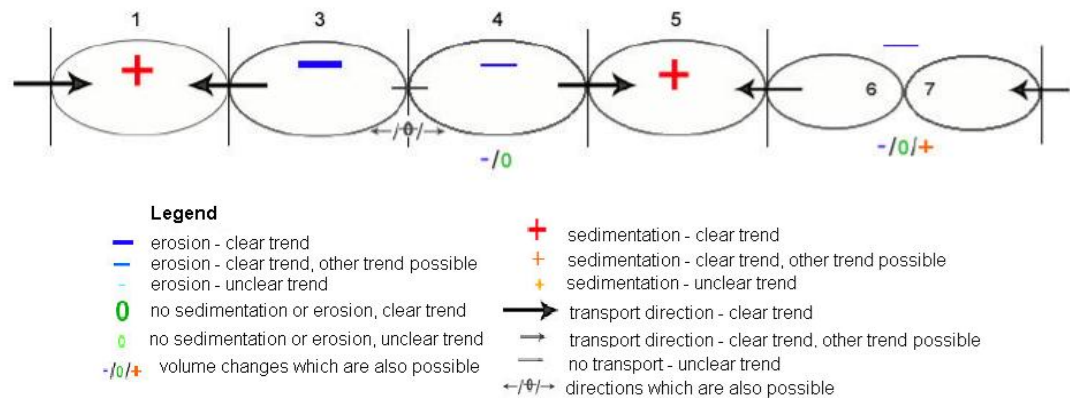


Figure A.10-7: Effect of the modified bathymetry on the net sediment transport, calculated from the average of the transport differences between 2002 and 1972 in the border areas Groenendaal (2005).

A.10.5 Possible Errors

In the first approach, errors are introduced by inaccurate measurements due to stochastic, systematic and variable systematic errors (Marijs and Parée, 2004) (See Paragraph 3.2.1 in main text). In this approach also dredging, dumping and sand mining during the considered period are taken into account. Errors on these data originate from the assumption of a conversion factor, inaccuracies concerning the distribution of volumes over different compartments and the errors in the reported dredged and dumped volumes (Nederbragt and Liek, 2004).

With the approach in this study errors are introduced by the selection of the cross-sections which represent the borders between the compartments. The transport can vary with more than 50% between two successive cross-sections (See comparison in Appendix A.10).

Also the model performance as regards the hydrodynamics and the sediment transport is important. The applied transport formulation influences the obtained volumes as well. The Engelund Hansen formulation typically gives lower values (30 to 50%) compared to Van Rijn. Also Kuijper et al. (2004) found that the type of sediment transport formula largely affects the results. As a result the presented results can only be interpreted qualitatively.